

SYSTEM DEVELOPMENT FOR ANALYSIS  
OF GAS TUNGSTEN ARC WELDING

By

Anna Katherine Albrecht

Thesis

Submitted to the Faculty of the  
Graduate School of Vanderbilt University  
in partial fulfillment of the requirements  
for the degree of

MASTER OF SCIENCE

in

Electrical Engineering

May, 2006

Nashville, Tennessee

**Approved:**

George E. Cook

Alvin M. Strauss

**Date:**

## ACKNOWLEDGEMENTS

I would like to thank all those with whom I have had the pleasure to work, especially, Dr. George E. Cook for his guidance and dedication. This work would not have been possible without him. I also would like to thank Dr. Strauss for his guidance. I really enjoyed working with everyone. This experience has taught me more than I ever thought it would. I also would like to thank Dr. Francis Wells for his help throughout all my educational plans. He supported me in my decision to go to graduate school. Without him, I would not be writing this. I will always remember my experiences, friends, and associates whom I have met while at Vanderbilt University.

## TABLE OF CONTENTS

	Page
ACKNOWLEDGEMENTS .....	ii
LIST OF FIGURES .....	v
LIST OF TABLES .....	xi
NOMENCLATURE .....	xii
 Chapter	
I. INTRODUCTION .....	1
Problem Statement .....	1
Approach .....	1
Equipment: .....	1
Welding Equipment .....	1
Imaging System and Macro Lens System .....	3
II. BACKGROUND .....	5
Gas Tungsten Arc Welding Process .....	5
Advantages and Disadvantages .....	9
Power Source .....	9
Alternating Current (AC) .....	11
Direct-Current Electrode Negative (DCEN) .....	11
Direct-Current Electrode Positive (DCEP) .....	11
The Electrode .....	12
Electrode Material .....	13
2% Thoriated Tungsten .....	14
2% Ceriated Tungsten .....	15
1½% Lanthanated Tungsten .....	15
Zirconiated .....	16
Pure Tungsten .....	16
Electrode Diameter .....	16
Grind Angle .....	17
Tip Diameter .....	17
Joint Types and Positions .....	20
Geometry of Weld Bead .....	21
Weld Pool Shape .....	22
Shielding Gas .....	26
Argon .....	27
Helium .....	27
Argon-Helium Mixtures .....	29
Argon-Hydrogen Mixtures .....	30
Multi Input Output System .....	30
Automatic Voltage Control .....	32
Applications of GTAW and Welding Automation .....	32
Digital Camera .....	33
Lens Selection .....	42
Digital Image Processing .....	45

Basic Image Processing Techniques . . . . .	47
Filtering . . . . .	49
Gradient and Laplacian Filters. . . . .	53
Smoothing Filters and Edge Enhancement Filters . . . . .	57
Fourier Transform . . . . .	61
Optimal and Sub-optimal Filters. . . . .	68
Fourier Domain Correlation . . . . .	69
Fast Fourier Transform . . . . .	71
High Speed Imaging System and Macro Lens Viewing . . . . .	72
Digital Camera and Macro Lens System . . . . .	72
Image Acquisition Board and Software . . . . .	76
III. EXPERIMENTAL METHOD . . . . .	79
Welding Parameters for the Gas Tungsten Arc Welding System . . . . .	79
Signal and Image Acquisition . . . . .	81
IV. HIGH SPEED DIGITAL IMAGING SYSTEM . . . . .	83
Viewer Program . . . . .	83
Spatial Filters . . . . .	87
Convolution . . . . .	88
LabVIEW Programming Definitions . . . . .	89
V. RESULTS . . . . .	95
VI. DISCUSSION . . . . .	96
VII. CONCLUSIONS AND RECOMMENDATIONS FOR FUTURE WORK . . . . .	98
APPENDIX . . . . .	100
A. LabVIEW Programs and Overview of Welding Process. . . . .	100
B. Dalsa Camera Data Sheets. . . . .	107
REFERENCES . . . . .	109

## LIST OF FIGURES

Figure	Page
1. The GTAW process. . . . .	5
2. GTAW process with an optional optical probe to collect specular reflections of the weld pool's surface. . . . .	6
3. The GTAW circuit. . . . .	7
4. Gas tungsten arc welding: (a) overall process (b) welding area enlarged. . . . .	8
5. GTAW Electrode Polarity. . . . .	11
6. Diagram of the electrode showing diameter, tip diameter, and included angle. . . . .	17
7. Arc shape and fusion zone profile as a function of electrode included angle. . . . .	20
8. Welding positions and primary joints. . . . .	21
9. Comparison of weld pool shapes under different travel speeds and the average grain growth direction. under different heat source travel speeds. . . . .	23
10. Comparison of weld pool shapes and grain growth under different travel speeds. . . . .	24
11. The different classifications of penetration. . . . .	25
12. Variation of heat input to the workpiece with power density of the heat source. . . . .	26
13. Arc welding depicted as a multiple-input, multiple-output system. . . . .	31
14. CCD architectures with different arrangements of image section and storage section: full frame transfer, interline transfer, and frame transfer. . . . .	34
15. Spectral sensitivity of silicon and the human eye. . . . .	38
16. Spectral characteristics of the red, green, and blue filters used in RGB color cameras. . . . .	38
17. Test pattern with different realizations of $\gamma$ ( $\gamma = 0.6, 1.0, 1.6$ from left to right). . . . .	39
18. Lens selection. . . . .	43
19. Diagram of a lens system. . . . .	45
20. A simple digital image: (a) The image and (b) the corresponding array of numbers. . . . .	48
21. Form of a typical point spread function $h(t)$ . . . . .	51
22. Digital Convolution: The output at a point is given by the sum of the input values around the point, each multiplied by the corresponding term of the $h$ array. To compute the next	

output value, the h array is shifted, and the multiply and sum operation repeated . . . . .	52
23. The Laplacian as pushing a pixel away from its neighbors. . . . .	59
24. The definitions for the forward and inverse transforms for each of these cases (The three letters starting at each line indicate Continuous/Discrete, 1 dimension or 2, and Forward or Inverse transform). . . . .	63
25. Comparison of standard and optical transforms: (a) The standard form of the Fourier transform in upper left, and (b) the transform rearranged into the optical form in upper right. (c), in lower left, shows the origin and coordinate systems for the two forms. The reordering to convert from one to the other in two dimensions is shown in (d). . . . .	67
26. Comparison of multiplication operations using spatial and Fourier correlation. . . . .	70
27. Photograph showing the overall layout of the macro camera system. The digital camera and the associated computer hardware is shown in the upper left area of the picture. . . . .	73
28. Macro camera imaging system showing linear array and digital frame grabber camera . in position for measurements Camera magnification is 28.86x. . . . .	74
29. The Dalsa CA-D1-0128A camera. . . . .	75
30. Photograph showing the orientation between the macro camera. the GTAW torch and the workpiece. . . . .	76
31. The IMAQ library palette shows basic, advanced, and color VIs. . . . .	78
32. Program used for saving images from camera system. . . . .	82
33. The main program which calls each subsequent programs. . . . .	84
34. Window of the program used to open images to be used by the viewer program. The block diagram can be seen in the appendix. . . . .	85
35. The Front Panel of the LabVIEW Viewer Program. Note: Begin 40 19 122, End 8 34 0, Gradient 74 71 255 The last number is cut off in the image. . . . .	86
36. Portion of LabVIEW Viewer Program Showing Convolution of the Image. . . . .	92
37. Portion of Labview Program Showing the Spreadsheet Command. . . . .	93
38. Front panel and block diagram of the LabVIEW subprogram used to get pixel data over each frame from the original image. Index and Index 2 corresponds to the coordinates of the pixel. . . . .	94
39. This is frame number 48 out of the 1800 frames in the image, 79d.log. . . . .	95

## LIST OF TABLES

Table	Page
1. Commonly Available Tungsten Electrodes. . . . .	14
2. Commercially sold tungsten types, their American Welding Society (AWS) and International Standards Organization (ISO) classifications, and the amount and type of oxide contained in the electrode. . . . .	14
3. Advantages and disadvantages of electrode tip diameters. . . . .	18
4. Advantages and disadvantages of electrode tapers. . . . .	19
5. Properties of shielding gases used for welding. . . . .	29
6. Gas Tungsten Arc Welding parameters for the welds (images of the welds) obtained. . . . .	81

## **Welding Terminology**

**Acetone** A flammable, volatile liquid used in acetylene cylinders to dissolve and stabilize acetylene under high pressure.

**Acetylene** A highly combustible gas composed of carbon and hydrogen. Used as a fuel gas in the oxyacetylene welding process.

**Air-Acetylene** A low temperature flare produced by burning acetylene with air instead of the carbon arc.

**Alloy** A mixture with metallic properties composed of two or more elements, of which at least one is a metal.

**Alternating current** An electric current that reverses its direction at regularly recurring intervals

**Arc length** The distance between the tip of the electrode and the weld puddle

**Arc voltage** the voltage across the welding arc

**Arc welding** A group of welding processes in which fusion is obtained by heating with an electric arc or arcs, with or without the use of filler metal.

**As welded** the condition of weld metal, welded joints, and weldments after welding and prior to any subsequent thermal, mechanical, or chemical treatments.

**Bare electrode** An arc welding electrode that has no coating other than that that incidental to the drawing of the wire.

**Base metal** The metal to be welded or cut. In alloys, it is the metal present in the largest proportion.

**Bead weld** A type of weld composed of one or more string of weave beads deposited on an unbroken surface.

**Beading** see string bead welding and weave bead.

**Bevel Angle** The angle formed between the prepared edge of a member and a plane perpendicular to the surface of the member.

**Buckling** Distortion caused by the heat of a welding process

**Buildup sequence** The order in which the weald beads of a multipass weld are deposited with respect to the cross section of a joint.



**Case hardening** A process of surface hardening involving a change in the composition of the outer layer of an iron base alloy by inward diffusion from a gas or liquid, followed by appropriate thermal treatment. Typical hardening processes are carbonizing, cyaniding, carbonitriding, and nitriding

**Coated electrode** An electrode having a flux applied externally by dipping, spraying, painting, or other similar methods. Upon burning, the coat produces a gas which envelopes the arc.

**Covered electrode** A metal electrode with a covering material which stabilizes the arc and improves the properties of the welding metal. The material may be external wrapping of paper, asbestos, and other materials or a flux covering.

**Crater** depression at the termination of an arc weld

**Critical Temperature** The transition temperature of a substance from one crystalline form to another.

**Concavity** The maximum perpendicular distance from the face of a concave weld to a line joining the toes.

**Current density** amperes per square inch of the electrode cross sectional area

**Cylinder** A portable cylindrical container used for the storage of a compressed gas.

**Defect** A discontinuity or discontinuities which, by nature or accumulated effect render a part or product unable to meet the minimum applicable acceptance standards or specifications. This term designates rejectability.

**DCEN Direct current electrode negative**

The arrangement of direct current arc welding leads in which the work is the positive pole and the electrode is the negative pole of the welding arc

**DCEP direct current electrode positive**

The arrangement of direct current arc welding leads in which the work is the negative pole and the electrode is the positive pole of the welding arc

**Depth of fusion** distance from the original surface of the base metal to that point at which fusion ceases in a welding operation

**Drag** The horizontal distance between the point of entrance and the point of exit of a cutting oxygen stream.

**Duty Cycle** The percentage of time during an arbitrary test period, usually 10 minutes, during which a power supply can be operated at its rated output without overloading.

**Electrode holder** A device used for mechanically holding the electrode and conducting current to it.

**Joint Penetration**

The maximum depth a groove weld extends from its face into a joint exclusive of reinforcement The temperature at which a metal begins to liquefy melting point

**Melting range** temperature range between solidus and liquidus

**Melting rate** the weight or length of electrode melted in a unit of time

**Pass** the weld metal deposited in one general progression along the axis of the weld

**Reverse polarity** the arrangement of direct current arc welding leads in which the work is the negative pole and the electrode is the positive pole of the welding arc

**Slag inclusion** non-metallic solid material entrapped in the weld metal or between the weld metal and the base metal

**String bead** A method of metal arc welding on pieces  $\frac{3}{4}$  in. (19mm) thick or heavier in which the weld metal is deposited in layers composed of strings of beads applied directly to the face of the bevel.

**Solidus** is the highest temperature at which a metal or alloy is completely solid

**Spall** small chips or fragments which are sometimes given off by electrodes during the welding operation. This common with heavy coated electrodes

**Spatter** the metal particles expelled during arc and gas welding which do not form a part of the weld

**Straight polarity** the arrangement of direct current arc welding leads in which the work is the positive pole and the electrode is the negative pole of the welding arc.

**Temper colors** colors which appear on the surface of steel heated at low temperatures in an oxidizing atmosphere

**Toe of the weld** The junction between the face of the weld and the base metal.

**Undercutting** An undesirable crater at the edge of the weld caused by poor weaving technique or excessive welding speed.

**Weave bead** type of weld bead made with transverse oscillation

**Weld** a localized fusion of metals produced by heating to suitable temperatures pressure and/or filler metal may or may not be used. The filler material has a melting point approximately the same or below that of the base metals, but always above 800 degrees F (427C)

**Weld bead** weld deposit resulting from a pass

**Weld gauge** a device designed for checking the shape and size of welds

**Weldment** is a unit composed of an assemblage of pieces welded together.

**Weld metal** that portion of a weld that has been melted during welding

**Weldability** the capacity of a material to form a strong bond of adherence under pressure or when solidifying from a liquid

**Welding leads**

a) **electrode lead** the electrical conductor between the source of the arc welding current and the electrode holder

b) **work lead** electrical conductor between the source of the arc welding current and the workpiece

**work lead** the electric conductor(cable) between the source of the arc welding current and the workpiece

## CHAPTER I

### INTRODUCTION

#### **Problem Statement**

The focus of this work was the development of equipment and image processing techniques to observe the melting characteristics at the leading edge of a gas tungsten arc weld.

#### **Approach**

A high speed digital imaging system, along with a macro lens imaging system, were used to obtain high quality images of the weld pool motion in a digital format for computer processing. Once in the computer, a LabVIEW viewer program [12] was used to view the images at various speeds. These images were further enhanced to bring out the leading edge of the weld. This was done by using Labview 5.1 along with the IMAQ Vision toolkit 4.1.1. Various image processing techniques, including filtering and convolution, were tried. Once the proper images were obtained, the Fast Fourier Transform and other techniques were used for the analysis of these images. The two main programs used for analyzing the weld pool motion were, Labview 5.1 and Matlab 5.3.

#### **Equipment**

##### ***Welding Equipment***

The GTA welding station consists of a welding table, welding torch, optical probe, and the workpiece to be welded. It also uses a TMC welding power supply [1] and controller. The welding torch and optical probe remains stationary while the workpiece transverses along with the table along a horizontal axis at a controllable speed. The

welding torch is equipped with a servosystem that can be used for automatic voltage control (AVC) or manual torch height. Information on this welding station can be found in the Ph.D. Dissertation [3].

The power supply is a Merrick TMC500 [1]. The TMC500 is a 45V, 500A DCEN class H linear amplifier used for constant current output control. It can deliver output current from 0 to 500A at a voltage from 0 to 45 volts for an indefinite period. This output current is controlled by supplying an input voltage ranging from 0 to 5 Volts to the “External Current Control” connection to provide an output current from 0 to 500 Amps. To operate in external current mode, a “Manual/External” toggle switch has to be set to “External” during the operating and arc ignition times. The automatic arc starter program was implemented during arc ignition time. The frequency response of the power source is in excess of 20 KHz. Direct current was used. The welding current is fed to a GTAW water cooled machine torch. The welding torch was moved up and down to maintain constant arc voltage. An Automatic Voltage Control system (AVC) is used to maintain a constant arc voltage over an entire run. Information on the power supply controller or AVC system can be found in the Ph.D. Dissertation [2].

The workpiece used in this research was a 1/8 inch x 4 inch x 18 inch cold rolled carbon steel, which can be purchased from a commercial supplier. The steel was wiped clean with denatured alcohol before use. The welding torch used a tungsten electrode, 2% thoriaed. The electrode tip angle is 60 degrees, included. Electrode tip to workpiece distance is approximately 0.015 in. The shielding gas was argon at a flow rate of 50 ft<sup>3</sup> hour. The workpiece is clamped to the top of a 25.4mm X 305mm X 610mm (1 inch x 12 inch x 24 inch) steel work table. The table can be adjusted so that multiple passes can be made on the same workpiece without disturbing the position of the weld pool relative to the macro camera. Spacers can be placed between the table and the workpiece to prevent direct heat loss into the table from the underbead area of the weld. The work table velocity is controlled by a variable speed electric motor. Welding speed can be continuously adjusted. For this research, the controlled welding speed was between 8.47 mm/s to 16.93 mm/s (20 in/min to 40 in/min). Low friction linear ball bushings support the work table. A precision ball screw assembly, driven by the motor, translates the work table. This provides quiet uniform translation to the workpiece [12].

### ***Imaging System And Macro Lens System***

An understanding of how modern electronic cameras function and the types of signals they produce is a key step in designing a successful system. The electronic camera is the most fundamental part of the imaging system. To work with signals as images, these signals need to get into the computer by way of the IMAQ-1424 frame grabber via the National Instruments software program LabVIEW. The IMAQ-1424 is discussed and how its RTSI interface is used to synchronize image and data acquisition with a PCI-MIO-16-E1 multifunction I/O board. The IMAQ PCI-1424 is a universal digital camera image acquisition board designed to acquire both monochrome and color images, as well as provide control for digital cameras. The board is designed to acquire data from cameras with resolutions of 8, 10, 12, 16, 24, and 32 bits.

Since the most fundamental part of the imaging system is the electronic camera. The progressive scan area camera, Dalsa CA-D1-0128, was used as the “eye” of the system. It was connected to the computer through a data and image acquisition board with the appropriate cables from the manufacturer. The acquisition board was installed in a PCI slot inside the computer. Also additional memory was needed and added to this computer. The camera was attached to the rear of the macro lens system [12]. The camera and the macro lens system was carefully adjusted to capture the weld pool image. This weld pool image was displayed frame by frame in real-time and saved on the computer for further analysis.

The Dalsa camera was mounted to the rear view port of the macro camera imaging system. Direct viewing was also available from a ground glass display screen at the rear view port. The top view port is normally used to mount a 35mm camera body or linear array using a standard 4x5 photographic mount [12]. Each view port was adjusted such that the geometric center of the view frame observes the same point on the weld pool surface. This macro camera and lens system enabled 28.86x magnification of the weld pool. The photo enlarger lens, 105mm, is attached to the front of a bellows type view camera. A lens of this focal length affords a reasonable compromise between the working distance (lens to weld pool distance) and the overall length of the macro camera imaging system, 3.035m (119.5in). This system with the two view ports allows both simultaneous measurement and direct observation of the weld pool. The weld pool image passes through an extension tube. The magnification of the camera is determined by:

$$L = fM \tag{1}$$

where M is the desired magnification, f is the focal length of the lens, and L is the extension tube length [12].

At the rear of the camera, a beam splitter is employed to provide simultaneous weld pool images to the two view ports. The beam splitter reflects 40 percent of the incident light to the top view port and the remaining light is transmitted to the rear view port. The optical axis of the camera is oriented 45 degrees to the horizontal and 90 degrees to the direction of travel. This allowed an unobstructed view of the weld pool while minimizing the amount of arc light viewed directly by the camera or reflected into the camera from the weld pool surface. As a result, no light filtering was required to reduce the arc light intensity for direct observation when weld currents were kept below 120 amperes. Simple adjustments to the lens aperture setting were all that was required. Observing welds with current settings below about 60 A proved challenging. Since arc light is reduced, the aperture must be opened to allow more light into the macro camera for proper viewing. By opening the aperture, field depth (the distance interval in front of the lens which is in clear focus) is reduced. Attaining clear focus across the entire width of the weld bead becomes difficult. The normal operating range for the macro camera, in its current state of development is, therefore, between 60 to 110 amperes. More information on this macro camera is in Delapp's paper [12].

Next, the focus will shift from the hardware end of image acquisition and processing to the software end. The NI-IMAQ Configuration Utility version 2.1 is a setup and diagnostic utility that configures parameters for your IMAQ board and tests if the board and camera are functioning correctly. Machine vision techniques were implemented using the Labview and IMAQ vision image processing toolkit. Advanced IMAQ Vision for LabVIEW version 4.1.1 and LabVIEW version 5.1 were used for acquiring, viewing, and analyzing the images that were obtained from the above mentioned camera system. Matlab version 5.3 and Microsoft Excel were also used for further image analysis. Plus it was good for comparing results with those from Labview. National Instruments also offers various Labview courses. The Labview Machine Vision and Image Processing Course version 1.0 was also used for reference and further advanced image processing ideas. These programs were used for enhancing the weld pool images and for extracting information from the weld pool.

## CHAPTER II

### BACKGROUND

#### Gas Tungsten Arc Welding Process

In the Gas Tungsten Arc Welding process (GTAW), also referred to as the Tungsten Inert Gas process (TIG) an electric arc is established between a tungsten electrode and the part to be welded. To start the arc a high voltage is used to break down the insulating gas between the electrode and the workpiece. Current is then transferred through the electrode to create an electrode arc. The metal to be welded is melted by the intense heat of the arc and fuses together either with or without a filler material. This GTAW process can be seen in Figure 1.

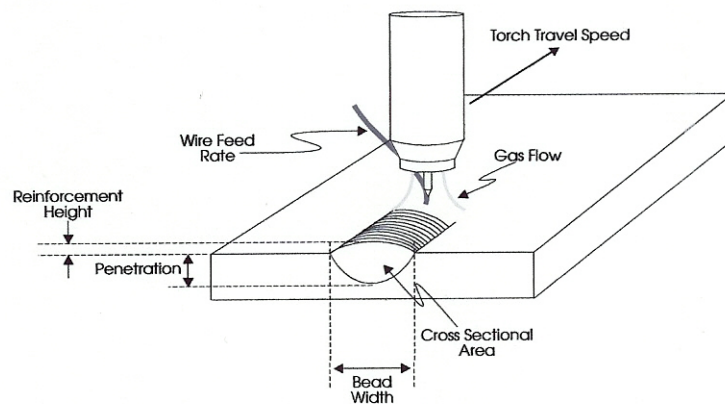


Figure 1. The GTAW process [4].

The purpose of welding is to join two pieces of metal by localized melting and re-solidification. Among the common arc welding processes is gas tungsten arc welding (GTAW). The other processes include flux-cored arc welding (FCAW), gas metal arc welding (GMAW), plasma arc welding (PAW), submerged arc welding (SAW), and



shielded metal arc welding (SMAW). An overview of these and other welding processes can be seen in Table A in Appendix A [5]. The welding process used in this work is an autogenous bead-on-plate GTA weld with a direct current electrode negative (DCEN) power source. This process, Figure 2, involves weld beads being made by the melting and solidification of the base metal without the addition of extra filler metal. Typically filler metal is not added when thinner materials, edge joints, or flange joints are welded. If needed, extra metal can be used to reinforce the weld joint supplied by a wire fed into the molten pool. Weld bead shapes should have smooth transitions with the base metal to avoid the development of stress concentration areas that fatigue and cause early failures. Undercutting, concavities, and other visual defects are detrimental.

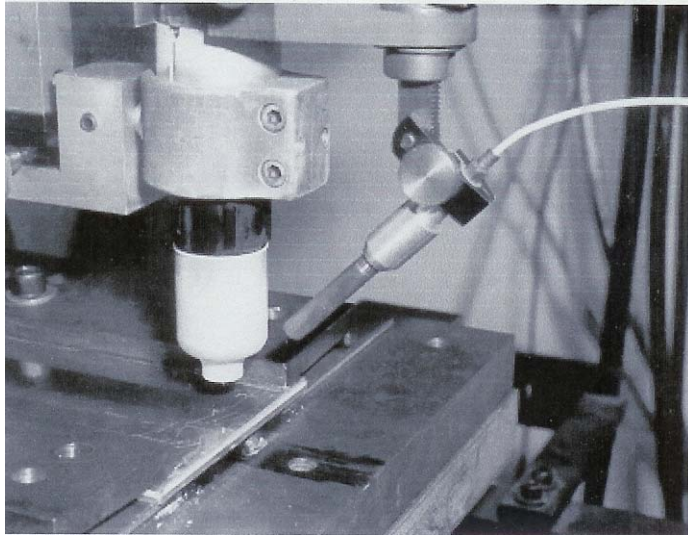


Figure 2. GTAW process with an optional optical probe to collect specular reflections of the weld pool's surface [4].

Gas tungsten arc welding is a method of welding in which the heat required for the melting of the base metal is supplied by an electric arc formed between a tungsten electrode and the base metal itself. This arc length can be measured in two different ways, the electrical and physical arc length. The electric arc extends from the workpiece upward to a point somewhat above the physical tip of the electrode. The distance above the tip is a

function of current, tip angle, arc voltage, and other factors. The physical arc length is defined as the electrode tip to workpiece distance. This distance is determined by direct measurement of the distance between the actual tip of the electrode and the original un-melted workpiece surface. The extremely high melting point of the tungsten allows the formation of the arc without causing the electrode to melt. The fact that the tungsten remains stable during the course of the welding operation results in the classification of GTAW as a non-consumable electrode process.

The high temperatures involved in the process, both at the electrode and in the weld pool, will result in almost instant oxidation if the process is not shielded from the atmosphere. For this purpose a shielding gas is conducted along the electrode to shield the pool from the atmosphere. This shielding gas surrounds the electrode and weld pool. The shielding gas is fed into the gas nozzle at a preset flow rate. The gas flow rate is typically in the range of 160cm<sup>3</sup>/s to 470cm<sup>3</sup>/s (20cfh to 60cfh) and maintained constant throughout the welding pass. The gas is usually argon or helium. Also to prevent overheating of the welding torch, coolant water is circulated in the torch as seen in Figure 3. The broad arc configuration of GTAW, and its much lower rate of energy input to the workpiece, results in a wide, high-volume melt and a more extensive heat-affected zone. These conditions can easily become a source of distortion, cracking, porosity, and stresses [4].

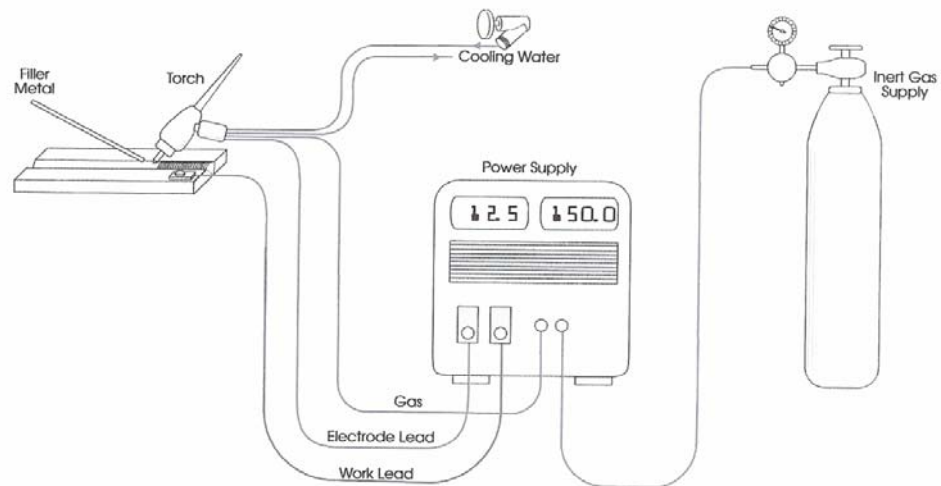


Figure 3. The GTAW circuit [4].

The torch holding the tungsten electrode is connected to a shielding gas cylinder as well as one terminal of the power source. The tungsten electrode is usually in contact with a water-cooled copper tube, called the contact tube, which is connected to the welding cable (cable 1) from the terminal. This allows both the welding current from the power source to enter the electrode and the electrode to be cooled to prevent overheating. The workpiece is connected to the other terminal of the power source through a different cable (cable 2). The shielding gas goes through the torch body and is directed by a nozzle toward the weld pool to protect it from the air. This process is illustrated in Figure 4. Protection from the air is much better in GTAW than in SMAW because an inert gas such as argon or helium is usually used as the shielding gas and because the shielding gas is directed toward the weld pool. For this reason, GTAW is also called Tungsten Inert Gas (TIG) welding. However, in special occasions a non inert gas can be added in a small quantity to the shielding gas. Therefore, GTAW seems a more appropriate name for this welding process. When a filler rod is needed, for instance, for joining thicker materials, it can be fed either manually or automatically into the arc.

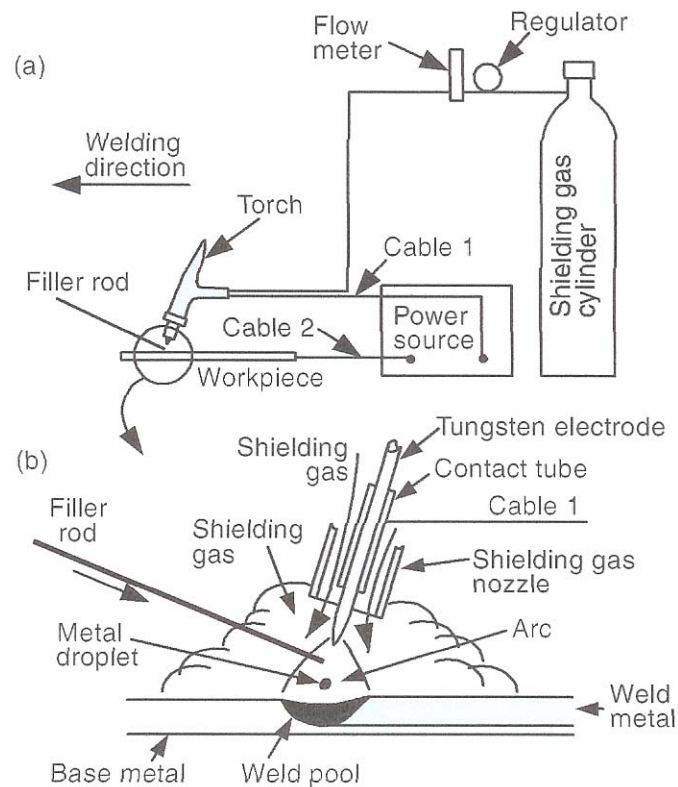


Figure 4. Gas tungsten arc welding: (a) overall process (b) welding area enlarged.

### ***Advantages And Disadvantages of Gas Tungsten Arc Welding***

Gas tungsten arc welding is suitable for joining thin sections because of its limited heat inputs. The feeding rate of the filler metal is somewhat independent of the welding current, thus allowing a variation in the relative amount of the fusion of the base metal and the fusion of the filler metal. Therefore, the control of dilution and energy input to the weld can be achieved without changing the size of the weld. It can also be used to weld butt joints of thin sheets by fusion alone, that is, without the addition of filler metals or autogenous welding. Since the GTAW process is a very clean welding process, it can be used to weld reactive metals, such as titanium and zirconium, aluminum, and magnesium. However, the deposition rate in GTAW is low. Excessive welding currents can cause melting of the tungsten electrode and results in brittle tungsten inclusions in the weld metal. However, by using preheated filler metals, the deposition rate can be improved. In the hot-wire GTAW process, the wire is fed into and in contact with the weld pool so that resistance heating can be obtained by passing an electric current through the wire. The arc welding process constitute an important segment of welding in manufacturing. The terminology and concepts of the Gas Tungsten Arc Welding process are as follows.

### ***Power Source***

Commercial arc welding power supplies are typically classified to operate in one of two modes: constant current (CC) or constant voltage (CV). The CC type power supply can operate using direct and alternating polarity, alternating current (AC) or direct current (dc). It is commonly used for the shielded metal arc welding process, gas tungsten arc welding process, and the plasma arc welding process. The constant voltage power source is typically preferred for continuous wire processes such as submerged arc welding, gas metal arc welding, and flux-cored arc welding. While commercial power supplies are generally classified as CC or CV machines, in many cases they exhibit a "drooping" volt-ampere characteristic, and in the case of CV machines sometimes are designed to exhibit a "rising" volt-ampere characteristic. Furthermore, many modern machines are designed to operate at a continuously variable volt-ampere characteristic, such that the machine setting can be optimized for the specific application. It is noted that for some applications a constant power characteristic, which remains a variable depending on the

application, is desired. The electrical power source usually provides controlled current, which is typically selected in the range of 50 to 500 Amperes. This current may be pulsed or constant. Further information can be obtained from Hartman's or Anderson's dissertation [4 and 2].

The power source is a fundamental component of all arc welding processes. The power source of the process can be either direct current (dc) or alternating current (ac) depending on the specific application. Alternating current (AC) is preferred for welding thin to moderately thick pieces of aluminum, magnesium, and some grades of stainless steel. In this case, dc is used on steel. Direct current with negative electrode (DCEN), also known as straight polarity, will provide more penetration and faster welding speed, especially with helium shielding gas. DCEN produces the maximum heat in the metal and the minimum heat in the electrode. To achieve deeper penetration when welding DCEN use smaller electrodes. On the other hand, direct current with the electrode positive (DCEP), also known as reverse polarity, is rarely used because of the problem of overheating the tungsten electrode, since DCEP generates the largest amount of heat in the electrode rather than in the base metal. Either polarity may be used when welding dc. However, the choice of polarity has a significant impact on the resulting weld. The GTAW electrode polarity can be seen in Figures 5 and 6 [7]. And the polarities, DCEN, and DCEP will be described further.

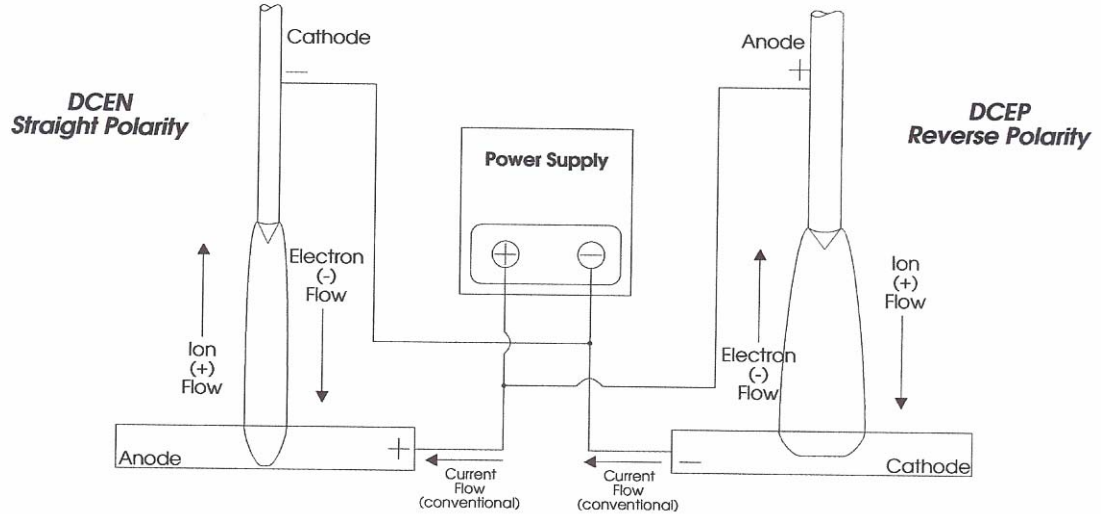


Figure 5. GTAW Electrode Polarity[4].

### **Direct-Current Electrode Negative (DCEN)**

Direct-current electrode negative, also called straight polarity, is the most common polarity in GTAW. The electrode is connected to the negative terminal of the power supply. As shown in Figure 6a, electrons are emitted from the tungsten electrode and accelerated while traveling through the arc. A significant amount of energy, called the work function, is required for an electron to be emitted from the electrode. When the electron enters the workpiece, an amount of energy equivalent to the work function is released. This is why in GTAW with DCEN more power (about two-thirds) is located at the work end of the arc and less (about one-third) at the electrode end. Consequently, a relatively narrow and deep weld is produced.

### **Direct-Current Electrode Positive (DCEP)**

Direct-current electrode positive is also called reverse polarity. The electrode is connected to the positive terminal of the power source. As shown in Figure 6b, the heating effect of electrons is now at the tungsten electrode rather than at the workpiece. Consequently, a shallow weld is produced. Furthermore, a large-diameter, water-cooled

electrodes must be used in order to prevent the electrode tip from melting. The positive ions of the shielding gas bombard the workpiece knocking off oxide films and producing a clean weld surface. Therefore, DCEP can be used for welding thin sheets of strong oxide-forming materials such as aluminum and magnesium, where deep penetration is not required.

### ***The Electrode***

Common to all arc welding processes is the electrode. The gas tungsten arc welding (GTAW) process, sometimes called tungsten inert gas (TIG) process, uses a non-consumable electrode from which an electrical arc is extended onto the welded metal workpiece. The arc causes localized heating of the workpiece metal and filler material resulting in localized melting of the metals. The arc is sustained between the electrode and the workpiece, which are separated by a small distance, usually in the 1.3 mm (0.050 in.) to 7.6 mm (0.300 in.) range. The intense heat developed by the arc melts the surface of the base metal to form a molten pool. Resolidification occurs when the heat source is removed.

Electrode material, diameter, grind angle, and tip diameter (flat) vary according to each welding application. Tables and guides are available identifying amperage ratings for a variety of grind angles and tip diameters. Where available, the welding equipment manufacturer's recommendations should be used as a starting point. In the absence of that, the information below offers some general rules of thumb to follow and may be modified according to the specific application. The choice of electrode material and geometry will always be a compromise affecting the following: shorter vs. longer electrode life, easier vs. more difficult arc starting, deeper vs. shallower weld penetration, wider vs. narrower arc and weld shape.

Welding should follow an equipment supplier's suggested procedures and dimensions first, because they have usually performed a lot of qualifying and troubleshooting work to optimize electrode preparation for their equipment. However, where these specifications do not exist or the welder or engineer would like to change those settings to possibly improve and optimize their welding, the following guidelines apply:

### ***Electrode material***

The electrode is made of tungsten (wolfram), typically compounded with a small amount (2-5%) of Thorium, measuring 2.4mm, (3/32in) in diameter, for increased electron emission efficiency. Tips were ground with a diamond wheel to maintain an included angle of 60°. Tungsten has characteristics of high melting point, low electrical resistance, and good heat conductivity. Pure tungsten has the disadvantage that in the cathode spot mode the tip of the electrode melts and becomes spherical causing the cathode spot, and hence the arc column to wander. The addition of thorium and zirconium lower the work function thus enabling greater current density of electron emissions at lower temperatures. Tungsten electrodes with 2% cerium or thorium have better electron emissivity, current-carrying capacity, and resistance to contamination than pure tungsten electrodes. As a result, arc starting is easier and the arc is more stable. The electron emissivity refers to the ability of the electrode tip to emit electrons. A lower electron emissivity implies a higher electrode tip temperature required to emit electrons and hence a greater risk of melting the tip.

For quite some time, tungsten manufacturers have added an oxide to pure tungsten to improve the arc starting characteristics and the longevity of pure tungsten electrodes. Table 1 shows four common tungsten electrodes along with their tip color. Table 2 lists the major commercially sold tungsten types, their American Welding Society (AWS) and International Standards Organization (ISO) classifications, and the amount and type of oxide contained in the electrode. The amount and type of oxide contained in the electrode and their uses are described in more detail below.



Table 1: Commonly Available Tungsten Electrodes

AWS Classification	Type	Tip Color
EWP	Pure Tungsten	Green
EWTh1	1% Thorium added	Yellow
EWTh2	2% Thorium added	Red
EW Zr	1/2% Zirconium added	Brown

Table 2: Commercially sold tungsten types, their American Welding Society (AWS) and International Standards Organization (ISO) classifications, and the amount and type of oxide contained in the electrode.

Material	AWS C	ISO C	Oxide Content
<b>2% Thoriated</b>	EWTh	WT	1.7-2.2% ThO <sub>2</sub>
<b>2% Ceriated</b>	EWTh	WC	1.8-2.2% CeO <sub>2</sub>
<b>1½% Lanthanated</b>	EWLa-	N/	1.3-1.7% La <sub>2</sub> O <sub>3</sub>
<b>1% Lanthanated</b>	EWLa	WL	0.8-1.2% La <sub>2</sub> O <sub>3</sub>
<b>Zirconiated</b>	EWZr	WZ	0.15-0.40% ZrO <sub>2</sub>
<b>Pure Tungsten</b>	EWP	W	None

### 2% Thoriated Tungsten

This is the most commonly used tungsten material because it was the first to display a significant improvement over pure tungsten. This is a good general use tungsten for DC applications, because it has a low work function and operates well even when overloaded with extra amperage. While many companies still use this material because it is specified as part of a qualified weld program, there is a definite migration to other tungsten types, namely 2% Ceriated and 1½% Lanthanated, due to their superior performance in most applications and the fact that they are non-radioactive. The thoria contained in 2% Thoriated tungsten is slightly radioactive and many welders

and safety officers are leading the move away from this material. The American Welding Society state the following on this issue [7]:

“Thoria is a low-level radioactive material. However, if welding is to be performed in confined spaces for prolonged periods of time or if electrode grinding dust might be ingested, special precautions relative to ventilation should be considered. The user should consult appropriate safety personnel. ... during the grinding of electrode tips there is generation of radioactive dust, with the risk of internal exposure. Consequentially, it is necessary to use local exhaust ventilation to control the dust at the source, complemented if necessary by respiratory protective equipment.”

### **2% Ceriated Tungsten**

This non-radioactive alternative to 2% Thoriated Tungsten is best when used primarily in DC welding at low currents. It has excellent arc starting capabilities at low currents and therefore it has become the standard for many orbital tube and pipe welding equipment manufacturers. In addition, it is often used in other low amperage applications where small or delicate parts are being welded. It would not be good for higher amperage applications, because the oxides migrate very quickly to the heat at the tip under these conditions and the oxide content and benefits are then removed.

### **1½% Lanthanated Tungsten**

This has been a very popular new material internationally and has recently been introduced in the United States. The 1½% content (as opposed to 2%) was chosen by two of the largest manufacturers as the optimum content amount based on scientific studies which showed that this content amount most closely mirrors the conductivity characteristics of 2% Thoriated Tungsten. Therefore, welders can usually easily replace their radioactive 2% Thoriated material with this tungsten and not have to make any welding program changes. It makes the switch quick and easy. In addition, one major manufacturer had an independent study performed on this material and it was presented at the 1998 American Welding Society Exhibition in Detroit, Michigan. In summary, 2% Thoriated, 2% Ceriated and two manufacturer's ½% Lanthanated were compared by observing tip erosion after 300

DC arc strikes at both 70 amps and 150 amps. In both cases, the 1½% Lanthanated tungsten showed the least amount of tip erosion. This material is also suitable for AC welding. Therefore, for optimizing the welding process, this is an excellent material to consider.

### **Zirconiated**

This material is used primarily for AC welding. The AWS states [7], "This electrode performs well when used with alternating current as it retains a balled end during welding and has a high resistance to contamination." This electrode has reduced in importance as other alternatives have become available. The recommendation is to try 1½% Lanthanated tungsten for your AC welding. Zirconiated tungsten has very poor performance in DC welding.

### **Pure Tungsten**

Like Zirconiated Tungsten, this tungsten is also only used for AC welding and there are better alternatives available. Try 1½% Lanthanated instead of this material. Different electrode materials offer various advantages in arc starting and electrode life. The following are the most commonly used electrode materials: 2% Cerium, 2% Thorium, Pure Tungsten, 1½% Lanthanum.

### ***Electrode Diameter***

The welding equipment supplier's recommendations and the American Welding Society recommendations are the best place to start with this variable. Keep in mind that as you increase the diameter of the electrode you are able to handle more amperage. For a given amperage, larger diameter electrodes are more difficult to start than smaller ones, but they will probably erode less rapidly. If you use too large an electrode for your amperage level, you are likely to experience arc instability. The electrode in Figure 6 shows the diameter, tip diameter, and included angle.

*General Formula:*                  Diameter x 1,500 = Average amperage for acceptable electrode life

(20-30 degree angle)

*Example:* .040" diameter x 1,500 = 60 amps maximum

*Rule of Thumb:* For a given amperage, larger diameters offer longer electrode life but may be more difficult to arc start at low amperages.

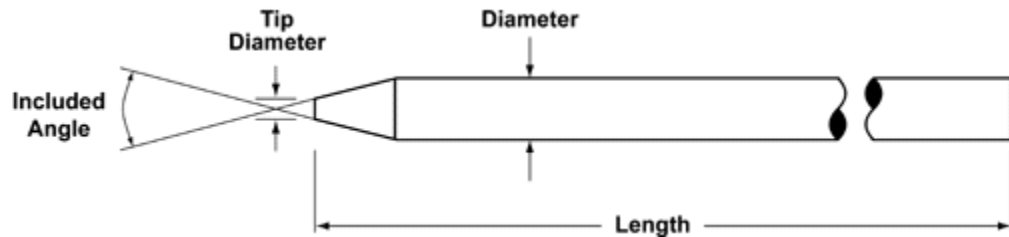


Figure 6. Diagram of the electrode showing diameter, tip diameter, and included angle.

### ***Grind Angle***

The tips of the electrode are ground to a specified included angle, the total angle across the electrode diameter, anywhere from 10 to 90 degrees. Generally the smaller tip angles are used in applications requiring low current and small electrode diameter, and greater angles for higher currents and larger electrode diameters. Sometimes the electrode point is truncated as well, resulting in a small flat area at the electrode tip. The electrode diameter values range typically from 1mm to 3.2mm (approximately 0.040 in. to 0.125 in.). For most materials the electrode potential is negative with respect to the workpiece, straight polarity, while a positive electrode, reverse polarity, is occasionally used as well. In this case an arc cleaning action is produced at the welded surface during the half cycle when the electrode is positive, resulting in substantial cleaning of contaminants on the workpiece.

### ***Electrode Tip Diameter***

Electrode Tip Diameter - Grinding an electrode to a point is sometimes desirable for certain applications, especially where arc starting is difficult or short duration welds on small parts are performed. However in most cases

it is best for a welder to leave a flat spot or tip diameter at the end of electrode. This reduces erosion at the thin part of a point and reduces the concern that the tip may fall into the weld. Larger and smaller tip diameters offer the following trade-offs as seen in Table 3:

Table 3. Advantages and disadvantages of electrode tip diameters

<b>Smaller Tip</b>	<b>Larger Tip</b>
Easier arc starting	Usually harder to start the arc
Potential for more arc wander	Good arc stability
Less weld penetration	More weld penetration
Shorter electrode life	More electrode life

***Flat/Tip Diameter***

*General Formula:* Amperage/4,000 = "Rule of Thumb" Flat Diameter

*Example:* 120 amps/4,000 = .030" "Rule of Thumb" Flat Diameter

*Rule of Thumb:* Use above calculation as a starting point for tip flat dimensions.

As with electrode angle/taper, smaller tip diameter (sharper electrode) offer better arc starting and a more stable arc at low amperages. Larger tip diameters offer longer electrode life.

### *Angle/Taper*

Electrode Taper - This is usually called out in degrees of included angle (usually anywhere between 14 degrees and 60 degrees). Below is a summary, Table 4, which illustrates how different tapers offer different arc shapes and features:

Table 4. Advantages and disadvantages of electrode tapers

<b>Sharper Electrodes</b>	<b>Blunter Electrodes</b>
Easy arc starting	Usually harder to start the arc
Handle less amperage	Handle more amperage
Wider arc shape	Narrower arc shape
Good arc stability	Potential for more arc wander
Less weld penetration	Better weld penetration
Shorter electrode life	Longer electrode life

Thus, sharper electrodes have less arc wander at lower amperages, more consistent arc starting, and a wider arc. Blunt electrodes can handle higher amperage levels and provide better weld penetration. Blunt electrodes last longer than sharper electrodes. As a rule of thumb, use 20-30 angles for up to 90 amps, average. Higher currents can use larger included angles. In AC welding, the electrode is typically balled up and used so there is no tip geometry to prepare. Therefore, this section is dedicated to DC welding.

To demonstrate graphically how the taper selection will effect the size of the weld bead and the amount of penetration, below is a drawing, Figure 7, that shows typical representations of the arc shape and resultant fusion

zone profile for different tapers. The fusion zone profile also depends on the electrode tip diameter (flat), arc gap, material to be welded, and the shielding gas used.

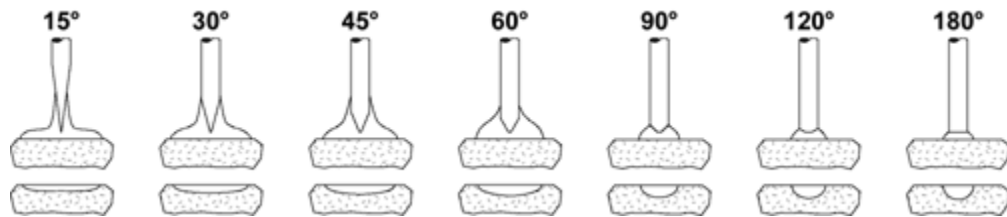


Figure 7. Arc shape and fusion zone profile as a function of electrode included angle.

### ***Joint Types And Positions***

Illustrated in Figure 8, the American Welding Society has defined four basic welding positions, the flat position, the horizontal position, the vertical position, and the overhead position [4]. They also defined five basic joint types. The intersection of the joined pieces is referred to as the welding joint. The joint type used for a given application, such as a corner joint, butt joint, etc, is primarily established by the geometry of the welded structure. Once a suitable joint has been selected, the appropriate weld type is determined. Most of these weld types require special preparation of the joint to accommodate the molten weld pool and the filler metal, if any is used. This preparation is commonly carried out by forming a groove in the joint. During welding the molten metal of the pool fuses into the bottom and sidewalls of the groove, providing a firm cohesion to the joined pieces. Joint. This research will focus strictly on autogenous welds on bead-on-plate welds performed in the flat position.

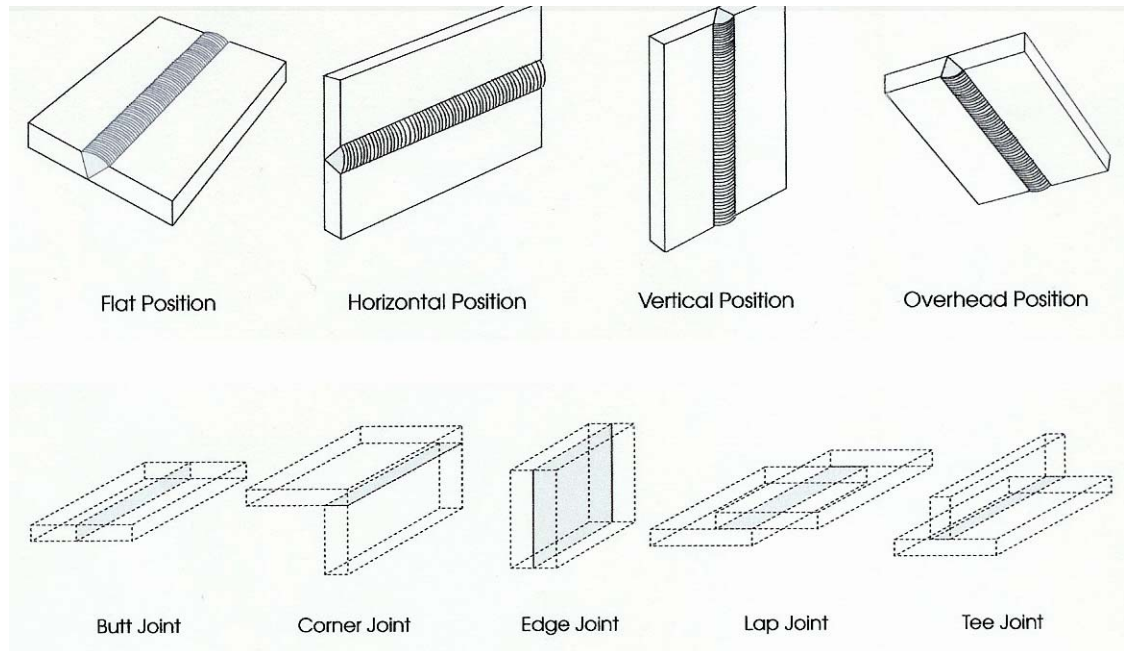


Figure 8. Welding positions and primary joints [4].

### ***Geometry Of Weld Bead***

The primary geometric features of the weld were illustrated in Figure 1. The geometry of the weld bead is of great interest to the welding engineer. The bead width, and thus the extent of the pool fusion into the joint sidewalls, is important from the standpoint of mechanical strength of the bonding formed by the weld. The penetration of the weld pool into the workpiece is important as well. In some cases full penetration is desired, where the pool bottom actually reaches the bottom side of the workpiece. To keep the molten metal from running away and leaving a gap at the joint, non-melting backing metal plates are frequently attached to the bottom side of the joint. In this case, it is desirable to maintain the heat input at a level sufficient to melt the bottom of the work piece, without penetrating into the backing plate. Partial penetration is usually employed in multiple –pass welding, where the welding groove is incrementally filled up with feed metal in a number of passes along the groove. The first pass is usually welded with full penetration and then the subsequent passes are superimposed with partial penetration on previous passes, until the entire groove has been filled. The total cross sectional area of the bead is of significance when the cross sectioned joint is examine. This area is an approximate indicator of the amount of metal deposited



into the groove for a given unit distance. Frequently, the strength of the welded joint is ensured by additional welding passes and filler metal deposition up to a fixed level above the workpiece top surface. The height of this addition is referred to as the reinforcement height.

Bead width, penetration, and cross sectional area are primarily governed by the net arc power (arc voltage multiplied by arc current, less power losses), torch travel speed, wire diameter and feed rate, and the workpiece metal type. Other parameters affect the dimensions of the weld bead to a lesser extent. The reinforcement height is, of course, primarily a function of the wire deposition rate during the reinforcement pass.

### ***Weld Pool Shape***

Weld pool geometry is primarily determined by two factors, the thermal conditions in and near the weld pool and the nature of the fluid flow. The volume of the weld pool is controlled to a large extent by the welding parameters. The arc current, arc voltage, and travel speed are the dominant parameters affecting the weld pool's volume. In general, the volume is directly proportional to the arc current and inversely proportional to the travel speed. In addition to affecting its volume, the speed of the moving heat source has a large influence on the overall shape of the weld pool. The effect that the speed of a moving heat source has on the topside bead shape is illustrated in Figure 9. The weld pool shape is circular at lower speeds and tends to become more elongated with increasing welding speed until the weld finally takes on a tear drop shape at fast welding speeds. Changes in the weld pool shape as the welding speed increases also changes the isotherms, and hence influences the fusion zone grain growth. The weld-metal grain structure, the grain size and the microstructure in the fusion zone and the surrounding base metal, of the completed weld contributes significantly to the mechanical properties of the weld, in general, and the joint integrity, in particular. Furthermore, the final weld-metal grain structure influences the existence and distribution of welding flaws, such as porosity, hydrogen-induced cold cracking, hot cracking, etc. In general, the average grain growth direction during solidification of a weld pool is approximately normal to the solid/liquid interface. For slow travel speeds in which the weld pool is elliptically or near-spherically shaped, the direction of the maximum temperature gradient is constantly changing from approximately 90 degrees to the weld interface at position A to nearly parallel to the weld centerline at position B1 (see Figure 9). Any given grain which is initially

unfavorably oriented will become more favorably oriented because the direction of the gradient changes. Those grains that are not completely eliminated continue to grow towards the centerline, thus resulting in a finer fusion zone grain structure. This process, known as “competitive growth”, eliminates or crowds out less favorably oriented grains with grains of more favorable orientation [4].

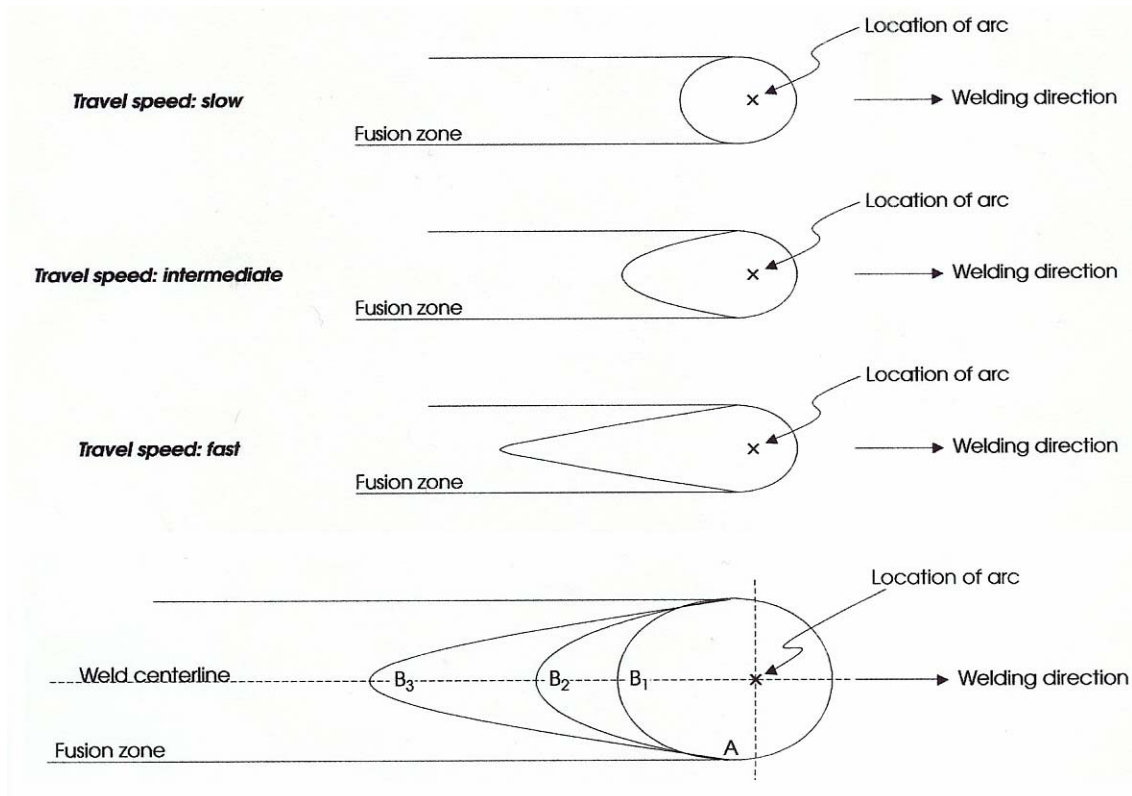


Figure 9. Comparison of weld pool shapes under different travel speeds and the average grain growth direction under different heat source travel speeds [4].

As the weld travel speed increases, the direction of the maximum thermal gradient becomes more invariant with respect to slower travel speeds. The elongated weld pool causes the temperature gradient at positions B2, for intermediate travel speeds, and B3, for fast travel speeds, to be no longer strongly directed toward the electrode. Consequently, the grain growth is highly columnar with very little change in direction. Figure 10 illustrates the results of fusion zone grain growth under different heat source travel speeds. Although the beyond the scope of this document, the solidification behavior in the fusion zone is a critical component to an overall weld quality

monitoring and control system. The fusion zone is the area of base metal melted as determined on the cross section of the weld. Further information on this topic can be found in [4].

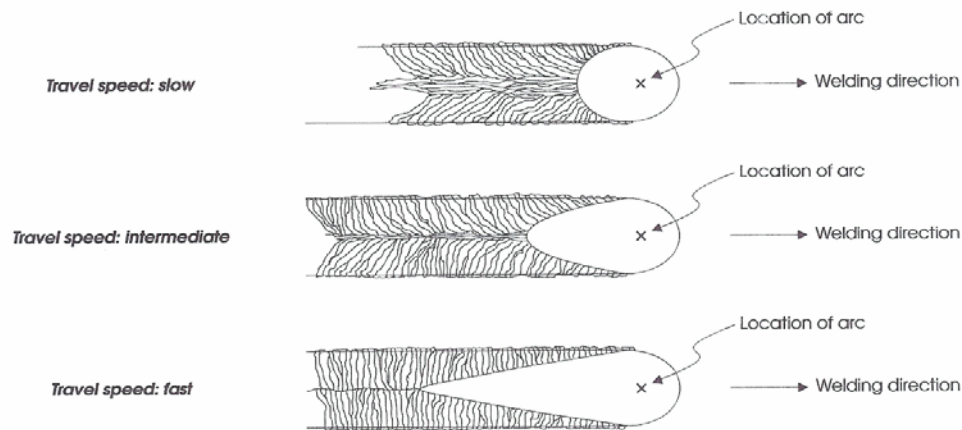


Figure 10. Comparison of weld pool shapes and grain growth under different travel speeds [4].

The motion in the weld pool is caused primarily by Lorentz forces and the arc plasma forces on the surface of the weld pool. The intensity of the motion increases both with the square of the arc current and with the melting point of the base material. Materials with high melting points such as iron, titanium, nickel, mild steel, stainless steel, and cobalt displayed very rapid motion causing more erratic changes in the flow pattern. The intensity of the molten metal fluid motion, indicative of higher melting point temperatures, is related to the degree of constriction of the anode spot. A higher melting point material favors a higher current density thus facilitating greater electromagnetic (EM) forces. Base metal materials with lower melting points, like aluminum, copper, and silver, displayed slower more regular fluid motion. This tendency to move more slowly and regularly is obviously more desirable in a welding control scenario since it affects the heat transfer and the depth of penetration. The five different classifications of penetration are illustrated in Figure 11.

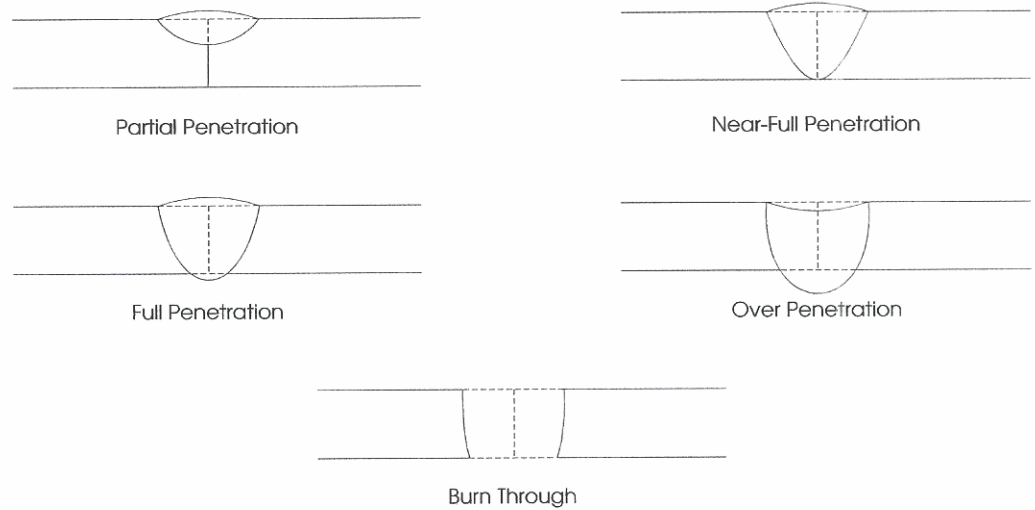


Figure 11. The different classifications of penetration [3].

The heat sources for the gas, arc, and high-energy beam welding processes are a gas flame, an electric arc, and a high-energy beam, respectively. The power density increases from a gas flame to an electric arc and a high-energy beam. As shown in Figure 12, as the power density of the heat source increases, the heat input to the workpiece that is required for welding decreases. The portion of the workpiece material exposed to a gas flame heats up so slowly that, before any melting occurs, a large amount of heat is already conducted away into the bulk of the workpiece. Excessive heating can cause damage to the workpiece, including weakening and distortion. On the contrary, the same material exposed to a sharply focused electron or laser beam can melt or even vaporize to form a deep keyhole instantaneously, and before much heat is conducted away into the bulk of the workpiece, welding is completed (1). Therefore, the advantages of increasing the power density of the heat source are deeper weld penetration, higher welding speeds, and better weld quality with less damage to the workpiece, as indicated in Figure 12.

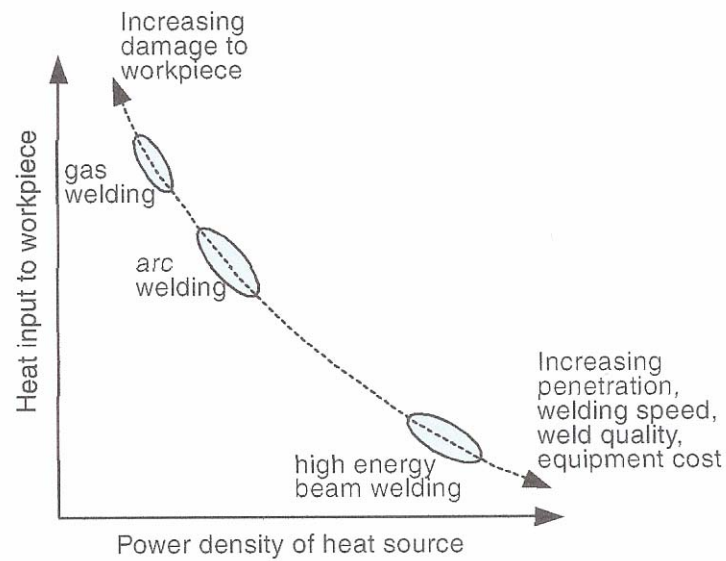


Figure 12. Variation of heat input to the workpiece with power density of the heat source.

### ***Shielding Gas***

Various gases are used for arc shielding. These can be inert gases, such as helium and argon, or they can be mixtures of these and other gases. Inert gases will not combine chemically with other elements. The other inert gases are neon, krypton, xenon, and radon, but they are too rare and expensive. The arc zone is filled with an inert gas to protect the tungsten electrode and molten material from oxidation and to provide a conducting path for the arc current. The inert shielding gas flows from the nozzle of the torch down and across the molten region of the weldment metal. Shielding gas is used to displace the air preventing oxygen and nitrogen from coming into contact with the molten metal and the hot tungsten electrode. Shielding gasses used are argon, helium or small percentages mixed with Argon. Shielding gas is normally chosen according to the material type to be welded and the type of metal transfer required. It is necessary to consult a welding procedure schedule for the particular material to be joined [13].

## **Argon**

Argon, in its pure form, is the most widely used as a shielding gas for Gas Tungsten Arc Welding (GTAW). A million cubic feet of air contains 93,000 cubic feet of argon [13]. Thus, this inert gas is relatively plentiful. Its mild thermal conductivity produces a narrow, constricted arc column which allows greater variations in arc length with minimal influence on arc power and weld bead shape. This characteristic makes it the preferred choice for manual welding. In addition, argon provides good arc starting due to its low ionization potential. This property allows argon to carry electric current well when compared to other shielding gases. For AC welding applications, argon is preferred over helium because of its superior cleaning action, arc stability, and weld appearance. When welding thicker aluminum alloys, greater than ¼ inch, argon is mixed with helium to enhance the thermal conductivity of the shielding gas [13].

While pure argon may be used for mechanized applications, depending on the base material, thickness and composition, argon-helium or argon-hydrogen blends promote higher welding travel speeds. The hotter arc characteristics of argon-helium blends also make them more suitable for welding metals with high thermal conductivity, such as copper [13].

## **Helium**

Helium, also an inert gas, has high thermal conductivity and high ionization potential, which produces higher arc voltages when compared to argon for a given current setting and arc length. Because of this, arcs in an atmosphere of helium produce a larger amount of heat. The increased heat input affects depth of penetration and its wider, less constricted arc column increases weld bead width. Helium is used in mixtures with argon and with active gases. Because of its light weight, helium tends to float away from the arc zone. Thus, higher flow rates are necessary [13].

The use of helium is generally favored over argon at the higher current levels which are used for the welding of the thicker materials, especially those having high thermal conductivity or relatively high melting

temperatures. It is often used for high-speed mechanized applications [13].

Although argon is widely used for AC welding of aluminum, pure helium has been successfully used for DCEN mechanized welding of this material. It produces greater penetration at higher travel speeds. However, surface oxides must be cleaned from the weld joint to obtain acceptable results, since the cleaning action of the AC arc is not present. Argon-helium mixtures are widely used with AC current when welding with aluminum alloys [13].

The physical properties of helium definitely offer advantages in some applications. However, due to its high ionization potential, it also produces a less stable arc and a less desirable arc starting characteristic than argon. Its higher cost and higher flow rates are also factors to be considered. In some cases, an argon mixture is used for igniting the arc and pure helium is used for welding. This technique is used for DC GTAW welding of heavy aluminum [13].

Argon is heavier than helium and slightly heavier than air thus providing better arc shielding while using lower flow rates. Since helium is much lighter than air it tends to float away from the weld zone. Argon is usually better for arc starting and operates at lower arc voltages than helium. When using helium, higher flow rates are required. Unlike argon, helium provides for a higher arc voltage which in turn generates more heat from the arc. For certain applications, small amounts of hydrogen, oxygen, or nitrogen may be added to the shielding gas in an effort to obtain more stable arc characteristics or higher arc voltages, and hence higher arc temperatures [13].

Both argon and helium can be used. Table 5 lists the properties of some shielding gases. As shown, the ionization potentials for argon and helium are 15.7 and 24.5 eV (electron volts), respectively. Since it is easier to ionize argon than helium, arc initiation is easier and the voltage drop across the arc is lower with argon. Also, since argon is heavier than helium, it offers more effective shielding and greater resistance to cross draft than helium. With DCEP or AC, argon also has a greater oxide cleaning action than helium. These advantages plus the lower cost of argon make it more attractive for GTAW than helium [13].

Because of the greater voltage drop across a helium arc than an argon arc, however, higher power inputs and greater sensitivity to variations in the arc length can be obtained with helium. The former allows the welding of thicker sections and the use of higher welding speeds. The latter, on the other hand, allows a better control of the arc length during automatic GTAW [13].

Table 5. Properties of shielding gases used for welding [13]

Gas	Chemical Symbol	Molecular Weight (g/mol)	Specific Gravity with Respect to Air at 1 atm and 0°C	Density (g/L)	Ionization Potential (eV)
Argon	Ar	39.95	1.38	1.784	15.7
Carbon dioxide	CO <sub>2</sub>	44.01	1.53	1.978	14.4
Helium	He	4.00	0.1368	0.178	24.5
Hydrogen	H <sub>2</sub>	2.016	0.0695	0.090	13.5
Nitrogen	N <sub>2</sub>	28.01	0.967	1.25	14.5
Oxygen	O <sub>2</sub>	32.00	1.105	1.43	13.2

### Argon-Helium Mixtures

Each of these gases (argon and helium), as explained above, has specific advantages. Argon-helium blends are basically used to increase the heat input to the base metal while maintaining the favorable characteristics of argon, such as arc stability and superior arc starting. This gas mixture is used for gas tungsten arc welding of nonferrous materials. The addition of helium is in percentages of 50% or 75%. This raises the arc voltage and increases the heat in the arc. It is used for DC welding when it is desirable to obtain higher heat input while maintaining the good arc starting behavior of argon. This blend is used primarily for high-speed mechanized and manual welding of nonferrous material (aluminum and copper) under 3/4 inch thick. It is used for welding heavier sections of aluminum, magnesium, and copper. The speed and quality of AC welding on aluminum can be improved with this blend. It is sometimes used for manual welding of aluminum pipe and mechanized welding of butt joints in aluminum sheet and plate [13].



### **Argon-Hydrogen Mixtures**

Hydrogen is often added to argon to enhance the thermal properties of argon. It increases the arc voltage and the heat in the arc. Its reducing effect improves the weld surface due to the reduced surface oxidation. The higher arc voltage associated with hydrogen increases the difficulty of starting the arc. For this reason, the lowest amount of hydrogen consistent with the desired result is recommended. Additions up to 5% for manual welding and up to 10% for mechanized welding are typical. This gas mixture should not be used for welding mild or low-alloy steels. Argon-hydrogen blends are primarily used on austenitic stainless steel (300 series), nickel, and nickel alloys. Hydrogen enhanced mixtures are not recommended to weld carbon or low-alloy steel, or any of the copper, aluminum, or titanium alloys since cracking or porosity will occur due to the absorption of hydrogen. Argon-hydrogen blends utilized as a purge gas are successfully applied to improve root appearance when TIG welding 300 series stainless pipe [13].

Normally, the shielding gases applied with this process are either argon or helium, inert gases. It's widely known that the shielding gas and also the arc current affect the arc voltage measured between the workpiece and the tungsten electrode. For the automatic welding process, the arc length is commonly a controlled variable which is indirectly controlled by controlling the arc voltage with a servo called the automatic voltage control [4].

### ***Multi Input Output System***

The gas tungsten arc welding process is, in general, a nonlinear multiple-input, multiple-output system, Figure 13 [8]. The arc welding process can be seen as a system transforming a number of input parameters to a corresponding set of output parameters. The input parameters are the controllable welding equipment parameters, welded materials, and other parameters, which affect the properties of the finished welds. Pre-selected weld parameters, indirect weld parameters, and other uncontrollable factors affect the weld quality of the gas tungsten arc weld. Pre-selected weld parameters are selected prior to the start of the welding process and they cannot be changed during the welding process. These parameters, variables, include the electrode type, size, and tip geometry, the torch nozzle size, and the shielding gas type. The indirect weld parameters of the welding process include the arc voltage, arc current, travel speed, shielding gas, and wire feed rate (for filler metal process). Indirect weld parameters are

parameters that can be modified in process. The other uncontrollable factors that can affect weld quality include clamping, heat sinks such as tack welds, heat buildup, backing, and impurities that might be found within the material, electrode, or shielding gas. These welding parameters are sometimes referred to as primary variables, or inputs to the welding system. Once the pre-selected variables are properly chosen, the quality of the weld can be controlled through proper selection and modification of the indirect weld parameters. The welding process, in general, has two principal problems. The first problem is that the relationship between the indirect welding parameters and the direct welding parameters are nonlinear in most cases. The second problem is that the variables are highly coupled. Thus, it is desired to determine a set of indirect welding parameters (IWP) that will produce the desired direct welding parameters (DWP). With the correct welding parameters, the process can be controlled without the need of human or computer intervention to change the necessary welding equipment settings [8].

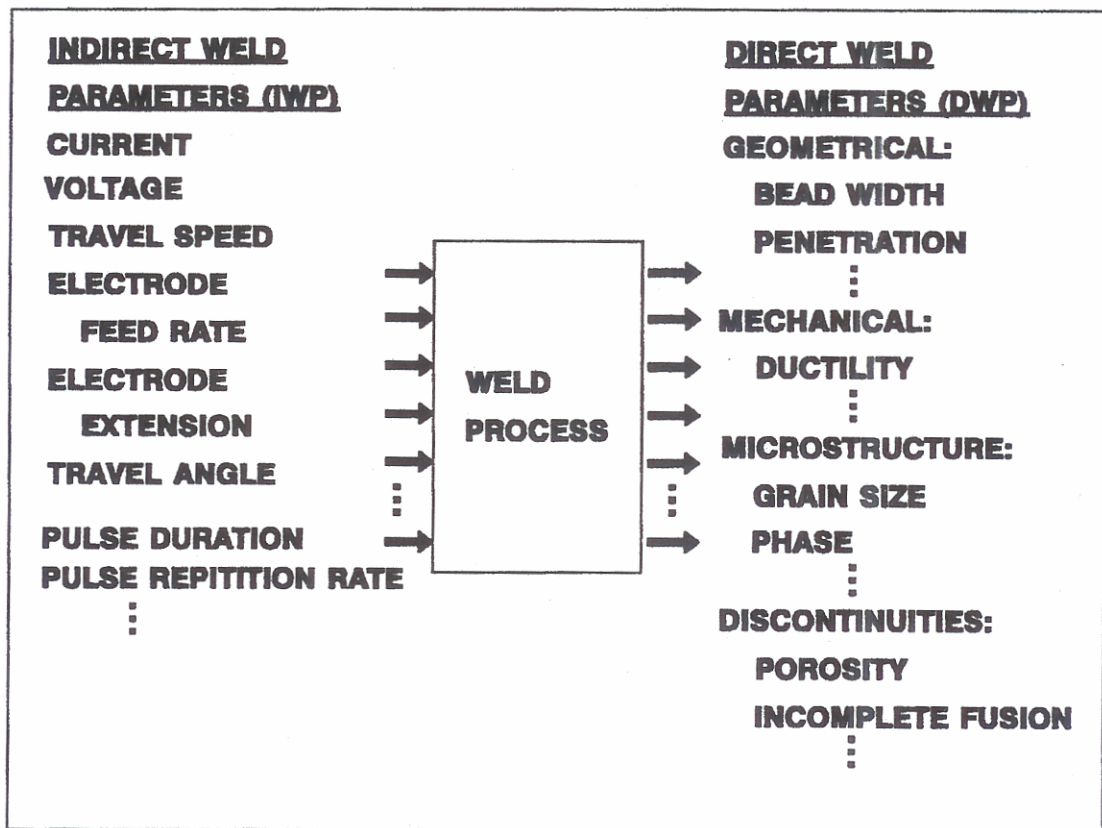


Figure 13. Arc welding depicted as a multiple-input, multiple-output system [8].

### ***Automatic Voltage Control***

In the GTAW process, the arc voltage must be accurately controlled through on-line arc length adjustment, or automatic voltage control (AVC), in order to maintain constant heat input. The welding torch position is controlled indirectly by controlling the arc voltage. At a constant input current, the arc voltage is a function of the electrode-to-workpiece distance. This means, as the electrode-to-workpiece distance ( $L_{arc}$ ) increases, so will the arc voltage ( $V_{arc}$ ). As a means to control the arc voltage, a dc servomotor is used to move the welding torch closer to the workpiece or farther away from the workpiece [5 and 4].

### ***Applications of GTAW and Welding Automation***

GTAW is typically performed manually, but it is sometimes integrated into fully automated or semi-automated systems. A skilled welder can manually change the parameters needed to achieve the desired weld pool. These welding parameters include weld current, voltage, travel speed and electrode orientation. The skilled welder can also make allowances for joint gaps, and other irregularities that could not be handled by precision automated machine welding. The skilled welder acquired the skill and knowledge from hours of practice and education of rule of thumb techniques. Explaining this knowledge to another person is difficult. Thus, fully automated systems offer precise and consistent joint preparation, which requires knowledge of the proper defined parameters for the system. The welding characteristics that are unobservable to humans are also necessary. Control algorithms are used in an attempt to circumvent a machine's lack of human intuition and decision making capabilities. This is done by applying conventional quantitative techniques of system analysis. The use of difference, differential, and integral equations are mainly used to model and control the mechanized aspects of welding. In some cases, such as penetration control or bead geometry, there are too many parameters involved. Thus, this process is impractical [4].

Welding automation is broken down into two basic categories: Semi-automatic and Fully Automatic. In semi-automatic welding, an operator manually loads the part(s) into the welding fixture. A weld controller then controls the torch/part motions and welding parameters to ensure a quality, repeatable weld. After the weld is completed, the operator then removes the completed part and the process begins again.

Fully automatic welding uses a custom machine or series of machines to load the workpiece, index the part or torch into position, effect the weld, monitor quality control, and then unload the finished product. Additional final

product quality checks may also be designed into the machine if necessary. Depending on the details of the specific operation, a machine operator may or may not be necessary

Applications that benefit most from automation have one or all of the following three basic requirements. The first is the quality or the critical function of the welds. The second is the repetitive weld on identical parts. The third is the parts with significant accumulated value prior to welding. Excellent candidates for automation include, but are not limited to precision devices such as batteries, capacitor cans, solenoids, sensors transducers & instrumentation, metal bellows & seals, relay cans & enclosures, light bulb elements, fuel filters, thermos flasks, medical components, nuclear devices, pipe to fittings, transformer cores, valve elements and airbag components. Companies that make limited quantities of products may benefit from a semi-automatic system but might not be candidates for fully automated welding systems

### ***Digital Camera and Lens System***

A general knowledge of cameras and charged coupled devices (CCDs), video signals, lighting techniques, and image processing is needed to develop a PC-based vision system. CCD is a type of solid-state camera. A solid-state camera focuses incoming light onto a light-sensitive, solid-state (semiconductor) sensor. These sensors are typically made up of a rectangular array (imagers) or a single line (line-scan) of equi-spaced, discrete light-sensing elements, called photo-sites. Each photo-site acts as an optoelectric converter because it becomes electrically charged to a level directly proportional to the amount of light that strikes it during a given time period, called the integration time [9].

The vital part of the optical system of a camera consists of a CCD-array. This is the light-sensitive part, or the thin silicon layer, of the camera. Photons reach this layer and break bonds between neighboring silicon atoms. This generates electron-hole pairs. During the exposure time, these photo electrons are collected in potential wells. A well can collect only a limited amount of electrons so the integration time has to be adjusted to prevent overflow. After integration, the charges stored in the image section are read out and measured. This determines the intensity of light. This is done by shifting each row sequentially into a serial register. Here one pixel after another is converted into a digital signal proportional to the charge. This signal can be transmitted and measured. It is

important to protect the storage section from light during the readout process to prevent smearing. Several CCD architectures with different arrangements of image section and storage section have been developed: full frame transfer, interline transfer, and frame transfer. The full frame architecture is the only one that needs an external shutter to prevent further photon collection during readout. The other architectures can shift the charges to a light-protected region before shifting to the serial register. The other architectures can shift the charges to a light-protected region before shifting to the serial register, Figure 14 [9].

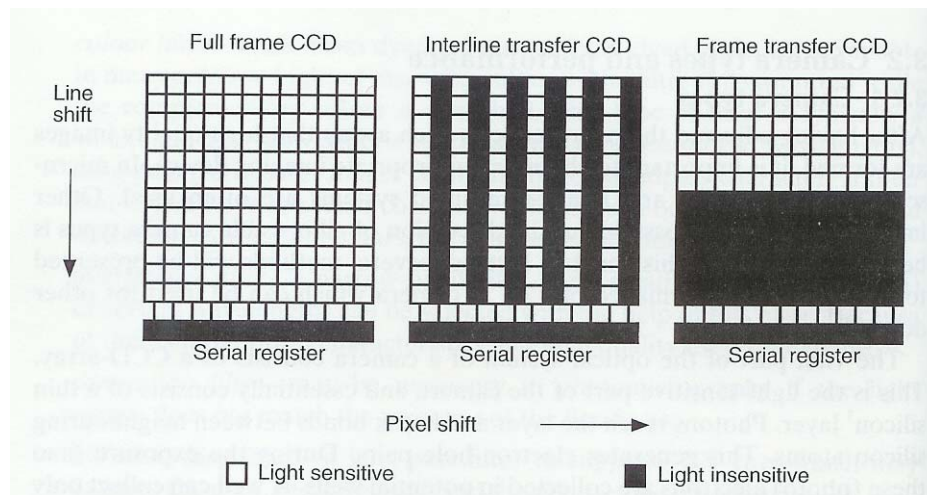


Figure 14. CCD architectures with different arrangements of image section and storage section: full frame transfer, interline transfer, and frame transfer [9].

In a CCD design, the charges that build up on all of the array photo-sites are linked or coupled together so that they can be transferred out of the array directly (digital output) or processed into a time-varying video signal (analog output). The two basic designs for transferring the accumulated charges out of a CCD array are frame-transfer (FT) and interline-transfer (IT), shown in Figure 14. The analog data received by the CCD camera has to be transformed to digital data before it can be processed by a computer. An analog-to-digital converter (ADC) has to be placed between camera and computer. Depending on the camera type different tools are possible. Some cameras have built-in interfaces to the computer while others need a frame grabber in between [9].

CMOS is a type of solid-state cameras. CMOS designs differ from CCD designs in the way the sensors are manufactured and how the charges are read out of the array. CMOS sensors are manufactured on standard

semiconductor production lines, while CCDs are manufactured on dedicated production lines. Thus, CMOS are relatively less expensive than CCDs. Onboard signal processing functionality can be added to CMOS at a fraction of the cost of CCDs. This allows CMOS sensors to be more tightly integrated into entire camera assemblies on a single production line than CCDs. CMOS sensors traditionally suffer from poor dynamic response when compared to CCDs. Due to video-conferencing and high-performance compact digital camera markets, research and development is being done to improve on the deficiencies in CMOS designs. Another advantage that CMOS sensors have over CCDs is that each photo-site in a CMOS sensor array can have its own amplifier and output circuitry. This allows each photo-site to be read out independently of the other photo-sites and eliminates the need for charge-coupling. It also gives CMOS sensors the ability to have much better onboard programmability for more efficient read-outs. CMOS sensors can be integrated easier with off the shelf digital signal processors for more powerful and smaller camera design [9].

Progressive-scan cameras operate by immediately transferring an entire frame at once from the image sensor without performing any line-interlacing. The obvious benefit of this design is in motion detection applications. In computer based image processing applications, the camera is used as the sensor and input device to a plug-in acquisition board inside a computer with a built-in display board that can handle the output of the acquisition board directly. Progressive-scan camera designs are used for computer based applications, because they incorporate direct digital output and eliminate many other time consuming and unnecessary processing steps [9].

Digital cameras have several technical advantages over analog cameras. The signal-to-noise ratio is typically higher by digitizing at the CCD camera rather than at the image acquisition board. This results in better image resolution. Most digital cameras come with 8- to 12-bit gray levels of resolution as a standard feature. This higher image resolution is often required in medical, machine vision, and thermal imaging applications. The IMAQ PCI-1424 is a digital image acquisition board designed to work with digital cameras from many manufacturers [9]. Digital cameras typically have one or more 8-, 10-, or 12-bit channels (or taps). These channels are the streams of digitized data from the CCD sensor array. For fast digital image acquisition, these channels can be read out in parallel from the camera. The IMAQ 1424 series boards has a 40 Mhz pixel clock and can acquire at a rate of 160 Mbytes/s [9]. An onboard memory buffer on your digital frame grabber enables acquisition at extremely high rates

while sustaining high-speed throughput and greater overall system performance. Thus digital cameras have major advantages over analog cameras. You can acquire at faster rates, have higher resolution, acquire bigger images, and trigger acquisitions with a deterministic time delay between the trigger assertion and image acquisition [9].

Video-based CCD cameras and scientific CCD cameras are suitable for different applications. An advantage of scientific cameras are its sensitivity. It also has optional settings that can be adjusted to the detected signal. The disadvantage is the high price compared to simpler video cameras. If modified to allow variable integration time, video cameras can be sufficient. Scientific CCD cameras or video-based CCD cameras suitable for image acquisition are offered by many manufacturers. It is difficult to compare these cameras since every camera has a different set of specifications. Often there is no explanation as to how the specifications have been measured. Thus, to determine the suitability of a camera type several aspects, signal-to-noise ratio, pixel size, fill factor, sensitivity, spectral sensitivity, quantum efficiency, linearity, densitometry, and binning should be studied [9].

Signal-to-noise ratio, SNR, is a number indicating the quality of the image. It is calculated from two independent images  $I_1$  and  $I_2$  of a homogeneous, uniformly illuminated area with the same mean value  $\mu$ . The variance  $\sigma^2$  depends on dark current, photon shot noise, and readout noise. This variance is calculated as [9]:

$$\sigma^2 = \frac{1}{2} \text{var}(I_1 - I_2) \quad (1)$$

Using these values the SNR is calculated as [9]:

$$\text{SNR} = 20 \log\left(\frac{\mu}{\sigma}\right) \text{ (dB)} \quad (2)$$

The SNR should be at least 20 dB. Lower SNR means that the image is too noisy for measurements. Ignoring possible noise sources, except the Poisson noise, makes it possible to determine the best SNR a camera can achieve. According to Poisson statistics, the maximal signal is  $N$ , photoelectrons, with a standard deviation of  $\sqrt{N}$ .

The resulting SNR according to Equation 2 is reduced to  $SNR = 10\log_{10}(N)$ . The maximum SNR for a camera can be determined by knowing the size of the pixels and the typical photoelectron density of modern cameras, which is about  $700 e^- \mu m^{-2}$ . For example, a camera with small pixels ( $6.8 \times 6.8 \mu m^2$ ) has a maximum SNR of  $10 \log_{10}(6.8 \times 6.8 \mu m^2 \times 700 e^- \mu m^{-2}) = 45$  dB. Large pixels ( $23 \times 23 \mu m^2$ ) lead to a maximum SNR of 56 dB [10]. The SNR is related to the size of the pixels, which means the larger the pixel the higher the possible SNR. Small pixel sizes are more limited with respect to noise, but offer a higher sampling density than larger pixels [9].

Fill factor indicates what percentage of the chip is actually light sensitive. For example, the frame transfer CCD chip, and the interline transfer CCD chip can have a fill factor of at most 50%, see Figure 14. As far as sensitivity, there are two types, the relative and the absolute sensitivity. The relative sensitivity is the number of photoelectrons needed to produce a change of one analog-to-digital converter unit (ADU). The absolute sensitivity of a sensor is determined as the minimum number of photoelectrons that can be detected which depends on the noise characteristics of the camera [9].

The spectral sensitivity of silicon and the human eye can be seen in Figure 15. The silicon layer used to detect light is not equally sensitive to different wavelengths. Silicon is opaque to wavelengths smaller than 400nm (UV light is blocked) and transparent to light of wavelength above 1100 nm (IR light). Within this interval the sensitivity increases until it reaches its maximum at about 1050 nm as shown in Figure 15 [9]. For color cameras the sensitivity is determined by the silicon sensitivity in combination with the filters used to separate the red, green, and blue signals, for example in Figure 16 [9].



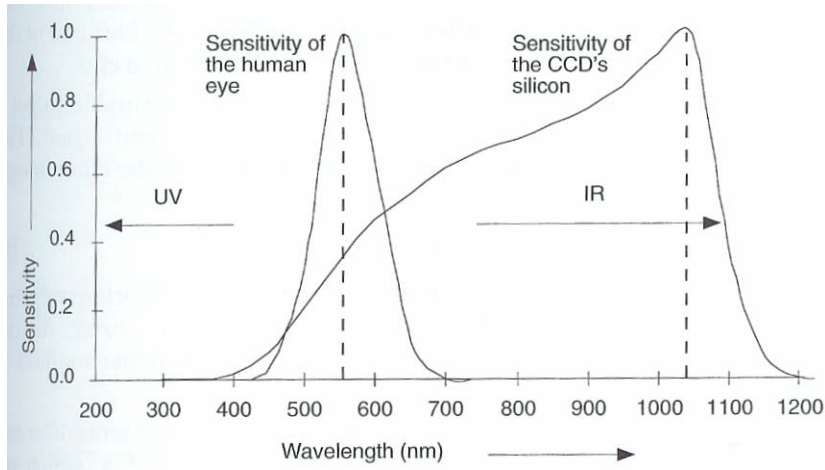


Figure 15. Spectral sensitivity of silicon and the human eye [9].

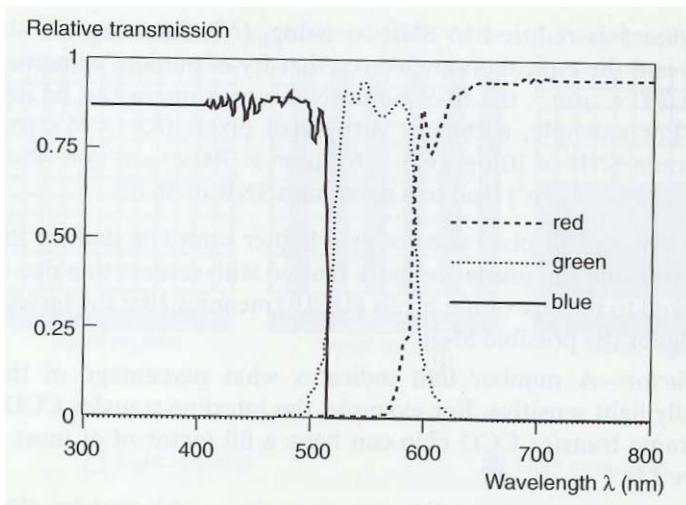


Figure 16. Spectral characteristics of the red, green, and blue filters used in RGB color cameras [9].

The quantum efficiency of the sensor material, is the relationship between the average number of incident photons and the average number of resulting photoelectrons. Not every photon causes an electron hole pair. But as the arrival of photons is determined by Poisson statistics, the number of photoelectrons is also Poisson distributed. The quantum efficiency depends on the wavelength of the incident light. For silicon it is about 50%, less for wavelengths tending to the blue end of the spectrum, and more for wavelengths tending to the infrared end [9].

It is desirable to get a linear response between the output signal and the input signal, especially for intensity measurements. The intensity of the output image depends on the intensity of the input image, the gain, the gamma value, and the offset [9]:

$$I_{\text{out}} = \text{gain} \cdot I_{\text{in}}^{\gamma} + \text{offset}$$

A linear response means that the offset is 0 and gamma is 1. The offset is almost never zero. There are several methods to correct for the non-zero offset after image acquisition. The type of camera influences the value of gamma. The ability to switch electronically between various values of gamma is offered in modern cameras. This influences the contrast of the image. If gamma is less than 1.0, the dynamic range of gray values is compressed. For values of gamma greater than 1.0, the dynamic range is expanded, Figure 17. To give the best possible contrast in the output image, some cameras have an automatic gamma correction. If intensity measurements have to be done, this should be turned off. Since different images acquired under different conditions will not be comparable [9].

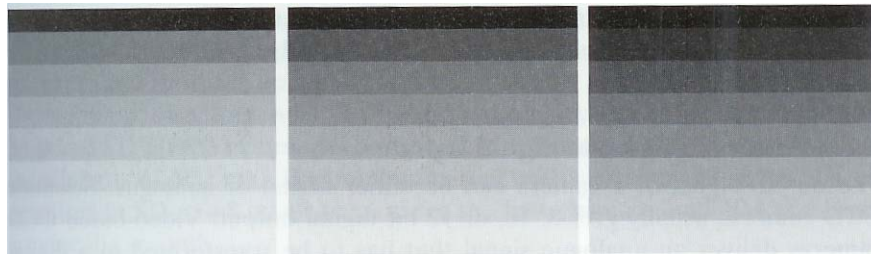


Figure 17. Test pattern with different realizations of  $\gamma$  ( $\gamma = 0.6, 1.0, 1.6$  from left to right).

The gain indicates the amplification of the input signal. Cameras may have automatic gain control (AGC) which sets the gain automatically to obtain the best contrast in the image. To enable intensity comparison between different images, this function should also be switched off. Sometimes it is possible to choose between different but fixed gain values, usually 1 x and 4 x. This can be used to adjust the camera sensitivity to the input signal. If the input signal is low the gain should be high [9].

Densitometry is the calibration for intensity measurements. Digital images can be used to measure intensity information in the object. The gray value of the digital image can easily be related to properties such as optical density. If the system is not linear, a calibration function has to be determined. First, take images of graded neutral-density filters and average the entire digital image. Second relate the known input intensity to the measured output intensity. Use flat field correction to remove the shading, if the images are distorted by uneven illumination [9].

A possibility to reduce noise is binning, which is a special readout method available with some cameras. It is possible to combine the charge of a number of neighboring pixels before digitization, instead of measuring every pixel. This causes the noise contribution to be relatively reduced. The resulting images consist of a reduced number of pixels which makes processing faster but also decreases the spatial resolution as well as the sampling density [9].

The camera's output signal can either be digital or analog. Scientific CCD cameras usually give 8, 10, or 12 bit digital output. Video-based CCD cameras deliver an analog signal that has to be transformed to a digital signal by a frame grabber. The resulting image differs in number of pixels in the horizontal direction from the expected number based on the camera chip specifications, depending on the specifications of the frame grabber. The combination of camera and frame grabber determines the sampling, not the camera alone, if a frame grabber is involved in the image acquisition. To measure quantities in images recorded by a camera, it is important to know how the original image is sampled by the camera pixels. The number of pixels in the horizontal and vertical directions indicate the resolution of the camera. These numbers are given by the manufacturer. The distance between two pixels on the CCD-array corresponds to a certain distance in the imaged object. It is possible that the sampling density (SD) in the x-direction of the chip differs from the SD in the y-direction. To determine the SD of the optical system a test pattern with known dimensions is needed. The actual size of the test pattern is compared to the size in pixels in the image [9].

$$SD = \frac{\text{size \{ (in pixels) \}}}{\text{size (in } \mu\text{m)}}$$

This has to be done in the x- and y-direction of the camera chip. The pixels of a camera are square, only if [9]

$$\frac{SD_x}{SD_y} = 1$$

It is impossible to produce an image that is identical to the original object. Only part of the light scattered or emitted from the object is collected due to the finite opening of the objective. This loss of light causes some of the information of the original object to be lost. Considering the effects in the Fourier domain, the lens can be characterized as a bandpass filter. This means only the frequencies between  $-2NA/\lambda$  and  $2NA/\lambda$  are transmitted and the other frequencies are suppressed. Thus, the frequency  $2NA/\lambda$  is called the cut-off frequency. An image that is to be processed in a computer has to be sampled at or above the Nyquist frequency, which is twice the cut-off frequency [9]:

$$SD_{Nyquist} = \left\{ \frac{4NA}{\lambda} \right\} \left\{ \frac{\text{pixels}}{\mu\text{m}} \right\}$$

Only then it is possible to reconstruct the original image based on the sampled image and avoid aliasing. Depending on subsequent image-processing steps, higher sampling may be necessary. For example, assuming sampling at the Nyquist frequency, the required SD can be determined for the two model objectives 25x/0.6 and 40x/1.3 assuming a wavelength of 500nm. The minimum required sampling density is  $4NA/\lambda$  resulting in  $SD = 4.8$  pixels per  $\mu\text{m}$  for the first objective and 10.4 pixels per  $\mu\text{m}$  for the second. It is advisable to sample at a higher frequency than proposed by the Nyquist theorem, if the aim of image acquisition is to analyze the image content. These images may be unsuitable for image analysis. This theorem yields images that look good. The accuracy of measurements in the image highly depends on the sampling density. Thus, for measurements in images with an allowable error of about 1%, the following numbers can be used as a rule of thumb. To measure the area, 10-20 samples are needed per average diameter. To measure length, 25 samples are needed per analog length. To measure certain texture features, 150 samples are needed per average diameter. And to measure small structures of the order

of micrometers, 15 to 30 samples per  $\mu\text{m}$  (2-4 times Nyquist frequency) are needed. Thus, the sampling density highly depends on the maximum allowable error of the measurement and the measurement method [9].

### ***Lens Selection***

Many applications require resolution of small particles. The challenge is to find the correct lens and camera to meet the requirements. When measuring small features, several camera and lens specifications determine how small a measurement you can make. The camera specifications are described in the camera user manual. The focal length is often printed on the lens. The minimum focal distance typically is in the lens catalog. For typical applications, the camera is selected first, based on the application. For example, the application may require a progressive scan camera for applications with motion. The camera sensor size (SS) is one of the parameters needed to resolve small objects. Next, select the lens to meet the camera requirements. To select the correct lens, select a lens with a focal length (FL) and minimum focal distance (D) to meet your requirements. It is important to know what lens will give you the resolution needed for the camera. For example, if 1 pixel is needed to inspect etched lines on a semiconductor that are 0.01 inches apart, the following calculations are needed, which are seen in Figure 18 [9]. One pixel is equal to 0.01 in.. Thus 640 pixels equals 6.40 in, which is the minimum FOV required. For the Sony XC-75, the SS equals 6.4 x 4.8 mm(640x 480) pixels. For the camera lens, the FL is 12mm and the minimum focal distance (D) is 8in.. Thus the FOV minimum equals 6.4 mm (203.2 mm/12 mm), which equals 4.27 inches. The etched lines can be resolved. To measure or resolve small objects, decrease the field of view by using a lens with a larger focal length. Also a lens with a short minimum focal distance specification can be used. Another option is to use a camera with a smaller sensor size that still maintains a high pixel density.

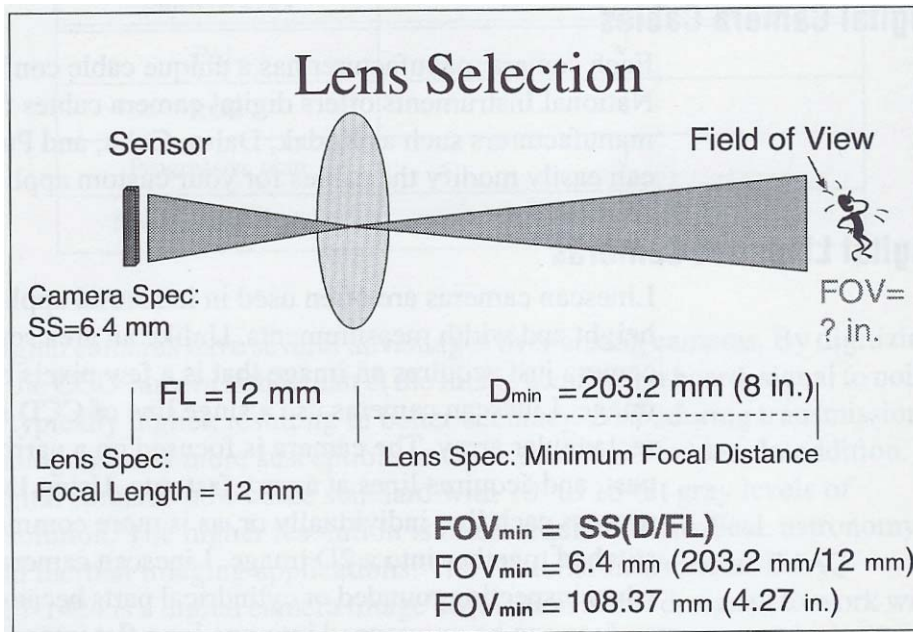


Figure 18. Lens selection [9].

A lens is a material that transmits light, with a special property: that an image of a distant object is formed a certain distance behind the lens. That distance is the focal length. The focal length is the primary characteristic of a lens. Several lenses can be combined to form a compound lens with effective focal length (EFL). The size, or field of view, of the image is proportional to the focal length. The other important parameter is the diameter, or aperture, of the lens. The brightness of the image depends on the aperture (as the square of the radius). The resolution of the image is the minimum distance between two separable points on the object. Obviously, it is better to have smaller resolution values.

Two distinct terms describe the focal lengths ( $f$ ) associated with every lens or lens system. The effective focal length (EFL) or equivalent focal length determines magnification and hence image size. The term  $f$  appears frequently in the lens formulas and tables of standard lenses. Unfortunately,  $f$  is measured with reference to principal points which are usually inside the lens so the meaning of  $f$  is not immediately apparent when a lens is visually inspected. The second type of focal length relates the focal plane positions directly to landmarks on the lens surfaces (namely the vertices) which are immediately recognizable. It is not simply related to image size but is

especially convenient for use when there is concern about correct lens positioning or mechanical clearances.

Examples of this second type of focal length are the front focal length (FFL, denoted  $f_f$ ) and the back focal length (BFL, denoted  $f_b$ ).

Field of view is the relationship between the angle of view and the distance of the object from the lens. The field of view varies with the focal length of the lens. In an imaging system depth of field refers to the distance in object space over which the system delivers an acceptably sharp image which is chosen by the user depth of field increases with increasing f-number For an imaging system depth of focus is the range in image space over which the system delivers an acceptably sharp image. This is the amount that the image surface could be moved while maintaining acceptable focus

The aperture is the opening in the lens that lets light in. The aperture ring controls the size of this opening, and thus the amount of light transmitted to the film. Apertures are indicated in f-numbers:  $f/4$ ,  $f/11$ , etc. The f-number is the ratio between the diameter of the aperture and the focal length of the lens:  $f/4$  means the aperture diameter is  $1/4$  the focal length of the lens (25mm on a 100mm lens);  $f/11$  means the aperture diameter is  $1/11$  the focal length of the lens (9mm on a 100mm lens). This is why larger f-numbers represent smaller aperture diameters, and vice versa.

A lens is a material that transmits light, conventional from left to right, which enables an image of a distant object to be formed a certain distance behind the lens, Figure 18. This distance is the focal length. The focal length is the primary characteristic of a lens. The magnification of a lens is a measure of the size of the object's image produced compared to the actual size of the object. A  $1/5X$  magnification means the object's image is  $1/5$  its actual size. Magnification can also be expressed as a reproduction ratio, which is the ratio between the size of the object's image and the object's actual size. A 3:1 reproduction ratio means the object's image is 3X the object's actual size; a 1:3 reproduction ratio means the object's image is  $1/3$  the object's actual size. Note Figure 19, the magnification is defined by the ratio of the height of the image ( $h'$ ) and the height of object ( $h$ ). The magnification is also the ratio of the back focal length ( $f'$ ) and the object distance (OD). Thus, these two ratios are equal.

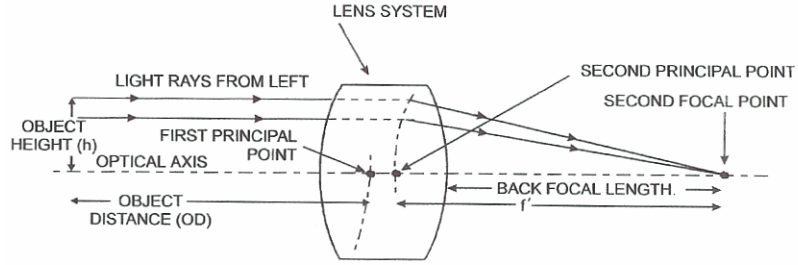


Figure 19. Diagram of a lens system

The mathematical formula, or the Thin Lens Equation, relates the object distances ( $o$ ) and image distances ( $i$ ) to the focal length ( $f$ ), the distance from the center of the lens to the focal point(s).

The Thin Lens Equation is

$$\frac{1}{o} + \frac{1}{i} = \frac{1}{f}$$

Related to this is the Thin Lens Magnification relationship:

$$M = -\frac{i}{o},$$

where the sign indicates whether the image is inverted (negative) or upright (positive).

### ***Digital Image Processing***

Technology is available to send acquired images directly to a computer for further processing and analysis. Using these images, the features of the object such as length, area, or intensity can be measured with the appropriate software. These results can be used to determine the quality of the object and to classify objects. Automated imaging systems have become more fast and accurate due to the progress of the industry. Another advantage is that results are reproducible if the set-up is unchanged. It is also easy to store results electronically for further processing at a later time or for comparison with other results.

For both image analysis and image processing, attention has to be paid to errors occurring during the image formation and acquisition. For image analysis, the quality may not always be critical since it involves an image as input and data as output. Some measurements might be done on noisy images or on unsharp images without losing



much accuracy. However, for image processing, the image quality has to be high since the output is an image too. The effort invested in getting high quality images is rewarded with less trouble in subsequent procedures. But, there are limitations with respect to the accuracy of the object representation. The optics, which form an image of the object on the sensor and the digitization process which happens in the camera, introduce errors or suppress parts of the object signal. Some of these limitations encountered in image acquisition can be compensated and/or eliminated.

Digital image processing is the computer processing of pictures or images that have been converted into numeric form. The purpose of this process is to understand and improve a digital image, which is a large array of numbers. Digital cameras produce digital images instead of the classic exposed film. In order to digitize photographs, scanners or microdensitometers can be used. The seven basic operations to enhance or improve an image and to extract information from it are as follows :

- a) Remove the blur from an image
- b) Smooth out the graininess, speckle, or noise in an image
- c) Improve the contrast or other visual properties prior to displaying the image
- d) Segment an image into regions such as object and background
- e) magnify, minify, or rotate an image
- f) remove warps or distortions from an image
- g) code the image in an efficient way for storage or transmission

There are other kinds of image processing, mainly optical and photographic, and electrical analog. Optical and photographic image processing includes the use of enlargers, lenses, and other techniques to scale, vary colors, reduce blur and so on in pictures. In each generation of the photographic process, there is a loss of image quality. Electrical analog image processing involves images that are converted into electrical signals. These signals are transmitted, received, and reconstructed as pictures. Electrical signals degrade by the physical limitations of the electrical components. Digital image processing has two main advantages, precision and extreme flexibility, over the other types. Digital image processing enables almost exact precision such that the image does not lose much of the

image quality. Also in digital image processing, more than one operation can be done at one time on sections of the image instead of just on the whole image. The main disadvantages of digital processing are its speed and expense, but as computer technology improves so will these. The use of personal computers and desktop workstations enables faster results. And there are less expensive equipment and programs available.

### ***Basic Image Processing Techniques***

To understand the properties of an image, the following image processing concepts are used. An image is a visual representation of an object or scene. In digital image processing, an image is a two dimensional array of numbers. The basic image, in Figure 20, has eleven lines and eleven samples per line. Each number in (b) corresponds to one small area of the visual image. This area is called a pixel, and the number gives the level of darkness or lightness of the area. For this example, the maximum value is white and zero is black. For other examples, this could be done vice versa with zero being white and the maximum value black. The shades of grey correspond to every number in between the zero and the maximum numbers. Zero is usually the minimum value of a pixel. The maximum value depends on how the number is stored in the computer. Each pixel can be stored as a single bit, which have values 0 and 1, or black and white. Another way is storing each pixel as a byte, which is 8 bits, thus the maximum value would be 255. Thus, depending on the computer architecture, other formats are possible. Halfword integer is 16 bits per pixel, and floating point is 32 bits per pixel. These allow greater precision and range of pixel values, but require, respectively, two and four times as much computer memory to store the image [11].

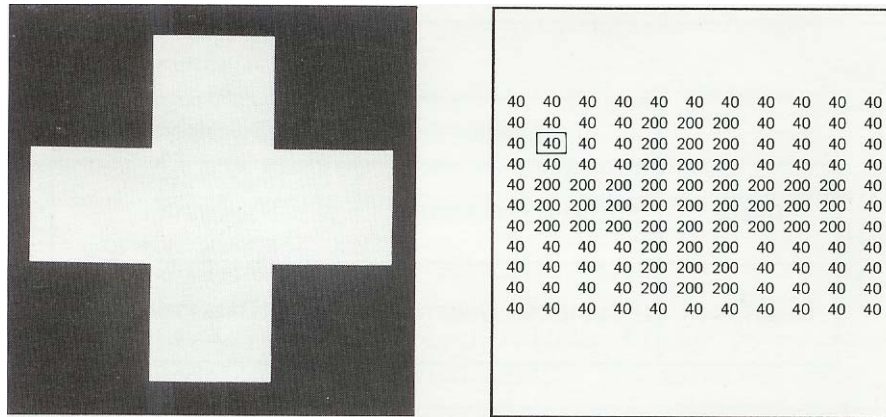


Figure 20. A simple digital image: (a) The image and (b) the corresponding array of numbers [11].

A pixel is each small area to which an integer number is assigned. It is also called a picture element. The spatial resolution of the pixel is the size of the physical area represented by a pixel. This size varies from nanometers to kilometers. Each pixel has its value, plus a line coordinate and sample coordinate, which gives the location in the array. Images are usually square with corresponding sizes of 256 X 256, 512 X 512, and 1024 X 1024. When dealing with color, the images may have three components red, green, and blue. These components are considered the bands of the image. They are also considered as three individual images which make up the whole image. They are aligned so that they superimpose which can be displayed with no shift or displacement between them [11].

An image histogram measures the distribution of the pixel values in an image. Given the mean  $\bar{v}$  and standard deviation  $\sigma$ :

$$\bar{v} = \frac{1}{n} \sum_{i,j} v(i,j) \quad \sigma = \sqrt{\frac{1}{n} \sum_{i,j} (v(i,j) - \bar{v})^2}$$

where  $n$  is the number of pixels in the image [11]. This can also be done by creating a table or plot giving the number of pixels having each possible value  $v$ . This is the image histogram,  $h(v)$ . If  $\eta_a$  is the number of pixels in the area over which the histogram is computed, then [11]

$$\sum_v h(v) = n_a$$

The normalized histogram is as follows [11]:

$$H(v) = \frac{h(v)}{n_a}$$

$H(v)$  is analogous to the probability density function. Thus, it is considered as the probability of a pixel having value  $v$ . In this case [11],

$$\sum_v H(v) = 1$$

For two bands and a specified area, a two dimensional table  $h(v, \omega)$  giving the number of pixels having value  $v$  in the first band and value  $\omega$  in the second may be computed. This is called the two dimensional histogram, the scatter plot or the scatter diagram, of the two bands. Similar to the one dimensional histogram, the two dimensional histogram satisfies:

$$\sum_v \sum_w h(v, \omega) = n_a$$

for  $n_a$  the number of pixels in the area of the histogram [11].

### **Filtering**

A reconstruction filter attempts to restore an image based on some knowledge of the degradation it has undergone, whereas an enhancement filter attempts to improve the quality of an image for human or machine interpretability. The enhancement filters include both high pass (edge enhancement) filters and low pass

(smoothing) filters [11]. In digital image processing, the mathematical basis for most filters is linear systems theory.

A system  $S$  is considered a black box with an input  $f(x)$  and output  $g(x) = S(f(x))$  [11]:

$$f(x) \rightarrow S \rightarrow g(x)$$

In one dimension,  $f(x)$  is the original image,  $g(x)$  the filtered output image, and  $S$  the filtering operation. From linear system theory, if a filter satisfies the conditions (linear and shift invariant), then output of the filter is expressed mathematically in the simple form [11]:

$$g(x) = \int f(t) h(x-t) dt \quad (3.1)$$

where  $h(t)$  is called the point spread function or impulse response. This function completely characterizes the filter. The integral expression is called a convolution integral which is written in short form as  $g = f * h$  [11]. In the digital case, the integral becomes a summation:

$$g(i) = \sum_{k=-\infty}^{+\infty} f(k) h(i-k) \quad (3.2)$$

and, although the limits on the summation are infinite, the function  $h$  is usually zero outside some range, as seen in Figure 21 [11].

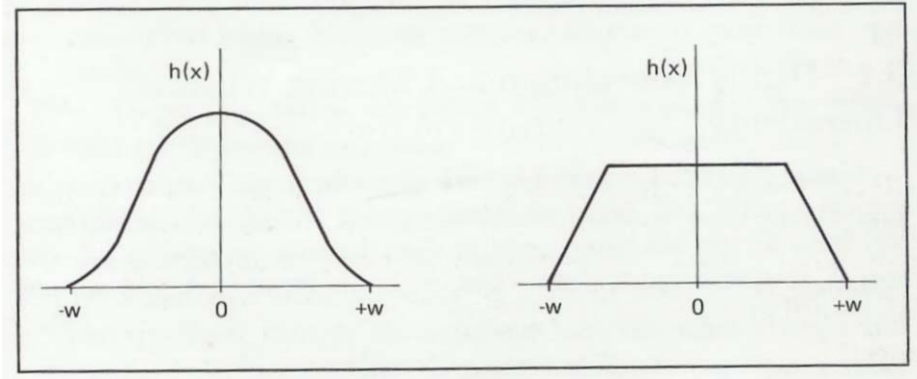


Figure 21. Form of a typical point spread function  $h(t)$  [11].

If the range over which  $h$  is non zero is  $(-\omega, +\omega)$ , then equation (3.2) may be written as [11]:

$$g(i) = \sum_{k=i-w}^{i+w} f(k) h(i-k) \quad (3.3)$$

The output  $g(i)$  at point  $i$  is given by a weighted sum of input pixels surrounding  $i$  where the weights are given by the  $h(k)$ . For the output at the next pixel  $i + 1$ , the function  $h(k)$  is shifted by one, and the weighted sum is recomputed. The full output is created by a series of shift-multiply-sum operations. This is called a digital convolution. In two dimensions,  $h(k)$  becomes  $h(k, l)$ . and equation (3.3) becomes a double summation [11]:

$$g(i, j) = \sum_{k=i-w}^{i+w} \sum_{l=j-v}^{j+v} f(k, l) h(i-k, j-l)$$

Thus,  $g(i, j)$  is created by a series of shift-multiply-sum operations as in Figure 22. The values of  $h$  are referred to as the filter weights, the filter kernel, or the filter mask. If  $h(k, l)$  is the point spread function, then the weights or filter mask is usually given as  $h(-k, -l)$ . To be symmetric,  $h(i, j)$  is usually chosen to be of size  $m \times n$  where both  $m$  and  $n$  are odd and  $m = n$ .

In some cases,  $h$  may be represented as the vector outer product of a vertical component vector  $h_v(l)$  and a horizontal component vector  $h_h(m)$ :

$$h(l,m) = h_v(l) h_h(m)^T$$

Then  $h$  is called separable. Separability is an important property computationally because it means that the filter may be applied by first convolving the image with the horizontal component  $h_h$  and then convolving the result with the vertical component  $h_v$ , or vice versa. This replaces a two dimensional convolution with two one dimensional convolutions, reducing the computations from the order of  $n^2$  to the order of  $2n$ .

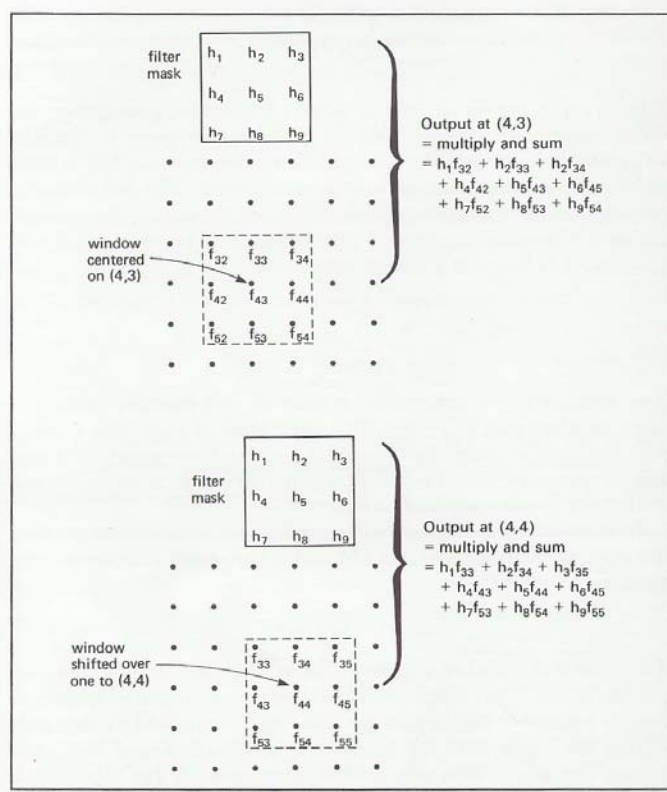


Figure 22. Digital Convolution: The output at a point is given by the sum of the input values around the point, each multiplied by the corresponding term of the  $h$  array. To compute the next output value, the  $h$  array is shifted, and the multiply and sum operation repeated [11].

In physical systems, the kernel  $h$  must be always non-negative. This results in some blurring or averaging of the image. In the sense of less blurring, the narrower  $h$ , the better the system. In digital imaging processing,  $h$  may be defined arbitrarily. This gives rise to many types of filters. By extending the basic idea of convolution, the weights of  $h$  may be varied over the image, and the size and the shape of the window varied. These operations are no longer linear, and are no longer convolutions. They become “moving window operations” which are very common in digital image processing. With this flexibility, a wide range of linear, non-linear, and adaptive filters may be implemented such as for edge enhancement or selective smoothing.

### Gradient and Laplacian Filters

The gradient and Laplacian operators are two filters applied to digital images as convolutions, which are related to the vector gradient and scalar Laplacian. These are defined for a continuous function  $f(x, y)$  of two variables as:

$$\text{Gradient: } \nabla f = \frac{\partial f}{\partial x} \bar{i} + \frac{\partial f}{\partial y} \bar{j} \qquad \text{Laplacian: } \nabla^2 f = \frac{\partial^2 f}{\partial x^2} + \frac{\partial^2 f}{\partial y^2}$$

where  $\bar{i}$  and  $\bar{j}$  are unit vectors in the  $x$  and  $y$  directions. The gradient operator applied to a continuous function produces a vector at each point whose direction gives the direction of maximum change of the function at that point, and whose magnitude gives the magnitude of this maximum change. A digital gradient may be computed by convolving two windows with an image, one window giving the  $x$  component  $g_x$  of the gradient, and the other giving the  $y$  component  $g_y$ :

$$g_x(i, j) = \text{mask}_x * n(i, j) \qquad g_y(i, j) = \text{mask}_y * n(i, j)$$



where  $n(i, j)$  is some neighborhood of  $(i, j)$  and \* represents the sum of products of the corresponding terms. The simplest set of masks is:

$$mask_x = \begin{matrix} -1 & 1 \end{matrix} \quad mask_y = \begin{matrix} -1 \\ 1 \end{matrix}$$

giving

$$g_x(i, j) = v(i, j + 1) - v(i, j)$$

$$g_y(i, j) = v(i + 1, j) - v(i, j)$$

This  $mask_x$  generates output values centered on the point  $(i, j + 1/2)$  and the  $mask_y$  generates output values centered on  $(i + 1/2, j)$ . To obtain values centered on  $(i, j)$ , masks symmetric about  $(i, j)$  are most often used. To get

$$g_x(i, j) = v(i, j + 1) - v(i, j - 1)$$

$$g_y(i, j) = v(i + 1, j) - v(i - 1, j)$$

the masks

$$mask_x = \begin{matrix} -1 & 0 & 1 \end{matrix} \quad \text{and} \quad mask_y = \begin{matrix} -1 \\ 0 \\ 1 \end{matrix}$$

are used. Other common masks are:

$$mask_x = \begin{pmatrix} -1 & 0 & 1 \\ -2 & 0 & 2 \\ -1 & 0 & 1 \end{pmatrix} \quad mask_y = \begin{pmatrix} -1 & -2 & -1 \\ 0 & 0 & 0 \\ 1 & 2 & 1 \end{pmatrix} \quad (\text{Sobel operators})$$

$$mask_x = \begin{pmatrix} -1 & 0 & 1 \\ -1 & 0 & 1 \\ -1 & 0 & 1 \end{pmatrix} \quad mask_y = \begin{pmatrix} -1 & -1 & -1 \\ 0 & 0 & 0 \\ 1 & 1 & 1 \end{pmatrix} \quad (\text{Prewitt operators})$$

Typical gradient masks for a larger window are:

$$\begin{array}{cc}
 \begin{array}{ccccc}
 -1/4 & -1/3 & 0 & 1/3 & 1/4 \\
 -1/3 & -1/2 & 0 & 1/2 & 1/3 \\
 \text{mask}_x = & -1/2 & -1 & 0 & 1 & 1/2 \\
 -1/3 & -1/2 & 0 & 1/2 & 1/3 \\
 -1/4 & -1/3 & 0 & 1/3 & 1/4
 \end{array}
 &
 \begin{array}{ccccc}
 -1/4 & -1/3 & -1/2 & -1/3 & -1/4 \\
 -1/3 & -1/2 & -1 & -1/2 & -1/3 \\
 \text{mask}_y = & 0 & 0 & 0 & 0 & 0 \\
 1/3 & 1/2 & 1 & 1/2 & 1/3 \\
 1/4 & 1/3 & 1/2 & 1/3 & 1/4
 \end{array}
 \end{array}$$

Sometimes the gradient is wanted as a magnitude  $g_m$  and an angle  $g_a$ .

These can be computed from  $g_x$  and  $g_y$  as:

$$\begin{aligned}
 g_m(i, j) &= \sqrt{g_x^2 + g_y^2} & \text{or} & & g_m(i, j) &= |g_x| + |g_y| \\
 g_a(i, j) &= \tan^{-1}\left(\frac{g_y}{g_x}\right)
 \end{aligned}$$

Another set of masks, called the Robert's operators, are not oriented along the  $x$ - and  $y$ - direction, but are nevertheless similar. They are defined on a  $2 \times 2$  window as:

$$\text{mask}_1 = \begin{pmatrix} 1 & 0 \\ 0 & -1 \end{pmatrix} \qquad \text{mask}_2 = \begin{pmatrix} 0 & 1 \\ -1 & 0 \end{pmatrix}$$

Whatever masks are used, the gradient operator produces a two element vector at each pixel, and this is usually stored as two new images, one for each component.

The Laplacian operator, which in one dimension reduces to the second derivative, is also computed by convolving a mask with the image. One of the masks that is used may be derived by comparing the continuous and digital cases as follows:

<i>Continuous</i>	<i>Digital</i>
$f(x)$	$v(i)$
$f'(x)$	$v'(i) = v(i) - v(i - 1)$
$f''(x) = \nabla^2 f(x)$	$v''(i) = v'(i) - v'(i - 1)$ $= [v(i) - v(i - 1)] - [v(i - 1) - v(i - 2)]$ $= v(i - 2) - 2v(i - 1) + v(i)$ $= (1 \ -2 \ 1)(v(i - 2) \ v(i - 1) \ v(i))$

(3.4)

giving the convolution mask (1 -2 1). In this form, the Laplacian at  $i$  is computed from values centered about  $i - 1$ .

To keep the Laplacian symmetric, it is normally shifted and given at  $i$  as:

$$(1 \ -2 \ 1) (v(i - 1) \ v(i) \ v(i + 1))$$

Also the sign is typically changed to give:

$$(-1 \ 2 \ -1) (v(i - 1) \ v(i) \ v(i + 1))$$

and this is a common form of the one dimensional digital Laplacian although mathematically it is the negative of the Laplacian. Different choices are available when extending this mask to two dimensions. Two standard masks are:

$\begin{matrix} & -1 & & & \\ -1 & & 4 & & -1 \\ & -1 & & & \end{matrix}$	$\begin{matrix} & -1 & -1 & -1 & \\ -1 & & 8 & & -1 \\ & -1 & -1 & -1 & \end{matrix}$
---	---

Again, this is the negative of the mathematical Laplacian.

A further result may be seen by rewriting the terms in equation (3.4) to give:

$$\begin{aligned} \nabla^2 v(i) &= 3v(i) - (v(i - 1) + v(i) + v(i + 1)) \\ &= 3v(i) - 3(\text{local mean at } i) \end{aligned}$$

showing that the Laplacian at  $i$  is proportional to  $v(i)$  minus the mean in a neighborhood of  $i$ .

The window masks given here for the gradient and Laplacian operators are fairly standard, but many other operators have been defined, in many cases using larger windows, say  $5 \times 5$ . Also, notice that the gradient gives both magnitude and direction information about the change in pixel values at a point, whereas the Laplacian is a scalar giving only magnitude. This was only to follow mathematical definitions and is not necessary. For example, a vector Laplacian can be defined whose  $x$  component is given by convolving the  $1 \times 3$  mask  $(-1 \ 2 \ -1)$  with the image, and whose  $y$  component is given by convolving the transposed  $3 \times 1$  mask.

### **Smoothing Filters and Edge Enhancement Filters**

Smoothing filters are designed to reduce the noise, or detail in an image. To improve the signal to noise ratio, multiple copies of the image can be averaged pixel by pixel. In most cases, only a single image is available. Thus, typical smoothing filters perform some form of moving window operation which may be a convolution or other local computation in the window. The basic problem of smoothing filters is to smooth out an image without blurring out the interesting features. Thus, edge-preserving smoothing were designed for this reason. Typical these filters are mean, weighted mean, mode, median, nearest neighbor, Sigma, etc.

Edge enhancement filters are the opposite of smoothing filters. Smoothing filters are low pass filters, while edge enhancement filters are high pass filters. Their effect is to enhance or boost edges. These filters are also referred to as edge detectors, a simple high pass filter. These filters may include a thresholding of the points into edge and non-edge categories, and even linking up of edge pixels into connected boundaries in the image. Examples of edge enhancement filters are Gradient, Laplacian, Marr, etc.

With gradient operators, only the magnitude is kept. Other methods keep both the magnitude and angle. The gradient in a given direction may also be computed. If the gradient at pixel  $p$  is considered as a vector  $(g_x, g_y)$ , then the gradient in the direction of vector  $d = (d_x, d_y)$  is  $g \cdot d$ . The gradient, moving across an edge, will start at zero, increase to a maximum, and then decrease back to zero. Thus, a broad edge is produced. The output from the

gradient operator is often thinned in order to identify only the central point as the edge. An example would be to keep only those gradient points that are a maximum in their direction. That is, let the gradient magnitude at a point be  $g_m$  and let the gradient direction, rounded to the closest of the 8 surrounding directions up, up-left, left, down-left, ..., be  $g_d$ . Then a point with a non-zero gradient is kept as an edge point only if  $g_m$  is greater than the gradient magnitude  $g_m$  of the two neighboring pixels in directions  $\pm g_d$ . Otherwise, set  $g_m$  to  $g_d$  to zero [11].

Another two forms of the edge enhancement filters are the Laplacian, which was described previously, and the Laplacian added back to the original image. Often a high pass filtered image is added back to the original image to boost edges yet maintain the underlying grey level information. But recall that the Laplacian operator, in this case, is the negative of the mathematical Laplacian. Subtracting it from the original gives:

$$v(i, j) - \nabla^2 v(i, j) \quad \text{or} \quad v(i, j) - \alpha \nabla^2 v(i, j)$$

where  $\alpha$  is an adjustable parameter. For  $\alpha = 1$ , the 3 x 3 plus-shaped window Laplacian-plus-original looks like:

$$\begin{array}{ccc|ccc|cc} 0 & 0 & 0 & & -1 & & & -1 & \\ 0 & 1 & 0 & + & -1 & 4 & -1 & = & -1 & 5 & -1 \\ 0 & 0 & 0 & & & -1 & & & & -1 & \end{array}$$

and the 3 x 3 square window looks like:

$$\begin{array}{ccc|ccc|ccc} 0 & 0 & 0 & & -1 & -1 & -1 & & -1 & -1 & -1 \\ 0 & 1 & 0 & + & -1 & 8 & -1 & = & -1 & 9 & -1 \\ 0 & 0 & 0 & & -1 & -1 & -1 & & -1 & -1 & -1 \end{array}$$

It has the effect of sharpening edges by pushing a pixel away from its neighbors. To understand this further, consider that the above masks reduce to (-1 3 -1) in one dimension, and thus the filter may be written as:

$$v_i + (v_i - v_{i-1}) + (v_i - v_{i+1})$$

This is illustrated in Figure 23.

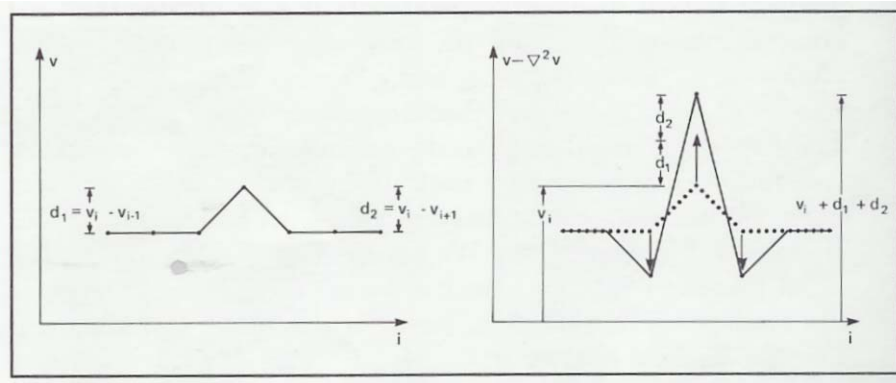


Figure 23. The Laplacian as pushing a pixel away from its neighbors [11].

The Laplacian-plus-original filter is analogous to the photographic process of unsharp masking. Equation (3.5) showed that the (negative) Laplacian of a function may be represented as the function minus its local mean. If the Laplacian is considered as  $v(i, j) - v_l(i, j)$  where  $v_l(i, j)$  is some low pass filtered version of the image such as the local mean, then the image minus the Laplacian, scaled by  $\alpha$ , is:

$$\begin{aligned} v(i, j) - \alpha \nabla^2 v(i, j) &= v(i, j) + \alpha(v(i, j) - v_l(i, j)) \\ &= \beta v(i, j) - \alpha v_l(i, j) \end{aligned} \quad (3.6)$$

which photographically, is unsharp masking.

In equation 3.6, the mean of the result is:

$$\beta \overline{v(i, j) - \alpha v_l(i, j)} = \beta \overline{v(i, j)} - \alpha \overline{v_l(i, j)}$$

and if the low pass filtered version has the same mean as the original, then this equals:

$$(\beta - \alpha) \overline{v(i, j)}$$

Therefore,  $(\beta - \alpha)$  is often chosen to be 1, so that the mean of the result is unchanged. Enhancement in the direction of the gradient can also be used for edge enhancement. An example of this filter is to compute the gradient at  $(i, j)$  and apply a one dimensional Laplacian operator in the direction of the gradient.

The Marr operators is another edge enhancement filter. These filters are of the form  $\nabla^2 G$  where  $\nabla^2$  is the Laplacian and  $G$  is the two dimensional Gaussian distribution. The idea behind these filters is to first smooth the image with a Gaussian shaped filter, and then find the edges (using the Laplacian) in the smoothed image. These filters are often used on images that have noisy and slowly varying patterns such as those from medical and robotics applications. They can be defined for any scale, depending on the size of the edges to be detected.

Like that for smoothing filters, high pass filters may be selectively applied. The filter:

```

If  $\nabla^2 v(i, j) < \text{threshold}$ 
     $v(i, j) = v(i, j) + \alpha \nabla^2 v(i, j)$ 
Else
     $v(i, j) = \overline{v(i, j)}$ 
Endif

```

where  $\alpha$  is a user-specified parameter, attempts to enhance edges (where  $\nabla^2$  is low) and suppress noise (where  $\nabla^2$  is high).  $\overline{v(i, j)}$  is the mean in some neighborhood of  $(i, j)$  [11].

More complex methods are also available. The problem is in trying to work well in the presence of noise. The list of filters for both low and high pass filtering is long. The results from filtering can be disappointing. Often improvements can be gained, however, if the geometry, imaging conditions, or nature of the noise or features of interest are incorporated in the filter. For example, if the features are known to be horizontally or vertically oriented, or the noise is known to be multiplicative and not additive, then perhaps the filter can be modified. Filter masks are only the starting point for a filter which may be adapted to a problem.

Apart from the adapting a filter to a specific problem, generalizations about the usefulness of the various filters are difficult. Of the smoothing filters briefly mentioned, the median and k nearest neighbor filters perform reasonably well in many applications. Most high pass filtering is concerned with detecting edges, and gradient methods are usually superior to Laplacian methods because they are less sensitive to noise and they also provide directional information which may be later be used to link edges and eliminate isolated edge points.

### **Fourier Transform**

The Fourier transform is a powerful tool for analysis and computation in many fields of mathematics and engineering. It has a wide variety of applications in image processing. Suboptimal image filtering and image pattern matching are two of these applications. In image processing, the term frequency is referred to as spatial frequency. This frequency is not related to the variations in time as in engineering studies. It is the frequency with which a signal or image varies as a function of spatial coordinates. Images with gradually varying patterns have low spatial frequencies, and those with much detail and sharp edges have high spatial frequencies. This type of frequency is the frequency components of an image, and will be computed using the Fourier transform.

The Fourier Transform  $F(\omega)$  of  $f(x)$  is defined as:

$$F(\omega) = \int_{-\infty}^{+\infty} f(x)e^{-j2\pi\omega x} dx$$



For  $j = \sqrt{-1}$ . If  $f$  is periodic,  $F$  will be non-zero on a discrete set of values; otherwise  $F$  will be a continuous function of  $\omega$ . If  $x$  is in units of spatial dimensions (meters),  $\omega$  is in units of spatial frequency (meters<sup>-1</sup>). There are limitations on the function  $f(x)$  for its transform to exist: it must be a piecewise continuous function with left and right-hand derivatives at every point. Assuming the transform exists for all cases of our interest, then the inverse transform also exists, transforming  $F(\omega)$  back to  $f(x)$ :

$$f(x) = \int_{-\infty}^{+\infty} F(\omega) e^{j2\pi\omega x} d\omega$$

Every  $f$  has a unique Fourier transform  $F(\omega)$ , and every  $F(\omega)$  has a unique inverse  $f$ , and vice versa. Thus,  $f$  and  $F$  transform back and forth. The symbol,  $FT$ , is used to denote the Fourier transform operator. And the symbol,  $F$ , is used to denote the transform. Thus,  $FT(f(x)) = F(\omega)$ . As an example,

$$\text{if } f(x) = \cos 2\pi\omega_0 x \quad \text{then} \quad F(\omega) = \begin{cases} \frac{1}{2} & \text{for } \omega = \pm \omega_0 \\ 0 & \text{elsewhere} \end{cases}$$

And if  $G(\omega_0) = 0$  then  $g(x)$  has no component of frequency  $2\pi\omega_0$ . The Fourier transform is linear:

$$FT[af(x) + bg(x)] = aFT(f(x)) + bFT(g(x))$$

and has the scaling and shift properties given by:

$$FT(f(ax)) = \frac{1}{|a|} F\left(\frac{\omega}{a}\right)$$

$$FT(f(x - a)) = F(\omega) e^{-j2\pi\omega a}$$

If there exists an  $\omega_0$  such that  $F(\omega) = 0$  for  $|\omega| \geq \omega_0$ , then  $f$  is said to be bandlimited at  $\omega_0$ .

These definitions and properties may be extended to functions defined not on a continuous interval, say  $(-a, a)$  or  $(-\infty, +\infty)$ , but on a discrete set of points  $x_i, i = 1, 2, \dots, n$ . The transform is then called the Discrete Fourier Transform. Both the continuous and the discrete transform may be extended from one to two dimensions. The Discrete Fourier Transform in two dimensions is the form typically used in image processing. Thus, it is considered the Fourier transform of a digital image. The definitions for the forward and inverse transforms for each of these cases are seen in Figure 24. The three letters starting at each line indicate Continuous/Discrete, 1 dimension or 2, and Forward or Inverse transform [11].

$$\begin{array}{ll}
 C2F & F(\omega, \nu) = \int_{-\infty}^{+\infty} \int_{-\infty}^{+\infty} f(x, y) e^{-j2\pi(\omega x + \nu y)} dx dy \\
 C2I & f(x, y) = \int_{-\infty}^{+\infty} \int_{-\infty}^{+\infty} F(\omega, \nu) e^{j2\pi(\omega x + \nu y)} d\omega d\nu \\
 D1F & F(h) = \frac{1}{\sqrt{n}} \sum_{k=0}^{n-1} f(k) e^{-j2\pi hk/n} \quad 0 \leq h \leq n-1 \\
 D1I & f(k) = \frac{1}{\sqrt{n}} \sum_{h=0}^{n-1} F(h) e^{j2\pi hk/n} \quad 0 \leq k \leq n-1 \\
 D2F & F(h, i) = \frac{1}{n} \sum_{k=0}^{n-1} \sum_{l=0}^{n-1} f(k, l) e^{-j2\pi(kh + li)/n} \quad 0 \leq h, i \leq n-1 \\
 D2I & f(k, l) = \frac{1}{n} \sum_{h=0}^{n-1} \sum_{i=0}^{n-1} F(h, i) e^{j2\pi(kh + li)/n} \quad 0 \leq k, l \leq n-1
 \end{array}$$

Figure 24. The definitions for the forward and inverse transforms for each of these cases (The three letters starting at each line indicate Continuous/Discrete, 1 dimension or 2, and Forward or Inverse transform) [11].

A property of the two dimensional Fourier transform is its separability. This may be expressed mathematically as:

$$F(\omega, \nu) = \int_{-\infty}^{+\infty} F_y(\omega, y) e^{-j2\pi\nu y} dy$$

where

$$F_y(\omega, y) = \int_{-\infty}^{+\infty} f(x, y) e^{-j2\pi\omega x} dx$$

This means that the two dimensional transform may be computed in two steps, first computing the one dimensional transforms for each value of  $x$  and then computing the one dimensional transforms of these results for each value of  $y$ .

A useful way of writing the equation for the discrete transform can be given by defining

$$z = e^{-j2\pi/n}$$

and then the matrix

$$\tilde{z} = \frac{1}{\sqrt{n}} \begin{pmatrix} 1 & 1 & 1 & \dots & 1 \\ 1 & z & z^2 & \dots & z^{(n-1)} \\ 1 & z^2 & z^4 & \dots & z^{2(n-1)} \\ 1 & z^3 & z^6 & \dots & z^{3(n-1)} \\ 1 & z^{n-1} & z^{2(n-1)} & \dots & z^{(n-1)(n-1)} \end{pmatrix}$$

That is,

$$Z(k,l) = z^{(k-1)(l-1)}.$$

Then the one dimensional discrete transforms may be expressed as:

$$F(h) = Zf(k) \quad \text{and} \quad f(k) = Z^T F(h)$$

and the two dimensional transform as:

$$F(h, i) = Zf(k, l)Z \quad \text{and} \quad f(k, l) = Z^{*T} F(h, i)Z^* \quad (5.1)$$

where  $F(h)$  and  $f(k)$  are vectors, and  $F(h, i)$  and  $F(k, l)$  are matrices. In this form, it can be seen that the direct computation of the one dimensional transform requires  $n^2$  multiples and the two dimensional requires  $n^4$ . Also, the separability of the transform can be seen: the two dimensional transform is equivalent to performing the one dimensional transform of all rows, and then performing the one dimensional transform of all columns of the result.

In the equations given, the discrete transform  $F$  is given for values of  $h$  (or for  $h$  and  $i$  in two dimensions) in the range  $[0, n-1]$ . For  $h = 0$ , the value of  $F$  is the constant or “dc” term. If the transform is displayed as an image, this constant term will be in the upper left corner, as in Figure 25(a). A more convenient way is to shift the transform to have the constant term in the center, Figure 25(b), and in this way it will match the more common presentation of the optical Fourier transform. These two forms of the transform, equivalent except the reordering of terms, are referred to as the “standard” and “optical” forms. The reason for this shift is illustrated in one dimension in Figure 25(c), showing the coordinate system for the computed transform and that for the best display. Part (d) shows the shifting of the two dimensional transform necessary to obtain the desired result. It can be shown that the result of this shifting can also be obtained by multiplying each pixel of the image to be transformed by  $(-1)^{(i+j)}$  where  $i$  and  $j$  are the line and sample coordinates of the pixel.

Mathematically, the transform is defined for complex valued functions and the results are complex valued functions. Digital images are real valued arrays, say  $n \times n$ , but nevertheless the output has a real and complex part, each  $n \times n$ . However, the transform of a real function is symmetric, so not all the  $2 \times n \times n$  resulting values are independent and there is no doubling of the amount of information. When displaying the transform of an image, what is displayed is  $|F(h, i)|$ , the magnitude of the complex number at each point. Because the dc or 0 frequency term is typically much larger than all others, it is sometimes set to zero before scaling for display, or the logarithm of the values in the magnitude image is taken before scaling.

One of the most useful properties of the Fourier transform is known as the Convolution Theorem. It states that if  $F$  is the transform of  $f$  and  $H$  is the transform of  $h$ , then

$$FT(f * h) = FT(f)FT(H)$$

This may be written in several equivalent ways:

$$f * h = FT^{-1}(FT(f)FT(h))$$

or

$$G = FH \text{ for } g = f * h \text{ and } G = FT(g)$$

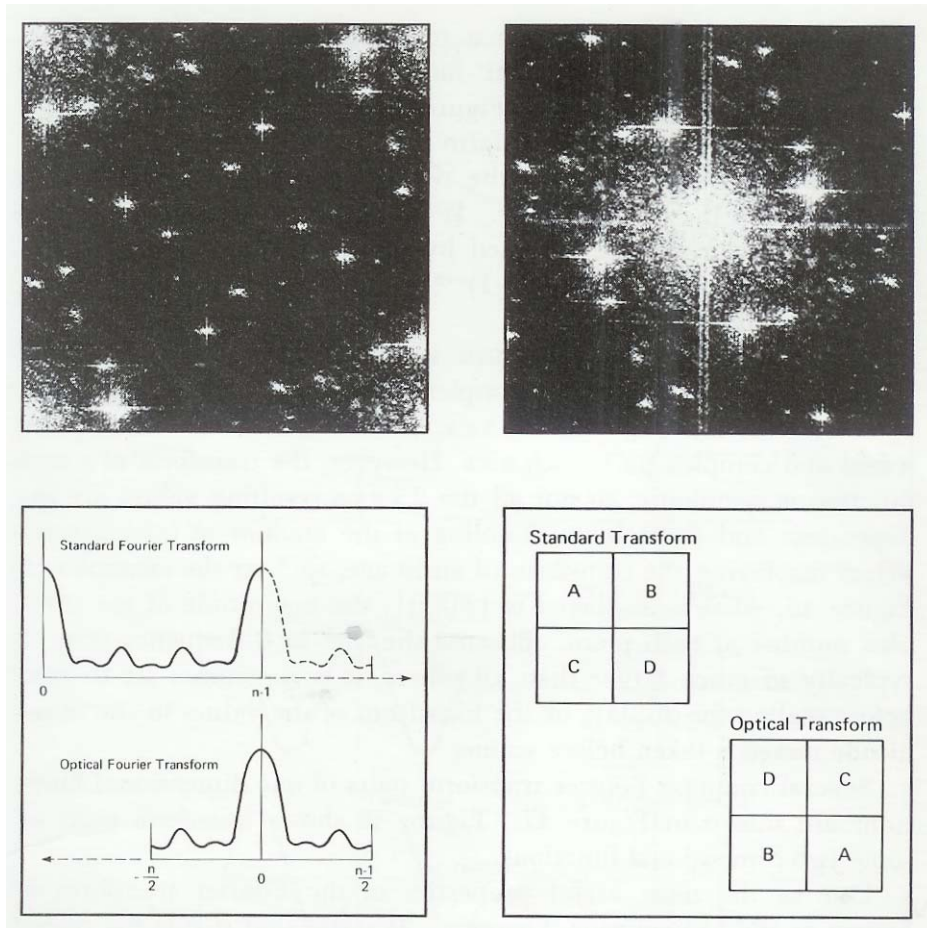


Figure 25. Comparison of standard and optical transforms: (a) The standard form of the Fourier transform in upper left, and (b) the transform rearranged into the optical form in upper right. (c), in lower left, shows the origin and coordinate systems for the two forms. The reordering to convert from one to the other in two dimensions is shown in (d).

This convolution in the spatial domain is equivalent to multiplication in the frequency domain. This provides an alternate way of convolving two signals. Instead of directly convolving  $f$  and  $g$ , we may take their transforms, multiply the transforms point-by-point, and take the inverse transform of the result. The same is true for correlating two signals, which is a similar operation.

The methods of Fourier analysis seem a natural choice for use in image filtering for two reasons. The first is computational efficiency. If a known, linear shift invariant filter  $h(k, l)$  is to be applied to image  $f(i, j)$ , the output  $g(i, j)$  may be generated as either a spatial convolution  $f(i, j) * h(k, l)$ , or, as described above, as  $FT^{-1}(FH)$ . There

may be a large computational savings in using the Fourier transforms. This will be discussed later in Fourier domain correlation.

Secondly, many imaging and optical systems can be analyzed using Fourier methods, and these naturally lead to filters that may be applied in the Fourier domain. Notice however, that the filter to be applied must be linear and independent of local image content. This is not the case for many of the adaptive, edge preserving filters discussed in this thesis. This is the reason Fourier filtering is typically used to compensate for the effects of an imaging or optical system, whereas adaptive spatial filters are used when the filtering is based on pixel value, gradients, and so forth. As an example, a common problem for astronomy images is to convert an image taken by one telescope system into one compatible with an image taken by another. This is often most easily done by modelling the optics as a linear system using Fourier methods, and then applying the filter in the Fourier domain. And even if no model of the imaging system is derived, the Fourier transform can still be used to help select a (linear) filter. The two dimensional transform of an image identifies the spatial frequency components, and by eliminating or attenuating suspected noise components in the transform, then taking the inverse transform, a filtered image is obtained.

### **Optimal and suboptimal filters**

In any case, when using Fourier methods,  $H$  is specified directly in the frequency space, and the problem of filtering becomes one of choosing  $H$ . Roughly corresponding to the two cases of having a model of the imaging system or not, there are two general categories of filters: optimal and suboptimal. Optimal filters are those that are designed to maximize certain goodness criteria and use either the model, or measurements or assumptions on the signal and noise properties; for example, the shape of their spectrum. The Wiener filter and the Matched detector are two categories of optimal filters that are derived using assumptions on the signal and/or noise. These topics are normally considered as image reconstruction, and are different from the other methods described in this thesis, which are heuristic and qualitatively evaluated. Literature is available which discusses the design and application of these filters in image processing.

Suboptimal filters are those for which  $H$  is chosen by heuristic guidelines or by trial-and-error. Standard filters, such as Ideal and Butterworth filters, may be applied to suppress the low or high frequencies. However, they may also produce artifacts in the filtered image. A common artifact is the “ringing” obtained in an ideal low pass filtered image. This can occur if high frequency terms are associated only with the noise in an image, and are completely eliminated.

Successful suboptimal filtering typically occurs when a specific frequency-dependent noise is to be removed from an image. An example is the noise coming from electrical signals in the imaging process and which can be visually observed in the image as periodic pattern. Another is the periodic noise induced in the digitization process of half-tone printed pictures in which the sampling frequency of the digitization interacts with the frequency of the printing matrix. In such cases, the noise component can often be observed as spikes in a display of  $|F(h, i)|$ . With appropriate software, the spikes can be outlined with a cursor, a filter constructed to attenuate those frequencies, and the filter applied. If the inverse transform can be computed rapidly, several filters can be tried to give a pleasing visual quality to the image.

### **Fourier Domain Correlation**

A second use of the Fourier transform in image processing is in performing correlations for pattern matching, which is sometimes called Fourier domain correlation. Several applications arise in which it is desired to know where a normally small pattern image or window  $W(i, j)$  best fits within another, larger array called the search area  $S(k, l)$ . One way of selecting where it best fits is to pick the point of maximum correlation. Because of the Convolution Theorem, the correlation may be done in the spatial domain, or in the Fourier domain. The Fast Fourier Transform (FFT) is an efficient algorithm for computing Fourier transforms, and by using the FFT, convolutions and correlations may often be computed more efficiently using the Fourier method than by direct spatial domain computations. Thus this use of the Fourier transform has no conceptual advantages but is strictly for computational efficiency.

To compare the computation times, correlation is used to locate a  $w \times w$  window  $W$  within a larger  $s \times s$  search area  $S$ . First,  $s$  is a power of 2. For a direct spatial correlation, each of the  $w \times w$  values of the window must



be multiplied by the corresponding elements of  $S$  in each position of  $W$  within  $S$ . Using the Fourier method, the two dimensional transforms of the search and of the window are performed and multiplied together. Then, the inverse transform of this result is performed. Using the FFT, a one dimensional  $s$  point transform requires  $2s\gamma$  real multiplies, where  $\gamma = \log_2 s$ . The number of multiplies required for both methods is summarized in Figure 26. The most efficient method for a given problem will depend on the specific sizes of the search and window arrays, and whether the search size is a power of 2. As examples, using the bottom line of the table, if we correlate a  $20 \times 20$  window in a  $32 \times 32$  search area, the ration of multiplies for the FFT method to direct spatial correlation is about 0.86. If the same  $20 \times 20$  area is to be located in a  $64 \times 64$  image, the ratio is about 0.33. Actual performance comparisons of the two methods, which includes the additions and other operations, have shown an even greater advantage for the FFT approach.

Using FFT:		$\gamma$ is given by $s=2^\gamma$			
2d FFT of window:	w lines s columns	x	s	point FFT:	w x $2s^\gamma$
2d FFT of search:	s lines s columns	x	s	point FFT:	s x $2s^\gamma$
Multiply transforms:					s x s x 4
2d inverse FFT:	s lines s columns	x	s	point FFT:	s x $2s^\gamma$
Total Multiplies for FFT:					$5(2^\gamma s^2) + 2^\gamma ws + 4s^2$
Using Spatial Correlation:					
Total Multiplies:					
s-w+1 lines x s-w+1 columns x w lines x w columns					
Ratio:	$\frac{\text{FFT}}{\text{Direct}}$	=	$\frac{5(2^\gamma s^2) + 2^\gamma ws + 4s^2}{(s-w+1)^2 w^2}$		

Figure 26. Comparison of multiplication operations using spatial and Fourier correlation [11].

This advantage becomes still greater if the Fourier transform of the window need not be computed each time. This may be the case if the window is a fixed pattern whose transform may be pre-computed, or if it is a special pattern whose transform may be computed analytically. In some cases, a normalization is necessary for

results computed using the Fourier method. In the spatial domain correlations, the window is usually normalized to have zero mean and sum of squares equal to one:

$$\overline{W(i, j)} = 0 \quad \text{and} \quad \sum_{i, j} W(i, j)^2 = 1$$

and, at each position of the  $W$  array within  $S$ , the  $w \times w$  elements of  $S$  are also normalized to have sum of squares equal to one:

$$\sum_{i, j} S(i, j)^2 = 1$$

where the sum is over the  $w \times w$  array overlaid by  $W$ . This local normalization cannot be included in the Fourier correlation and if it is necessary, must be done as a later step.

This is just two out of the many applications of the Fourier transform in image processing. Other applications include its use in reconstruction (optimal) filtering, in image coding and compression, in image analysis and evaluation, and in computing shape descriptors for objects.

### **Fast Fourier Transform**

The fast Fourier transform is a computationally efficient method for performing discrete-time spectral analysis. Fourier methods require no prior knowledge of the underlying structure of the signal. A limitation of the FFT is that its frequency resolution is dependent upon the number of samples available. Thus, to have better frequency resolution, the data needs to be longer. Whenever using Fourier methods, best results are obtained when physical considerations of the problem or image map well onto the Fourier model. This is often the case when deriving a linear filter describing an optical system such as a telescope or microscope. It is also the case when a periodic component or lattice is to be identified in an image. For this reason, Fourier methods are often used on images from astronomy, microbiology, images of repetitive structure such as crystals, and so on. In other problems,

this is not the case, and a Fourier solution may give poor results. For example, remote sensing images are usually not filtered with Fourier methods because there is no reason for suppressing or enhancing certain spatial frequencies and, for these images, the filters that are used are typically non-linear or the filter kernels are small and easily implemented as spatial convolutions [11].

### ***High Speed Imaging System And Macro Lens Viewing***

#### **Digital Camera And Macro Lens System**

A Dalsa camera was mounted to the rear view port of the macro camera imaging system, Figure 27. Direct viewing was also available from a ground glass display screen at the rear view port. The top view port is normally used to mount a 35mm camera body or linear array using a standard 4x5 photographic mount [12]. Each view port was adjusted such that the geometric center of the view frame observes the same point on the weld pool surface. This macro camera and lens system enabled 28.86x magnification of the weld pool. The photo enlarger lens, 105mm, is attached to the front of a bellows type view camera. A lens of this focal length affords a reasonable compromise between the working distance (lens to weld pool distance) and the overall length of the macro camera imaging system, 3.035m (119.5in). This system with the two view ports allows both simultaneous measurement and direct observation of the weld pool. The weld pool image passes through an extension tube. The magnification of the camera is determined by:

$$L = fM \tag{1}$$

where M is the desired magnification, f is the focal length of the lens, and L is the extension tube length [12].

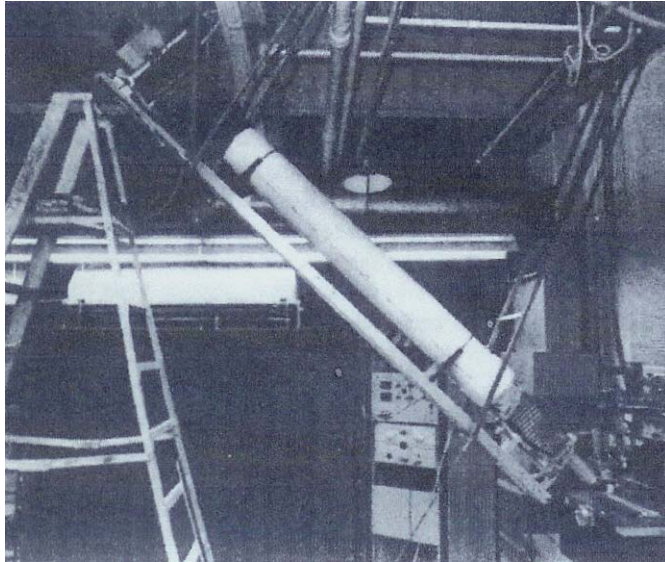


Figure 27. Photograph showing the overall layout of the macro camera system. The digital camera and the associated computer hardware is shown in the upper left area of the picture. [12]

At the rear of the camera, a beam splitter, Figure 28, is employed to provide simultaneous weld pool images to the two view ports. The beam splitter reflects 40 percent of the incident light to the top view port and the remaining light is transmitted to the rear view port. The optical axis of the camera is oriented 45 degrees to the horizontal and 90 degrees to the direction of travel. This allowed an unobstructed view of the weld pool while minimizing the amount of arc light viewed directly by the camera or reflected into the camera from the weld pool surface. As a result, no light filtering was required to reduce the arc light intensity for direct observation when weld currents were kept below 120 amperes. Simple adjustments to the lens aperture setting were all that was required. In practice the weld pool is positioned in the view frame such that the area of interest is placed under the cross hairs of the ground glass display screen. This focused image of the weld pool displayed on the ground glass view screen. The current settings of the welds were mostly kept around 80 A to 90 A, since observing welds with settings below 60 A proved challenging. Since arc light is reduced, the aperture must be opened to allow more light into the macro camera for proper viewing. By opening the aperture, field depth (the distance interval in front of the lens which is in clear focus) is reduced. Attaining clear focus across the entire width of the weld bead becomes difficult. The normal operating range for the macro camera, in its current state of development is, therefore, between 60 to 120 amperes. More information on this system is in Delapp's paper [12].

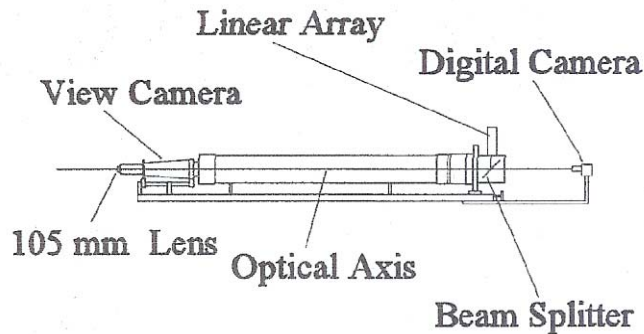


Figure 28. Macro camera imaging system showing linear array and digital frame grabber camera in position for measurements Camera magnification is 28.86x. [12]

The most fundamental part of the imaging system is the electronic camera. The progressive scan area camera, the Dalsa CA-D1-0128A (Figure 29) which is comparable to the DS-11-16K7H, enabled the real time signal acquisition, processing, and display of the images. Within the CA-D1 camera, a driver board provides bias voltages and clocks to the CCD image sensor, a timing board generates all internal timing, and an output board processes the video for output. Data sheets on this camera are attached in the appendix. The IMAQ-1424 is discussed and how its RTSI interface is used to synchronize image and data acquisition with a PCI-MIO-16-E1 multifunction I/O board. Next, to work with these signals as images, the IMAQ-1424 board enabled these signals to be opened as images by the National Instruments' software program, Labview.



Figure 29. The Dalsa CA-D1-0128A camera [6].

Before installing the appropriate software to the computer for grabbing the image from the camera, all the hardware was added. This included the memory, and the I/O data acquisition board. Then, the Dalsa camera was connected to the back of the computer through the data and image acquisition board with the appropriate cables from the manufacturer. This signal processing board, that was installed in a PCI slot inside the computer, enabled real time signal acquisition, processing, and display. The camera was then mounted high enough to be added to the rear of the macro lens system [12]. The camera and the macro lens system were carefully adjusted to capture the weld pool image, Figure 30. Using the Labview viewer program, this weld pool image was displayed frame by frame in real-time saved on the computer for further analysis. This viewer program will be discussed later.

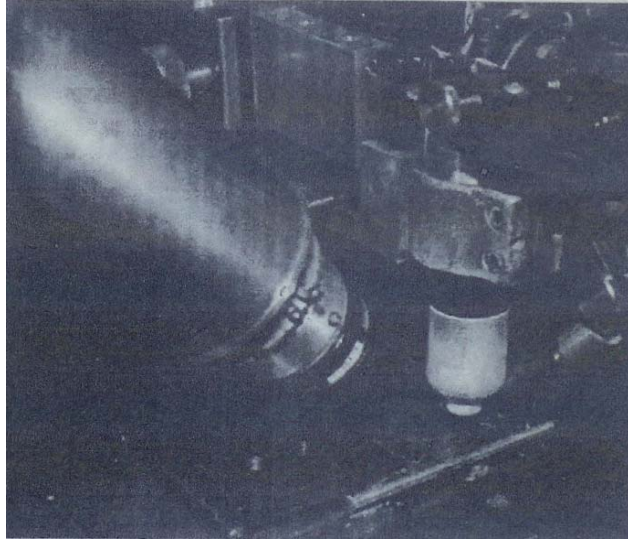


Figure 30. Photograph showing the orientation between the macro camera, the GTAW torch and the workpiece. [12]

### **Image Acquisition Board and Software**

The IMAQ PCI-1424 is a universal digital camera image acquisition board designed to acquire both color and monochrome images, as well as provide control for digital cameras. This board can acquire from up to four image sources simultaneously and from cameras with resolutions of 8, 10, 12, 16, 24, and 32 bits. The other option is the IMAQ 1408 series which is available for PCI, PXI, and CompactPCI. The 1408 is a high-accuracy image acquisition board for analog, monochrome, and StillColor acquisition. The board can acquire from standard (RS-170, CCIR, NTSC, and PAL) as well as nonstandard video. The board has four video channels and four I/O lines that can be used as triggers or for simple digital I/O. The 1408 also has the Real-Time System Integration (RTSI) bus for routing timing and triggering signals between other IMAQ boards and DAQ boards [9].

The NI-IMAQ driver software gives you the high-level control of National Instruments IMAQ hardware. NI-IMAQ performs all of the computer and board-specific tasks to make it easy to acquire images. No register-level programming is needed. NI-IMAQ contains the NI-IMAQ Configuration Utility for configuring your board. The utility allows you to set up your board and acquire images to test your board and camera. NI-IMAQ includes LabVIEW VIs for image acquisition. These VIs supply all functionality needed to acquire images with or without a trigger [9].

The NI-IMAQ Configuration Utility is a setup and diagnostic utility that configures parameters for your IMAQ board and tests if the board and camera are functioning correctly. After installing an IMAQ board in your system, you must run the NI-IMAQ Configuration Utility to select the type of video signal connected to the IMAQ board. You can select a standard video type (RS-170, CCIR, NTSC, or PAL) or configure a file for a nonstandard video signal. To test the board's configuration, the configuration utility allows you to acquire images from your camera [9].

All parameters that are configured in the NI-IMAQ Configuration Utility for a board are associated with an interface name. More than one interface name enables several different configurations for one board. The interface name is used to refer to the board in LabVIEW. `Img0` is the default interface name, and its information is stored in an interface (.iid) file and includes board serial number, camera file associated with each channel on the board, default channel, lookup table, and settings for the video synchronization signals [9].

All parameters configured for a camera type are stored in a camera (.icd) file. The camera file is then associated with a specific channel on an IMAQ board. The camera file includes information about the video signal timing and the input signal range of the video signal [9].

The LabVIEW Image Acquisition (IMAQ) Library contains VIs to control National Instruments IMAQ boards. The IMAQ Library subpalette contains VIs for image acquisition, triggering, and adjusting board parameters. The LabVIEW IMAQ VIs are organized into three levels, Figure 31 [10]:

- Basic VIs, which allow you to acquire images and get or set attributes
- Advanced VIs, which include VIs for triggering and allow you to wait for a hardware event
- Color VIs, which allow you to perform a StillColor acquisition



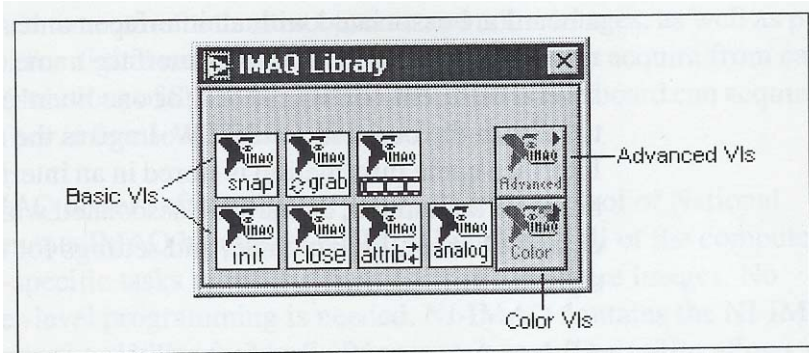


Figure 31. The IMAQ library palette shows basic, advanced, and color VIs [10].

Three image acquisition types are available in LabView. Snap, grab, and sequence allow for single-shot or continuous acquisition and single or multiple buffer acquisition. Also, it is possible to link or coordinate a vision action or function with events external to the computer. This can be done using triggered image acquisition, which is available in Labview. There are many programming VIs available, depending on the application. A few of these VIs will be discussed later.

## CHAPTER III

### EXPERIMENTAL METHOD

#### *Welding Parameters for the Gas Tungsten Arc Welding System*

Using the camera system and welding system described above, the images of the weld pool were obtained. The correct welding parameters, current, voltage, and travel speed, enable the welds to have better penetration. If the wrong parameters were selected, then excessive arc light would be going into the camera system. Thus, the formation of the weld surface ripples would not be visible. Any slight variation of these welding parameters, also including shielding gas, and surface impurities, could have a dramatic effect on the pool size, and the pool's vibration. The following information is needed to improve the weld and image quality.

The metal at the leading edge of the weld pool melts while solidification takes place at the trailing edge of the pool as the arc moves along the workpiece. The travel speed, along with the welding voltage and current, takes part in controlling the amount of heat delivered to the weld at any point. The heat input (in Joules per unit of distance) is proportional to  $P/v$ , where  $P$  is the net power and  $v$  is the travel speed. [4] Thus, the gas tungsten arc welds were obtained using a workpiece made of 10/18 cold rolled steel, with dimensions of 1/8 inch X 4 inches X 8 inches. The first image, 79a.log, was achieved from a weld on a cold workpiece on spacers. The AVC was off. The shielding gas was 45 ft<sup>3</sup> hour. The current and voltage were 80 Amps and 9.8 Volts, respectively. The image was aligned such that the leading edge was in the 12 o'clock position. The f stop of the lower and upper camera was adjusted to 8/11 and 5.6, respectively. The travel speed on the dial was 30 in/min (12.70 mm/s).

The next image, 79b.log, was also on a cold workpiece. The travel speed on the dial was changed to 36 in/min (15.24 mm/s). The rest the same as the first image. The third image, 79c.log, was also on a cold workpiece. The travel speed on the dial was 36 in/min (15.24 mm/s). The current and voltage was 81 Amps and 10.1 Volts, respectively. The rest the same as the second image. There seemed to be lots of lower frequencies, possibly due to

something being bumped. The fourth image, 79d.log, was on the same workpiece as the previous image. The travel speed on the dial was changed to 25 in/min (10.58 mm/s). Everything else is the same as before. The fifth image, 79e.log, was also on the same workpiece with a new travel speed on the dial of 20 in/min (8.47 mm/s). It probably was over-penetrating, due to the jumping around of the image. The sixth image, 712a.log, was on a cold workpiece with a travel speed on the dial of 30 in/min (12.70 mm/s). A new tank of gas was used. The current and voltage was 80 Amps and 10 Volts, respectively. The leading edge of the weld pool was along the 12 o'clock position. The AVC was off. The f stop of the lower and upper camera was adjusted to 4.5 5/6 and 2.8, respectively. The seventh image, 712b.log, was on the same workpiece as the previous weld. Everything was the same, except the travel speed on the dial was changed to 20 in/min (8.47 mm/s). The eighth image, 712c.log, was on a cold workpiece with a travel speed on the dial of 30 in/min (12.70 mm/s). The current and voltage was 90 Amps and 10 Volts, respectively. The f stop of the lower and upper camera was adjusted to 16/22 and 2.8/4, respectively. The ninth image, 712d.log, was on the previous workpiece with travel speed on the dial of 30 in/min (12.70 mm/s). The current and voltage was 120 Amps and 9.9 Volts, respectively, at the end of the weld. The f stop of the lower and upper camera was adjusted to 5.6/8 and 4, respectively. The final two images, 712e.log and 712f.log, were on a sanded workpiece with travel speed on the dial of 30 in/min (12.70 mm/s). The current and voltage was 80 Amps and 10 Volts, respectively. This information is summarized as follows in Table 6.

**Table 6. Gas Tungsten Arc Welding parameters for the welds (images of the welds) obtained.**

Image	Travel speed	Current	Voltage	F stop low	F stop upper	Workpiece condition
79a.log	12.70 mm/s	80 Amps	9.8 Volts	8/11	5.6	cold
79b.log	15.24 mm/s	80 Amps	9.8 Volts	8/11	5.6	cold
79c.log	15.24 mm/s	81 Amps	10.1 Volts	8/11	5.6	cold
79d.log	10.58 mm/s	81 Amps	10.1 Volts	8/11	5.6	
79e.log	8.47 mm/s	81 Amps	10.1 Volts	8/11	5.6	
712a.log	12.70 mm/s	80 Amps	10 Volts	4.5 5/6	2.8	cold
712b.log	8.47 mm/s	80 Amps	10 Volts	4.5 5/6	2.8	
712c.log	12.70 mm/s	90 Amps	10 Volts	16/22	2.8/4	cold
712d.log	12.70 mm/s	120 Amps	9.9 Volts	5.6/8	4	
712e.log	12.70 mm/s	80 Amps	10 Volts	5.6/8	4	sanded
712f.log	12.70 mm/s	80 Amps	10 Volts	5.6/8	4	sanded

### ***Signal and Image Acquisition***

The program used to save the weld pool images to the computer is illustrated in Figure 32. It is able to display the image in real-time and save the image on the computer. To display the image, the display button and the zoom factor are selected. The zoom factor allows the size of the pop up window to be adjusted with the image in it. By selecting call viewer, the separate viewer program will open and display the image allowing the images to be manipulated. To save the image, palette, number of frames to lock and the ROI (region of interest) are set first before running the program. The palette is set to temperature, gray, binary, gradient, or rainbow. This is beneficial depending on the application. The number of frames to lock selects the number of frames in the image to be saved. For example, if 1800 is selected, 1800 frames of the image are saved. The ROI specifies a specific region of the image, so the whole image does not have to be saved. Once these parameters are set, select “stop, write global, restart”. This marks the beginning position of the image to be saved and continues to collect the data until the press to save button is pressed. Then the user will be prompted to select a name and a destination to save the image on the

computer. After that portion of the image is saved, it will continue to display the image giving you the option to save more or to exit the program using the exit button. The other buttons, line profile and histogram, are optional for display purposes. The press to select ROI is used to save a portion of the displayed image and not the whole image. The images are saved as a .log file format, so it can be opened by the labview viewer program.

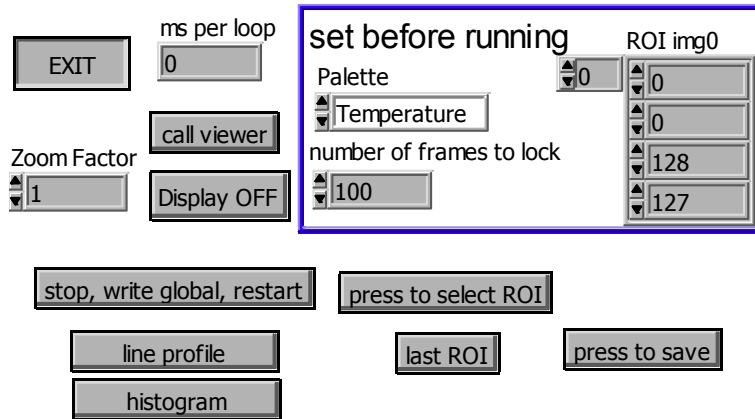


Figure 32. Program used for saving images from camera system.

## CHAPTER IV

### HIGH SPEED DIGITAL IMAGING SYSTEM

#### *LabVIEW Viewer Program*

Using the National Instruments Labview software, a viewer program was developed to play back frame by frame the recorded sequence of digitized images. The viewer program, used by David Delapp and W. Hofmeister, was modified further to improve the image quality and extract information [12]. This was done using various imaging processing techniques, which will be discussed later in this thesis. This program also enabled playback of the images at slower or faster speeds. The movable cursors in the program were positioned at various locations, or pixels, in the image. This provided the light intensity at each pixel in the image from frame to frame. Thus the time-domain analysis of the light intensity over the entire length of the data file was analyzed. The light intensity fluctuations and their corresponding Fast Fourier Transform can be performed on a single pixel over the span of the data file's images. Through the analysis of the individual pixels, time and frequency data was obtained. Frequency content of the fluctuations in light intensity reflected from the crests of the weld surface ripples were then related back to the ripple spacing,  $S_R$  and the weld travel speed according to:

$$F_R = V_t / S_R$$

where  $F_R$  is the ripple frequency,  $V_t$  is the weld travel speed, and  $S_R$  is the spacing between ripples [12].

Images were collected at the rate of 300 frames per second which was found by analyzing a frame by frame image of a stopwatch. A similar technique was used to determine the resolution of the camera system. In this case, the resolution was obtained by recording images of a ruler. The pixel resolution was found to be 0.74706 mm/pixel in the direction of the weld pool movement. This will be discussed in more detail later.

The Labview program consists of the main program [4], Figure 33, which calls all the subsequent programs. This program opens the sub-programs, get data from file, pyrometer, mask, viewer, thresholds, and area

and size. The get data from file and the viewer programs were the only ones used in the analysis of the image. The data set is the image file, .log file, that was saved previously. The file name will appear in the data set window. This file can be opened using the get data from file program. Once the file is opened, the viewer program is used to play the image back frame by frame at a controllable speed. This viewer program was enhanced dramatically to the point where only the basic structure was the same. By using the Labview Imaq Vision image processing toolkit, this program was modified to improve the image quality and to save the results.

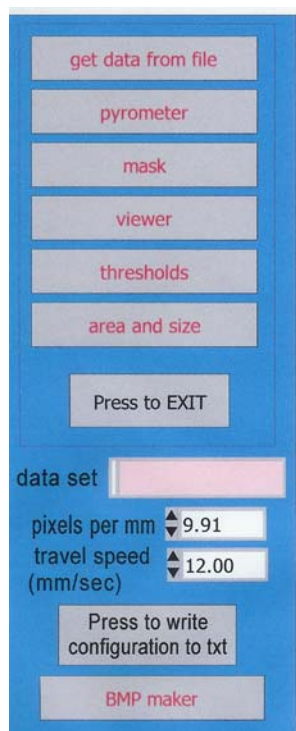


Figure 33. The main program which calls each subsequent programs [4].

In order to get the images into the viewer program, the get data from file program window, Figure 34, was used. First the file type needs to be selected as control, as seen in the figure. By selecting the press to read button, the file directory where the image is saved can be accessed to select the image file, .log file. This information appears in the spaces after the start directory and the current data set. Now the viewer program can be accessed from the main program. This program was used to play the image back and to analyze the weld pool. As a note, all the

Labview programs discussed includes both a front panel and a block diagram. Since the viewer program was enhanced, this program's front panel and block diagram will be discussed in greater detail.

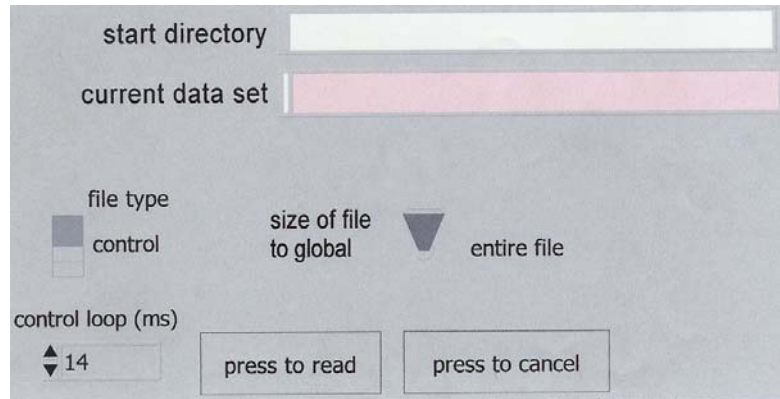


Figure 34. Window of the program used to open images to be used by the viewer program. The block diagram can be seen in the appendix.

The LabVIEW viewer program was used to analyze the leading edge of the weld pool. It includes both the front panel, Figure 35, and the block diagram, as seen in the Appendix A. An FFT can be performed on a specific pixel over all recorded frames, using the movable cursor in the viewer program. A program was also created to save this information to a text file. This FFT is related to the spacing between weld ripples. The light reflected from the weld bead is fluctuating in time, with respect to this pixel. Thus, a dominant frequency peak corresponds to a dominant ripple spacing. The dominant peaks were consistently around 10.5 Hz and 11.5 Hz. A few can be seen between 2 to 5 Hz and around 7 Hz. The FFTs of adjacent pixels parallel to the direction of travel are similar, because the weld specimen is moving relative to a particular pixel. Each of these adjacent pixels have a similar light intensity history, which is displaced by an increment of time. Thus, it is related to the pixel resolution and weld travel speed. Note, that each of the columns of pixels are parallel to the direction of travel, since the image was transposed in the programming of the viewer program. By selecting a pixel on the weld pool surface, its FFT peaks do not correspond to those of the weld ripples. The magnitude of these peaks is considerably smaller. Thus, this implies that the weld ripples are not the result of weld pool surface waves [12]. The FFT of each column of pixels



was also performed using the technique described below. This FFT was performed along the direction of travel of the weld ripples for a particular frame. This resulted in peaks around 50 Hz and 120 Hz, but these peaks varied greatly from plot to plot. These plots can be seen in the following section. When performing the FFT on pixels from the edge of the weld toward the center, the peaks climb to higher frequencies. More ripples exist per unit length near the weld center than near the edge. To determine any relationship between the ripple spacing and weld travel speed, the FFT should be placed along the weld centerline. Ripple frequency and travel speed have a near linear relationship [12].

The viewer program was modified to perform various image processing techniques. Many filtering techniques were tried, but only a few worked the best. The one chosen for this program filters the image using a linear filter IMAQ convolute along with IMAQ Getkernel in Labview terms. The kernels can be gradient, laplacian, smoothing, or gaussian. In the program shown, kernel code 1503 was used. Many other codes were also tried, but gradient and gaussian worked the best in this case. These image processing filtering techniques will be discussed briefly before explaining the code.

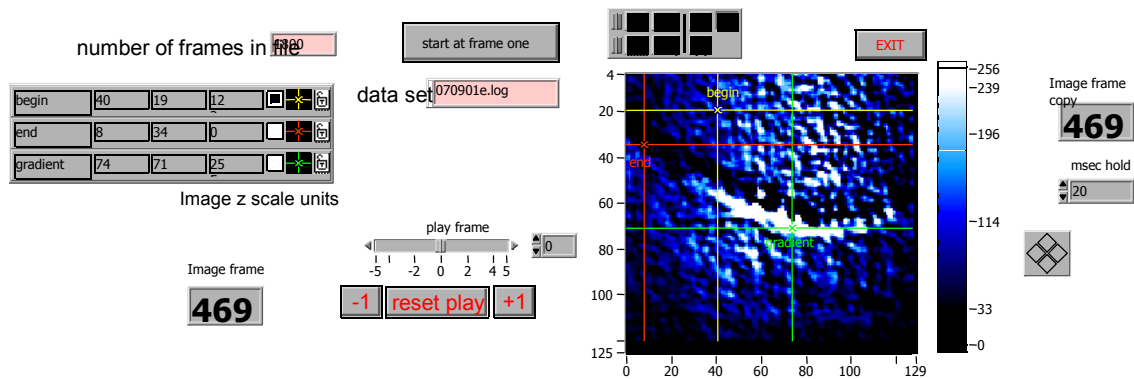


Figure 35. The Front Panel of the LabVIEW Viewer Program. Note: Begin 40 19 122, End 8 34 0, Gradient 74 71 255 The last number is cut off in the image.

## Spatial Filters

In order to get the desired information, linear spatial filters or convolution filters can be used to remove noise, smooth, and transform the image. Spatial filters alter pixel values with respect to variations in light intensity in their neighborhood. The neighborhood of a pixel is defined by the size of a matrix, or mask of pixels. This matrix or mask surrounds and is centered on the pixel itself. These filters can be sensitive to the presence or absence of light intensity variations. Spatial filters can serve a variety of purposes, such as the detection of edges along a specific direction, the contouring of patterns, noise reduction, and detail outlining or smoothing. Spatial filters can be divided into two categories, highpass and lowpass. Highpass filters emphasize significant variations of the light intensity usually found at the boundary of objects. Lowpass filters attenuate variations of the light intensity. They have the tendency to smooth images by eliminating details and blurring edges. In a 3x3 matrix, the value of the central pixel derives from the values of its eight surrounding neighbors. A 5x5 matrix specifies 24 neighbors, a 7x7 matrix specifies 48 neighbors, and so forth. If  $P_{(i,j)}$  represents the intensity of the pixel P with the coordinates (i,j), the pixels surrounding  $P_{(i,j)}$  can be indexed as follows for a 3x3 matrix [9]:

$P_{(i-1,j-1)}$	$P_{(i,j-1)}$	$P_{(i+1,j-1)}$
$P_{(i-1,j)}$	$P_{(i,j)}$	$P_{(i+1,j)}$
$P_{(i-1,j+1)}$	$P_{(i,j+1)}$	$P_{(i+1,j+1)}$

A linear filter assigns to  $P_{(i,j)}$  a value that is a linear combination of its surrounding values. For example,

$$P_{(i,j)} = (P_{(i,j-1)} + P_{(i-1,j)} + 2 P_{(i,j)} + P_{(i+1,j)} + P_{(i,j+1)}).$$

A nonlinear filter assigns to  $P_{(i,j)}$  a value that is not a linear combination of the surrounding values. For example,

$$P_{(i,j)} = \max(P_{(i-1,j-1)}, P_{(i+1,j-1)}, P_{(i-1,j+1)}, P_{(i+1,j+1)}).$$

The highpass linear filters are the Gradient and Laplacian filters. The lowpass linear filters are the Smoothing and Gaussian filters. The highpass nonlinear filters are the Gradient, Roberts, Sobel, Prewitt, Differentiation, and Sigma filters. The lowpass nonlinear filters are the Median, Nth Order, and Lowpass filters.

### Convolution

A convolution is a mathematical function that replaces each pixel by a weighted sum of its neighbors. The matrix defining the neighborhood of the pixel also specifies the weight assigned to each neighbor. This matrix is called the convolution kernel. For each pixel  $P_{(i,j)}$  in an image (where  $i$  and  $j$  represent the coordinates of the pixel), the convolution kernel is centered on  $P_{(i,j)}$ . Each pixel masked by the kernel is multiplied by the coefficient placed on top of it.  $P_{(i,j)}$  becomes the sum of these products.

The pixel neighborhood, the pixels surrounding  $P_{(i,j)}$ , is defined by the 3x3 matrix:

$P_{(i-1,j-1)}$	$P_{(i,j-1)}$	$P_{(i+1,j-1)}$
$P_{(i-1,j)}$	$P_{(i,j)}$	$P_{(i+1,j)}$
$P_{(i-1,j+1)}$	$P_{(i,j+1)}$	$P_{(i+1,j+1)}$

and the coefficients of the kernel,  $K$ , is defined by the 3x3 matrix:

$K_{(i-1,j-1)}$	$K_{(i,j-1)}$	$K_{(i+1,j-1)}$
$K_{(i-1,j)}$	$K_{(i,j)}$	$K_{(i+1,j)}$
$K_{(i-1,j+1)}$	$K_{(i,j+1)}$	$K_{(i+1,j+1)}$

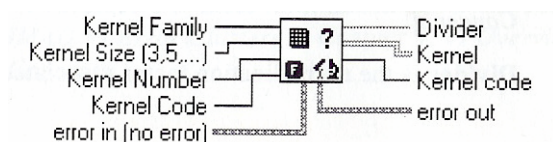
The result of the convolution operation is defined to be  $P_{(i,j)} = [\sum(K_{(a,b)} \times P_{(a,b)})] / N$ . The pixel  $P_{(i,j)}$  is given the value  $(1/N)\sum K_{(a,b)}P_{(a,b)}$ , with  $a$  ranging from  $(i-1)$  to  $(i+1)$ , and  $b$  ranging from  $(j-1)$  to  $(j+1)$ .  $N$  is the normalization factor, equal to  $\sum K_{(a,b)}$  or 1, whichever is greater [9]. If the new value  $P_{(i,j)}$  is negative, it is set to 0. If the new value  $P_{(i,j)}$  is greater than 255, it is set to 255 (for a 8-bit image). The greater the absolute value of a coefficient  $K_{(a,b)}$ , the more the pixel  $P_{(a,b)}$  contributes to the new value of  $P_{(i,j)}$ . If a coefficient  $K_{(a,b)}$  is null, the

neighbor  $P_{(a,b)}$  does not contribute to the new value of  $P_{(i,j)}$  (note  $P_{(a,b)}$  might be  $P_{(i,j)}$  itself [9]). The transfer function of the filter is equivalent to a weighted differentiation, and produces a sharpening or highpass filter, if the kernel contains both negative and positive coefficients. Highpass filters include Laplacian and gradient filters. The transfer function of the filter is equivalent to a weighted summation or lowpass filter, if all coefficients in the kernel are positive. Lowpass filters include Gaussian and smoothing filters.

Each of these filters, Laplacian, gradient, Gaussian and smoothing, use a kernel matrix as described above. A Laplacian Filter is used to highlight the variation of light intensity around a pixel. The Laplacian filter extracts the contours of objects in an image. This filter is omnidirectional. Thus, it does not have a preferred direction, unlike the gradient filter. A gradient filter highlights the variations of light intensity along a specific direction, which has the effect of outlining edges and revealing texture. It is used to highlight areas in an image where there are significant variations in pixel intensity which usually occur near edges in the image. Gaussian filters are averaging filters, which are used to attenuate the variations of light intensity in the neighborhood of a pixel. These filters smooth the overall shape of objects and attenuates details in the image. Smoothing filters are also used to attenuate the variations of light intensity in the neighborhood of a pixel. The smoothing effect of smoothing filters is more pronounced, unlike that of the Gaussian filters [9].

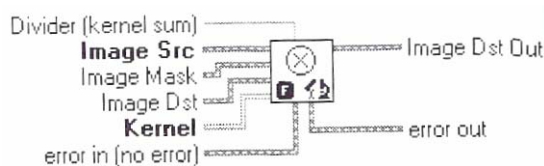
### LabVIEW Programming Definitions

Knowing the theory behind the code helps in understanding the viewer program. The following IMAQ Getkernel, and IMAQ Convolute information is taken from the Labview Imaq Vision for G Reference Manual [10]. IMAQ Getkernel [10] reads a predefined kernel. This VI uses the contents of a convolution catalog (imaqknl.txt). This VI outputs a specified kernel after reading the kernel-associated code. This code consists of three separate units, Kernel Family, Kernel Size, and Kernel Number. If you already know the code, you can enter it directly with Kernel Code. This operation can be seen in Figure 25.



Kernel Family determines the type of matrix. The valid values are between 1 and 4, each associated with a particular type. This value corresponds to the thousandth unit in the research code. Gradient is 1. Laplacian is 2. Smoothing is 3. Gaussian is 4. Kernel Size (3,5,7, ...) determines the horizontal and vertical matrix size. The values are 3,5, and 7, corresponding to the convolutions 3 x 3, 5 x 5, and 7 x 7 supplied in the matrix catalog. This value corresponds to the hundredth unit in the researched code. Kernel Number is the matrix family number. It is a two-digit number, between 0 and n, belonging to a family and a size. A number of predefined matrices are available for each type and size. Kernel Code is a code that permits direct access to a convolution matrix cataloged in the file imaqknl.txt. Each code specifies a specific convolution matrix. This input is used under the conditions that it is connected and is not 0. The kernel located in the file then is transcribed into a 2D G array that is available from the output Kernel. The user can use the codes to specify a predefined kernel as well as to create new user-coded kernels. The coding syntax is simple to employ and is broken down in the following manner. Fsnn, where F is the kernel family (1 to 4), S is the kernel size (3,5, and so forth), and nn is the kernel number (based on the family and size of the kernel). Error in (no error) is a cluster that describes the error status before this VI executes. Divider is the normalization factor associated with the retrieved kernel. Kernel is the resulting matrix. It corresponds to a kernel encoded by a code specified from the inputs Kernel Family, Kernel Size, and Kernel Number or a from a code directly passed through the input Kernel Code. This output can be connected directly to the input Kernel in IMAQ Convolute. Kernel code indicates the code that was used to retrieve the kernel. Error out is a cluster that describes the error status after this VI executes. For kernel code 1503, the kernel family is gradient, the kernel size is 5 x 5, and the kernel number (nn) is 03.

IMAQ Convolute [10] filters an image using a linear filter. The calculations are performed either with integers or floating points, depending on the image type and the contents of the kernel. This operation can be seen in Figure 36.



Divider (kernel sum) is a normalization factor that can be applied to the sum of the obtained products. Under normal conditions the divider should not be connected. If connected (and not equal to 0), the elements internal to the matrix are summed and then divided by this normalization factor. Image Src is the image reference source. It must be an 8-bit or RGB image. Image Mask is an 8-bit image that specifies the region in the image to modify. Only pixels in the original image that correspond to the equivalent pixel in the mask are replaced by the values in the lookup table (provided that the value in the mask is not 0). All pixels not corresponding to this criteria keep their original value. The complete image is modified if Image Mask is not connected. Image Dst is the reference of the image destination. If it is connected, it must be the same type as the Image Src. Kernel is a 2D array that contains the convolution matrix to be applied to the image. The size of the convolution is fixed by the size of this array. The array can be generated by using standard G programming techniques or the VIs IMAQ GetKernel or IMAQ BuildKernel. If the dimensions (XY) produced by this array are not greater than 3, the filter is considered null and the output image is identical to the input image. Error in (no error) is a cluster that describes the error status before this VI executes. Image Dst Out is the reference to the destination (output) image which receives the processing results of the VI. If the Image Dst is connected, then Image Dst Out is the same as Image Dst. Otherwise, Image Dst Out refers to the image referenced by Image Src. Error out is a cluster that describes the error status after this VI executes. Any image connected to the input Image Dst must be the same image type connected to Image Src. The image type connected to the input Image Mask must be an 8-bit image. The connected source image must have been created with a border capable of supporting the size of the convolution matrix. A 3 x 3 matrix must have a minimum border of 1, a 5 x 5 matrix must have a minimum border of 2, and so forth. The border size of the destination image is not important. A convolution matrix must have odd-sized dimensions so that it contains a central pixel. The function does not take into account the odd boundary, furthest out on the matrix, if one of the Kernel dimensions is even. For example, if the input Kernel is 6 x 4 (X=6 and Y=4), the actual convolution is 5 x 3. Both the sixth line and fourth are ignored. Remember, the second dimension in a G array is the vertical direction (Y). Calculations made with an 8 bit or 16 bit Image Src input are made in integer mode provided that the kernel contains only integers. Calculations made with a 32-bit floating-point Image Src input are made in floating-point mode. Note that the processing speed is correlated with the size of the kernel. A 3 x 3 convolution processes nine pixels while a 5 x 5 convolution processes 25 pixels.

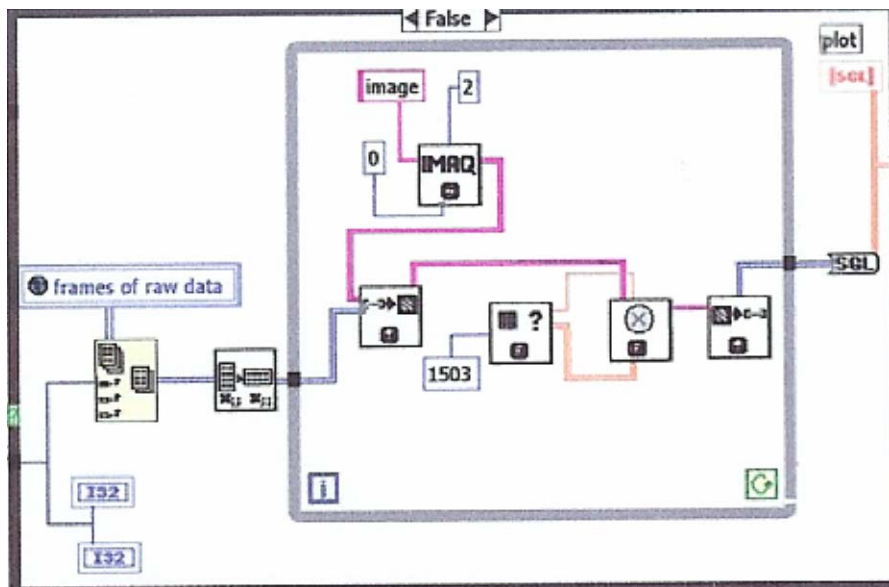


Figure 36. Portion of LabVIEW Viewer Program Showing Convolution of the Image

After convolution of the image, each frame of the image was saved in a spreadsheet form by simply adding the spreadsheet command block, in the labview viewer program which is seen in Figure 37. This spreadsheet command block converts a 2D or 1D array of single-precision (SGL) numbers to a text string and writes the string to a new byte stream file or appends the string to an existing file [10]. As an option, the data can be transposed. This VI opens or creates the file before writing to it and closes it afterwards. This VI is used to create a text file readable by most spreadsheet applications. This VI calls the Array to Spreadsheet String function to convert the data.

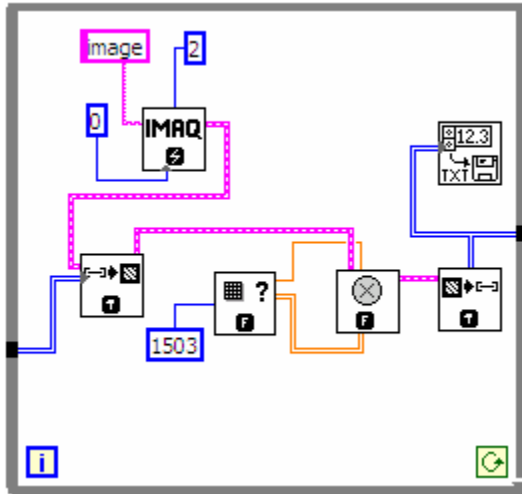
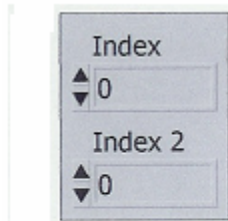


Figure 37. Portion of Labview Program Showing the Spreadsheet Command

Also the pixel data from the original image was saved by selecting the coordinates of each pixel. By entering these coordinates into the following program, Figure 38, the results would be the pixel intensity values for that particular pixel over every frame saved to a text file (.txt file). Thus, for 1800 frames, the file would have 1800 pixel intensity values for those coordinates. This was useful for performing the FFT and the pixel intensity history. The drawback of this is that if looking at many pixels, it takes time to enter all the coordinates. Therefore, there are many different options for saving the data needed.



### Front Panel



### Block Diagram

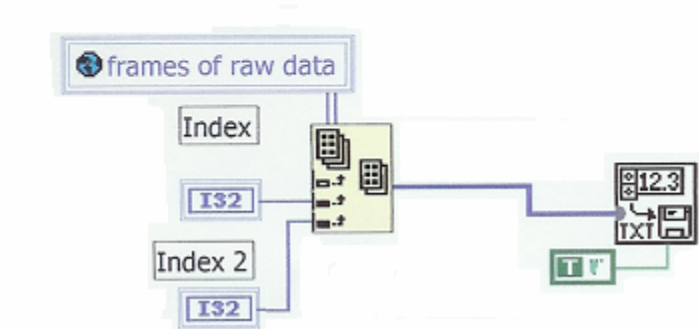


Figure 38. Front panel and block diagram of the LabVIEW subprogram used to get pixel data over each frame from the original image. Index and Index 2 corresponds to the coordinates of the pixel.

## CHAPTER V

### RESULTS

A PC-based vision system was developed for viewing and analyzing melt-off characteristics at the leading edge of a GTA weld. A Labview program was used to observe the images of the weld. This program was further enhanced, using Labview's IMAQ Vision toolkit. This enabled various filtering operations to be performed on the images, such as convolution and edge enhancement operations. It is a valuable tool for image processing and image analysis. The Labview program also performs the FFT on the images. For comparison, Matlab 5.3 was used to perform the FFT on the image. A Matlab program was also used to monitor the changes in the pixel intensity values.

Using the Labview program, the images observed showed distinct changes in the leading edge of the weld pool. There were 1800 frames in each image. A frame of one of these images, 79d.log, is illustrated in Figure 39.

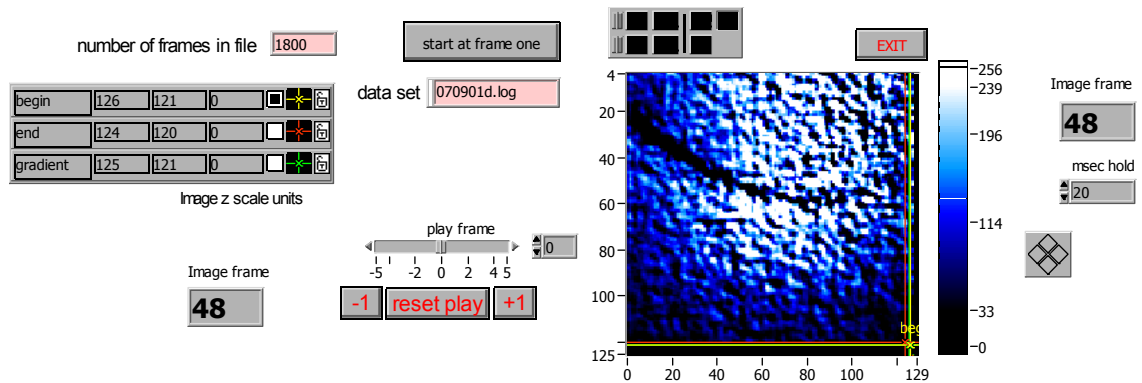


Figure 39. This is frame number 48 out of the 1800 frames in the image, 79d.log.

## CHAPTER VI

### DISCUSSION

A general knowledge of cameras and charged coupled devices (CCDs), video signals, lighting techniques, and image processing is needed to develop a PC-based vision system for the study of gas tungsten arc welds. The progressive scan area camera, Dalsa CA-D1-0128, is the most fundamental part of the imaging system. Equally important, the macro lens camera, minimized the amount of arc light viewed directly by the camera or reflected into the camera from the weld pool surface [12]. Once the cameras were correctly positioned to get the appropriate image of the weld pool and its leading edge, only the basic camera adjustments, such as the lens aperture setting, were needed to improve the image quality.

The aperture setting controls how much light is allowed into the cameras. For the best lighting results, currents were kept between 60 Amperes and 120 Amperes. Clear focus across the entire width of the weld bead is difficult. And the correct welding parameters, current, voltage, and travel speed, enable the welds to have better penetration. Any slight variation of these welding parameters, also including shielding gas, and surface impurities, could have a dramatic effect on the pool size, and the pool's vibration.

An understanding of how modern electronic cameras function and the types of signals they produce is a key step in designing a successful system. To work with these signals as images, these signals need to get into the computer by way of a frame grabber via the National Instruments software program LabView. The IMAQ-1424 RTSI interface is used to synchronize image and data acquisition with a PCI-MIO-16-E1 multifunction I/O board. This board enabled the images to be saved for further analysis.

Using the National Instruments software program, Labview 5.1, the viewer program was modified to improve the visual appearance of the leading edge of the weld. This was done using various image processing

techniques. Many filtering techniques were tried, but only a few worked the best. The one chosen for this program filters the image using a linear filter IMAQ convolute along with IMAQ Getkernel, with a kernel code of 1503, in Labview terms. Matlab 5.3, along with Labview 5.1, were used to perform the Fast Fourier Transform (FFT) on the pixels in the image over all 1800 frames. The FFT from both of these programs were compared for accuracy.

This FFT is related to the spacing between weld ripples. The light reflected from the weld bead is fluctuating in time, with respect to this pixel. Thus, a dominant frequency peak corresponds to a dominant incremental melt-off spacing. The FFTs of adjacent pixels parallel to the direction of travel are similar, because the weld specimen is moving relative to a particular pixel. Each of these adjacent pixels have a similar light intensity history, which is displaced by an increment of time. Thus, it is related to the pixel resolution and weld travel speed. Note, that each of the columns of pixels are parallel to the direction of travel, since the image was transposed in the programming of the viewer program. Using Matlab 5.3, the FFT on each column of a frame was also performed. Thus, these FFTs are performed in the same direction as the direction of travel of the weld incremental melt-off. By selecting a pixel on the weld pool surface, its FFT peaks do not correspond to those of the weld incremental melt-off. The magnitude of these peaks is considerably smaller. Thus, this implies that the weld melt-off variations are not the result of weld pool surface waves. When performing the FFT on pixels from the edge of the weld toward the center, the peaks climb to higher frequencies. More melt-off variations exist per unit length near the weld center than near the edge. To determine any relationship between the melt-off spacing and weld travel speed, the FFT should be placed along the weld centerline. The FFT of each column of pixels was also performed. This resulted in peaks near 50 Hz and 120 Hz. Also the pixel intensity history was plotted over the 1800 frames. The development of equipment and imaging analysis techniques were necessary to get a high quality image and to observe the melting characteristics at the leading edge of a gas tungsten arc weld.

## CHAPTER VII

### CONCLUSIONS AND RECOMMENDATIONS FOR FUTURE WORK

A PC-based vision system was developed for viewing and analyzing melt-off characteristics at the leading edge of a GTA weld. This system may be used for studying solidification characteristics. A general knowledge of cameras and charged coupled devices (CCDs), video signals, lighting techniques, and image processing were needed to develop this system. The progressive scan area camera, Dalsa CA-D1-0128, and the macro lens camera were positioned to get the appropriate image of the weld pool and its leading edge. Clear focus across the entire width of the weld bead is difficult. For the best lighting results, currents were kept between 60 Amperes and 120 Amperes. Also, the correct welding parameters, current, voltage, and travel speed, enabled the welds to have better penetration. Any slight variation of these welding parameters, including the shielding gas, could have a dramatic effect on the pool size, and the pool's vibration.

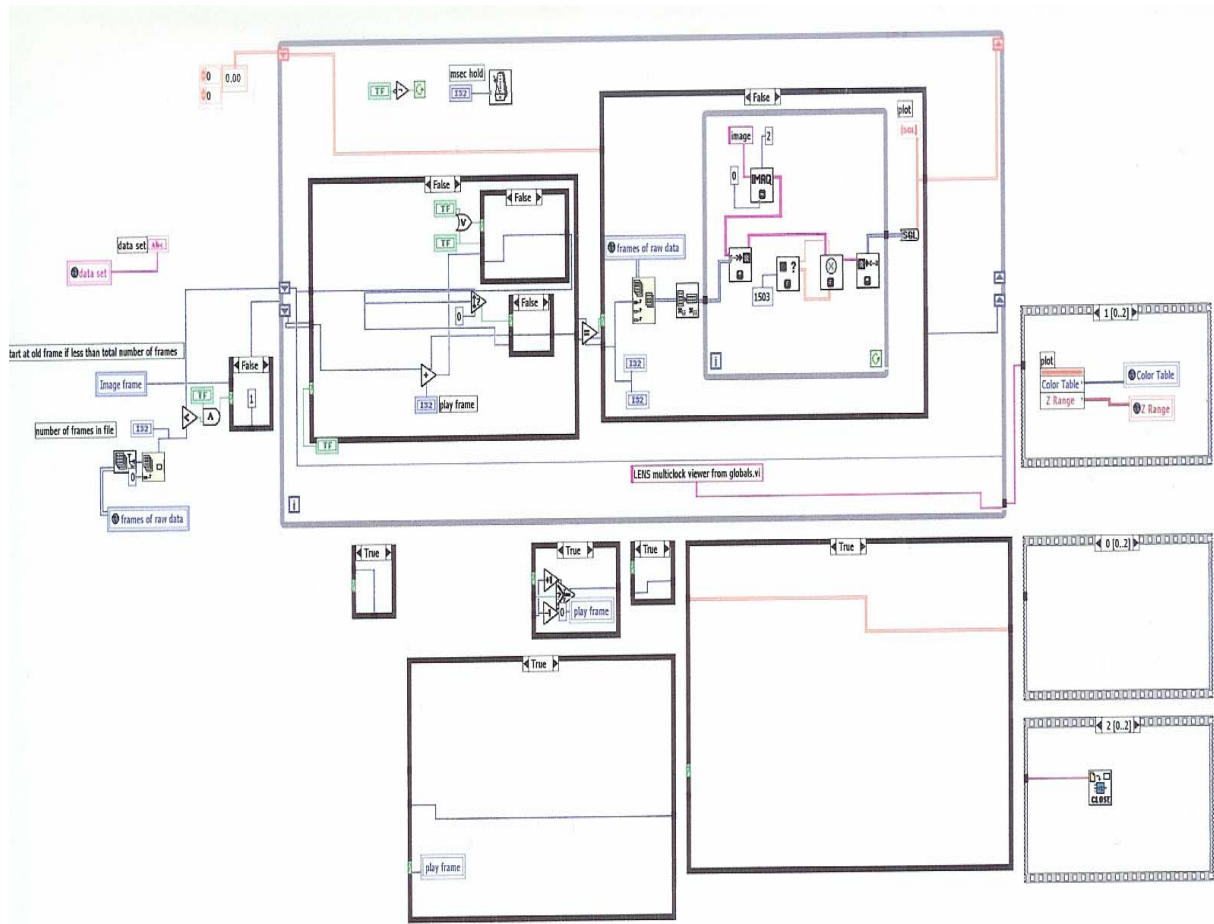
The image acquisition was accomplished by using a frame grabber via the National Instruments software program LabView. The IMAQ-1424 RTSI interface is used to synchronize image and data acquisition with a PCI-MIO-16-E1 multifunction I/O board. This board enabled the signals from the camera to be saved as images on the computer. Using the National Instruments software program, Labview 5.1, the viewer program was modified to improve the visual appearance of the leading edge of the weld. This was done using various image processing techniques. Matlab 5.3, along with Labview 5.1, were used to perform the Fast Fourier Transform (FFT) on the pixels in the image over all 1800 frames. The FFT from both of these programs were compared for accuracy. Also the pixel intensity in the images were compared over each frame.

With further work, including extensive weld testing, this system could be used to quantify the incremental melt-off at the leading edge of a GTA weld under certain conditions. From the images used in this research, the incremental melt off could not be quantified. Only a few of the images were clear enough to observe the leading edge. The obstacles in observing the leading edge included too much glare, which is seen in the image file,

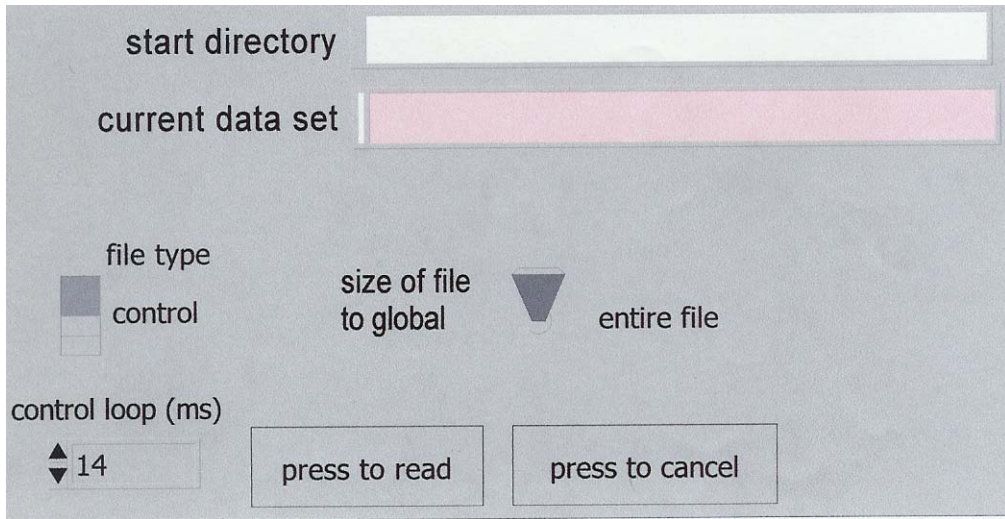
070901b.log. Impurities such as slag could be seen in the image, 100901a.log. The image, 070901e.log, was from an over penetration weld. The change in the leading edge was so small, a pixel or two, in these images from frame to frame. If the images were speed up too much, some of the information would be lost. The images obtained were only a small portion of the single pass weld. If more of the weld could have been captured, such as the whole pass of the weld, it would improve the ability to quantify the melt-off .

The ability to quantify the incremental melt-off rate at the leading edge of a GTA weld would be useful in various applications. It also would be used to improve the quality of the welds used in various fields, such as in the ship building and the aviation industries. A model could be developed using this information to improve the penetration and quality of the weld. The obvious desire is to develop an automated system, using a defined set of parameters, to produce quality welds.

## Appendix A LabVIEW Programs and Overview of Welding Process

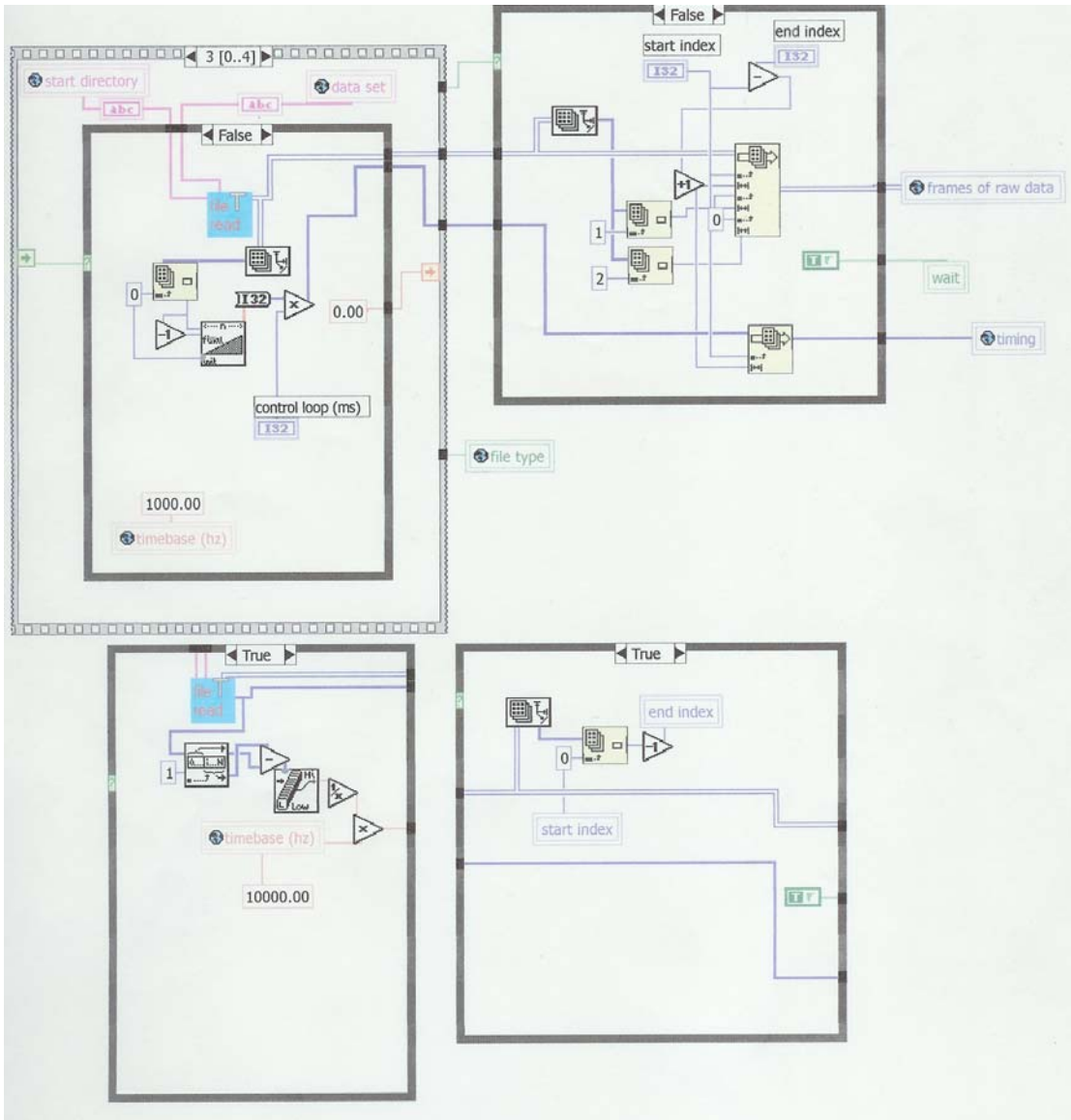


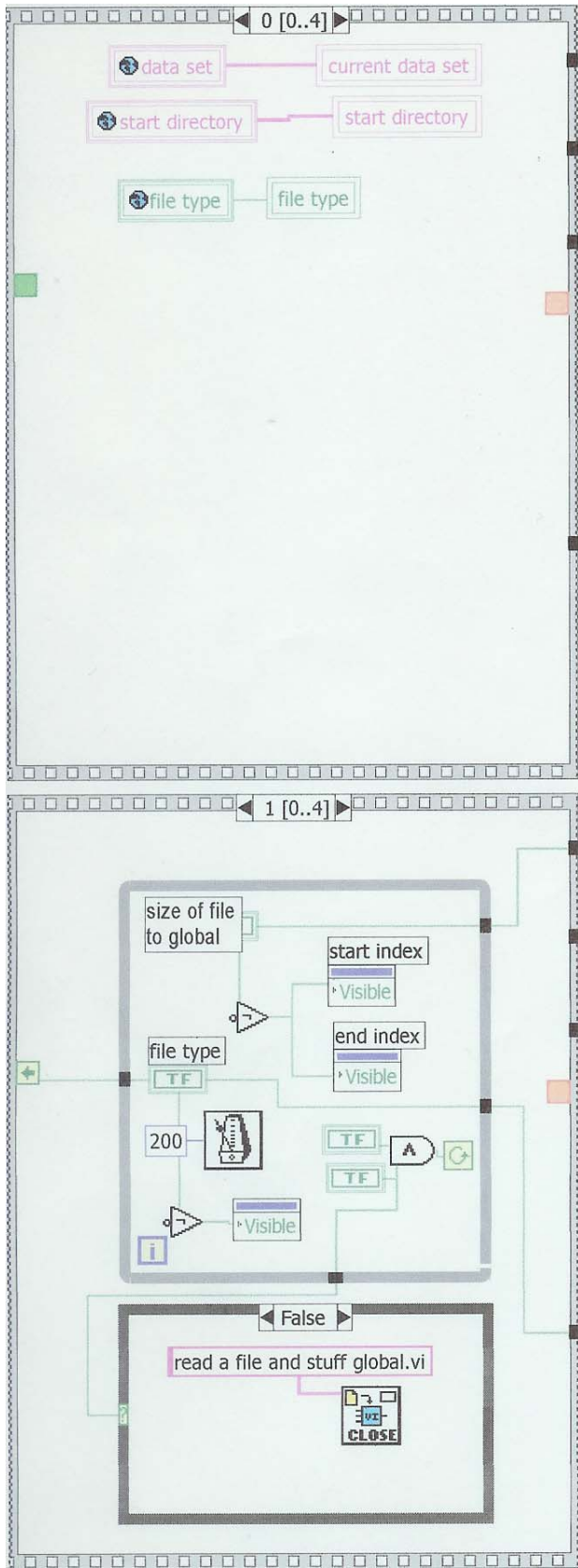
The Block Diagram of the Labview Viewer Program

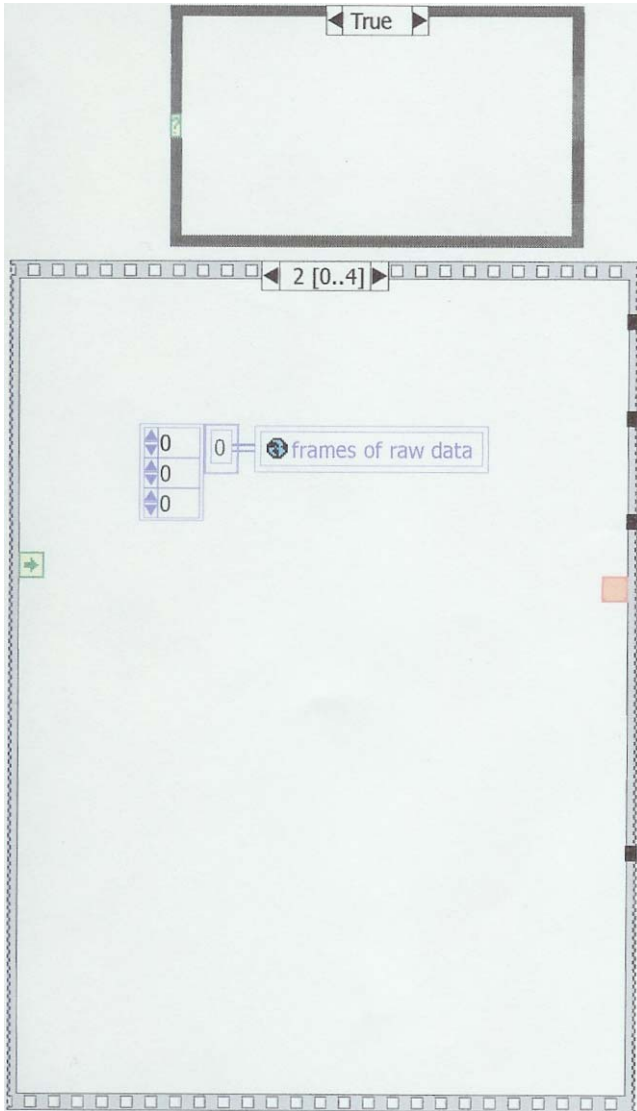


This is front panel of the LabVIEW program to save the weld pool images to a file. The following four pages are the block diagrams of this program.









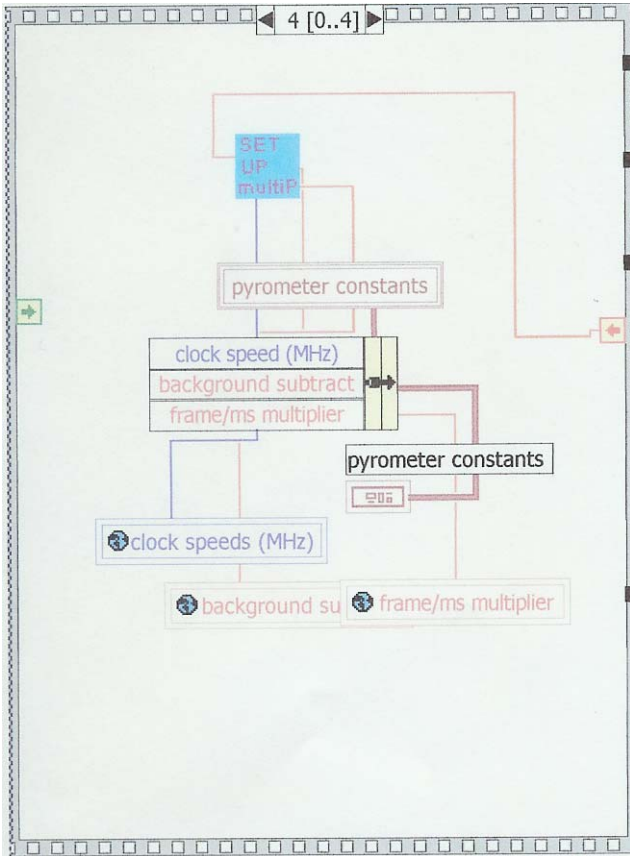


Table A Overview of Welding Processes<sup>a</sup>

Material	Thickness <sup>b</sup>	SMAW	SAW	GMAW	FCAW	GTAW	PAW	ESW	OPW	EBW	LBW
Carbon steels	S	X	X	X		X			X	X	X
	I	X	X	X		X			X	X	X
	M	X	X	X		X			X	X	X
Low-alloy steels	T	X	X	X		X		X	X	X	X
	S	X	X	X		X			X	X	X
	I	X	X	X		X			X	X	X
Stainless steels	M	X	X	X						X	X
	T	X	X	X				X		X	X
	S	X	X	X		X			X	X	X
Cast iron	I	X		X					X	X	
	M	X		X		X			X	X	
	T	X		X		X			X	X	
Nickel and alloys	S	X		X		X			X	X	X
	I	X		X		X			X	X	X
	M	X		X		X			X	X	X
Aluminum and alloys	T	X		X				X		X	
	S			X		X			X	X	X
	I			X		X			X	X	X
	M			X		X			X	X	X
	T			X					X	X	X

<sup>a</sup> Process code: SMAW, shielded metal arc welding; SAW, submerged arc welding; GMAW, gas-metal arc welding; FCAW, flux-cored arc welding; GTAW, gas-tungsten arc welding; PAW, plasma arc welding; ESW, electroslag welding; OPW, oxyfuel gas welding; EBW, electron beam welding; LBW, laser beam welding.

<sup>b</sup> Abbreviations: S, sheet, up to 3 mm ( $1/8$  in.); I, intermediate, 3–6 mm ( $1/8$ – $1/4$  in.); M, medium, 6–19 mm ( $1/4$ – $3/4$  in.); T, thick, 19 mm ( $3/4$  in.) and up; X, recommended.

## CA-D1 Progressive Scan Area Camera Product Info

[View Data Sheet](#)



Product ID CA-D1-0128

### Searchable Features

Feature	Unit	Specs
Total Data Rate	MHz	15
Max. Frame Rate	fr/sec	736
Pixel Size	µm	16x16
Resolution		128x128
Number of Camera Outputs		1



### Other Features

- 128x128 resolution
- 16µm square pixels, 100% fill factor
- Up to 15MHz data rate
- Single 8-bit output; 12-bit option available
- RS422 data
- Vertical and horizontal binning options
- Multi-camera synchronization

### Description

High frame rates, large pixels, an easy-to-interface single tap, and output options such as pixel binning and 12-bit digitization make this progressive scan area camera adaptable to a wide range of applications. DALSA's patented modular architecture provides a high-performance camera with the reliability, flexibility, and cost-effectiveness of high-volume interchangeable parts.

# DALSA CA-D1 Cameras

High frame rates, large pixels, and easy-to-interface single outputs make these progressive scan area cameras adaptable to a wide range of applications.

## Features

- 128x128, and 256x256 resolution,
- 16µm x 16µm pixels, 100% fill factor
- Frame transfer architecture—no shutter required
- Single output
- Up to 15MHz data rate
- 8-bit or 12-bit digital data in RS422 format
- Vertical and horizontal binning options
- Multi-camera synchronization

## Description

The CA-D1 series cameras feature the IA-D1 sensors in single output cameras providing data at up to 15MHz. This allows maximum frame rates of 736 frames per sec (CA-D1-0128A) or 203 frames/sec (CA-D1-0256A).

The CA-D1 cameras use DALSA's patented modular architecture. This system of connecting circuit modules through standardized busses allows DALSA to build a high performance modular camera using the reliability, flexibility, and cost-effectiveness of high-volume interchangeable parts. Within the camera, a driver board provides bias voltages and clocks to the CCD image sensor, a timing board generates all internal timing, and A/D boards process the video and digitize it for output. Contact DALSA for further information.

## Applications

The CA-D1 cameras are ideally suited for use in:

- Motion tracking
- Instrumentation
- High frame rate imaging

## Sensor

The CA-D1 cameras use the IA-D1 area scan image sensors for high speed, high resolution performance. The sensors use a frame transfer architecture. The pixel size is 16µm x 16µm with a 100% fill factor (all of the image area is photo-sensitive) to achieve maximum quantum efficiency within the pixel. Figure 1 shows the block diagram of the sensor.



Table 1. Camera Configurations

Specification	A Model	T Model
Pixel Pitch	16µm	16µm
Aperture, 0128	2.1 x 2.1mm	2.1 x 2.1mm
0256	4.1 x 4.1mm	4.1 x 4.1mm
Lens Mount	C-mount	C-mount
Data Bits	8	12
Max. Data Rate	15MHz	10MHz
Max. Frame Rate, 0128	736fps	490fps
0256	203fps	136fps
Data Format	RS422	RS422
Data Channels	1	1

Example Configuration: CA-D1-0256A

resolution model

Analog output models also available. Contact DALSA

## Operation

### Power Supplies

Cameras provide optimum performance using well-regulated linear supplies. The power supply requirements indicated below are adequately overrated to accommodate all models and operating conditions.

Voltage	Current Draw	Notes
+15V	300mA	Specified at 40°C ambient. Tolerance for all supplies: ■ ± 50mV ■ <5mV ripple.
+5V	1500mA	
-5V	200mA	
-15V	100mA	

### Optical Interface

The CA-D1 cameras provide a mount for a C-mount lens. The image sensor's frame transfer architecture means the camera does not require a shutter for most applications.

## REFERENCES

- [1] Hussam El-Dean E.H. Eassa. Electric Arc Welding Control with a High Performance Power Source. Ph.D. dissertation, Vanderbilt University, May 1983.
- [2] Kristinn Andersen. Synchronous Weld Pool Oscillation for Monitoring and Control. Ph.D. dissertation, Vanderbilt University, May 1993.
- [3] Robert Joel Barnett. Sensor Development for Multi-Parameter Control of Gas Tungsten Arc Welding. Ph.D. dissertation, Vanderbilt University, May 1993.
- [4] Daniel Anthony Hartman. Model Analysis of GTA Weld Pools for Penetration Control. Ph.D. dissertation, Vanderbilt University, December 1999.
- [5] Cook, George E., Andersen, K., Fernandez, K.R., Shepard, M.E., and wells, A. M., Jr. "Electric Arc Sensing for Robot Positioning Control." In International Trends in Manufacturing Technology – Robotic Welding, pp.181-216. Edited by J. D. Lane. London, England:IFS (Publications) Ltd, 1987.
- [6] *Welding Handbook*, Vol. 1, 7<sup>th</sup> ed., American Welding Society, Miami, FL, 1976, pp. 2-32.
- [7] *Welding handbook*, Vol. 2, 7<sup>th</sup> ed., American Welding Society, Miami, FL, 1978, pp.78-112,296-330.
- [8] Cook, George E. "Robotic Arc Welding: Research in Sensory Feedback Control." IEEE Transaction on Industrial Electronics, vol. IE-30, No.3, (August 1983):252-268.
- [9] "Labview Machine Vision and Image Processing Course Manual." National Instruments Corporation, 1998.
- [10] "BridgeVIEW and LabVIEW, IMAQ Vision for G Reference Manual." National Instruments Corporation, 1997.
- [11] Wayne Niblack. "An Introduction to Digital Image Processing." pp. 2-48. London, England: Prentice-Hall International (UK) Ltd, 1986.
- [12] The Development of a GTAW Observation System  
D.R. Delapp, D.A. Hartman R.J Barnett G E Cook A M Strauss. ASM International, June 1999.
- [13] Cary, Howard B. "Modern Welding Technology." pp. 2-48. Englewood Cliffs, NJ: Prentice-Hall Inc. 1979.